Ordered Mesoporous Materials as Catalysts

Harun Tüysüz, Ferdi Schüth

Max-Planck Institut für Kohlenforschung, Kaiser-Wilhelm-Platz 1, 45470 Mülheim an der Ruhr, Germany

Contents

Abstract

After their discovery in the early 1990s, ordered mesoporous materials have become one of the most widely investigated classes of materials, and applications have been considered in many areas, in particular in catalysis. They have attracted attention because of their unique properties such as high surface areas, controllable compositions, crystallinity, thermal and chemical stability, tailored porosities, narrow pore size distributions, concave surface curvatures, surface functionalities, as well as the opportunities they offer for incorporation of catalytically active and selective species. This chapter is focused on the properties of ordered mesoporous solids that distinguish them from more conventional porous catalytic materials. Emphasis is placed on history, development, and methods of synthesis of ordered mesoporous materials.

ABBREVIATIONS

1D one-dimensional
2D two-dimensional
3D three-dimensional
3-MPTS 3-methacryloxypropyltrimethoxysilane
ALD atomic layer deposition
APTES 3-aminopropyltriethoxysilane
BET Brunauer–Emmett–Teller
BJH Barrett–Joyner–Halenda
Boc *t*-butoxycarbonyl
Bpy bipyridyl
CMK-X carbon molecular sieves from KAIST (CMK-3 and CMK-5 are ordered
    mesoporous carbon materials with mono- and bimodal pore size distribution, respectively)
CTA cetyltrimethylammonium
CVD chemical vapor deposition
DBT dibenzothiophene
DPP 1,3-diphenylpropane
DTBP 2,6-*tert*-butyl phenol
EPR Electron Paramagnetic Resonance
FDU-X Fudan University ordered mesoporous materials series
FSMs folded sheet materials
FTIR Fourier transform infrared
FTO fluorine-doped tin oxide
HMS hexagonal mesoporous silica
HDS hydrodesulfurization
ITQ-X Instituto de Tecnología Química zeolite series
IRMOF isoreticular metal-organic framework
KIT-6 Korea Advanced Institute of Science and Technology cubic ordered mesoporous silica
KSW-X a type of mesoporous material
MCM-41/-48 Mobil composition of matter no. 41/48 (hexagonally and cubic ordered
    mesoporous silica)
MFI mordenite framework inverted (a type of zeolite structure)
MMCT metal-to-metal charge transfer
MMSs mesoporous molecular sieves
MOF metal-organic framework
MSU-(V,X) Michigan State University mesoporous materials series
Nafion®-SAC-13 fluorosulfonic acid Nafion® polymer on amorphous silica
NMR nuclear magnetic resonance
SBA-15/-XX Santa Barbara mesoporous silica series
SBU secondary building unit
ODH oxidative dehydrogenation
OM ordered mesoporous
OMC ordered mesoporous carbon
OMM ordered mesoporous material
PAMAM polyaminoamide
PAN polyacrylonitrile
Pc phthalocyanine
PEO polyethylene oxide

PMA phosphomolybdic acid
PPO polypropylene oxide
PTA phosphotungstic acid
P-123 $EO_{20}–PO_{70}–EO_{20}$, Pluronic® P-123
PVP polyvinylpyrrolidone
SEM scanning electron microscopy
SFS perfluoroalkylsulfonic acid
STY space–time yield
T_{50} light-off temperature
TEM transmission electron microscopy
TEOS tetraethyl orthosilicate
THF tetrahydrofuran
TMB trimethylbenzene
TMCS trimethylchlorosilane
TMOS tetramethyl orthosilicate
TMSI trimethylsilylimidazole
TMS trimethylsilane
TON turnover number
TS titanium silicalite
TTAB tetradecyltrimethylammonium bromide
TUD-X Technical University Delft mesoporous materials series
TVCS trivinylchlorosilane
VPI a zeolite framework type
VPO vanadyl pyrophosphate
XRD X-ray diffraction

1. INTRODUCTION

Since their discovery in the early 1990s *(1–3)*, ordered mesoporous materials (OMMs) have become one of the most widely investigated classes of materials for catalysis—and also for other applications, as documented by a large number of review papers *(4–37)*. This development is a consequence of both the potentially useful practical properties, such as extremely high surface areas, high pore volumes, narrow pore size distributions, and ordered pore systems, as well as of the intellectual fascination of these materials, and the opportunities they offer for rational design via templating by supramolecular aggregates and, more recently, ordered mesoporous solids themselves. Figure 2.1 is a summary of the exceptional structural and textural properties that characterize OMMs, as exemplified by MCM-41, and the most frequently used techniques to measure these properties, such as X-ray diffraction (XRD), N_2 adsorption, transmission electron microscopy (TEM), and scanning electron microscopy (SEM).
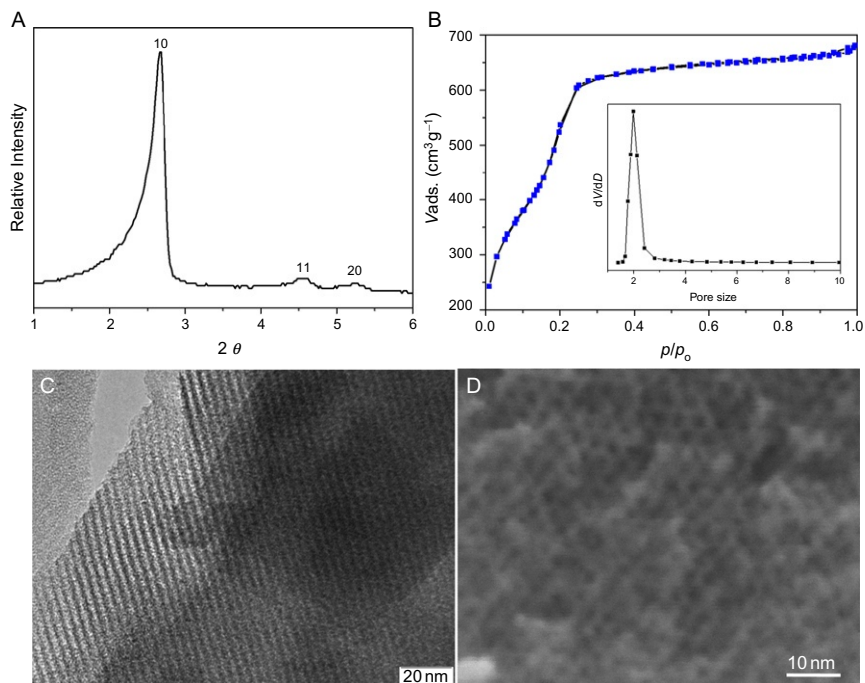
Figure 2.1 Low-angle XRD pattern (A), N₂ sorption isotherms and pore size distribution (B), TEM (c) and SEM images (D) of ordered mesoporous MCM-41 silica. The low-angle XRD pattern shows the (10), (11), and (20) reflections associated with the *p6mm* hexagonal symmetry. N₂ sorption isotherms show three well-defined stages: monolayer–multilayer adsorption on pore walls, reversible capillary condensation, and multilayer adsorption on the external surface. The isotherm is a typical type IV isotherm (for mesoporous materials). MCM-41 has a Brunauer–Emmett–Teller (BET) surface area of approximately $1500 \text{ m}^2 \text{ g}^{-1}$, a pore volume of $0.920 \text{ cm}^3 \text{ g}^{-1}$ and a pore diameter of 2 nm (Figure B, inset). The TEM image shows the regular hexagonal array of uniform channels of MCM-41 in a 2D projection, whereas the SEM image presents the ordered channel structure extending to the surface of the material.

With respect to catalytic applications of ordered mesoporous solids, the scientific community—specifically the zeolite community in which these materials were discovered—directed the early years of research toward applications that would be typical of zeolites, such as acid–catalyzed reactions and epoxidations on framework-substituted materials. One can speculate whether the research would have evolved with a different emphasis if these materials had been discovered, for instance, by the sol–gel community, or in another scientific subfield. The history of the discovery cannot be changed, but by now it seems clear that the domain of applications of ordered mesoporous solids in catalysis will differ from that of zeolites.

One reason for the difference is that one of the most distinctive properties of zeolites, the shape selectivity that results from their crystallographically defined pore system, will probably be exhibited only in exceptional cases by OMMs, even though their pore size distributions are almost as narrow as those of zeolites if one accounts for the thermal motion of atoms in zeolites under typical catalytic conditions. The pore sizes of OMMs are of the order of several nanometers and, on this scale, shape selectivity cannot be expected. If molecules reach a size of several nanometers, they typically have a high number of degrees of freedom and there exist many different conformers with similar energies but different molecular dimensions. This variability in size precludes a discrete cutoff between pores in which a molecule will fit and those in which it will not fit, as is characteristic of zeolites. Thus, shape selectivity will not be observed under most circumstances.

However, ordered mesoporous solids provide other characteristics that can make them unique in specific catalytic applications. This chapter is focused on properties that distinguish ordered mesoporous solids from more conventional catalytic materials, with examples chosen to show how such properties have been exploited. In many cases, the specific advantages and effects of the mesostructure are not evident from the published data, and consequently these reports are not addressed here. This issue is particularly a concern with respect to the patent literature, because in patents it is often not obvious why a particular material would be advantageous in a given application. Our focus in this chapter implies that it is not a comprehensive account of catalysis by OMMs—the literature of these materials is already so vast that it would be impossible to cover it completely in a single chapter (the search terms ("MCM-41" and *catal**) alone gave more than 5000 hits in Web of Science at the time of writing of this manuscript). We attempt to direct the reader towards those catalytic applications in which OMMs have an advantage that offsets the higher costs typically associated with their use; the chapter is not organized along the lines of reaction classes or materials classes that have been typical of reviews of OMMs in catalysis. For a more comprehensive coverage of the ever-growing literature of this topic, the reader is referred to several review papers, which partly cover the patent literature (4) and which for the most part are organized with respect to reaction classes (14,15,17,18,21,38–40).

2. COMPARISON WITH OTHER POROUS MATERIALS

Although the discovery of OMMs, as discussed above, has opened a new dimension in the science of porous solids, one should keep in mind that there are quite a few competing materials that can be equally well employed

in specific processes. The competing materials are briefly discussed in the following section, and their specific advantages and disadvantages are highlighted. The materials and their properties are summarized in Table 2.1.

2.1. Zeolites

Zeolites were initially perceived as the closest relatives of ordered meso-porous solids, especially of ordered mesoporous silicas and alumosilicates. However, it has now become clear that OMMs have at least as much in common with xerogels as with zeolites. Zeolites have clear advantages over ordered mesoporous solids. As a consequence of their crystalline nature, their pore systems are extremely well ordered, and their pore size distributions are very narrow. However, the most important advantages of zeolites with re-spect to catalytic applications are their strongly acidic sites *(41)*, in combina-tion with the rather high hydrothermal stabilities of high-silica zeolites (or stabilized zeolites such as ultrastable zeolite Y) *(42)*. Moreover, for large-scale applications, catalyst costs are important. Although it is difficult to judge how expensive OMMs would be if produced on the same scale as zeolites, it is probable that they would be substantially more expensive than commodity zeolites, which sell at prices on the order of $1 \, \text{€} \, \text{kg}^{-1}$. Specialty zeolites synthesized with the help of organic templates, however, have prices in the same range as those anticipated for ordered mesoporous silica and alumosilicates.

One essential feature of mesoporous materials, however, is not attained in the currently available zeolites (and it is difficult to implement): The upper pore size limit for the more thermally stable zeolites is about 0.8 nm (which is characteristic of Y-type zeolites). Less stable materials, such as VPI-5, have pore sizes of 1.3 nm *(43)*; and in recent years, zeolitic materials, especially germanium-containing forms, have been synthesized that make even the mesopore size range accessible *(44)*. However, for most catalytic applica-tions, the thermal stabilities of the mesoporous varieties of zeolite are not sufficient. Therefore, the pore size range substantially exceeding 1 nm, which is interesting for reactions that are not possible at all or significantly mass transfer-limited in zeolites, can be accessed only with OMMs. An example is the conversion of higher molecular weight hydrocarbons.

Fabrication of nanosized particles of zeolites *(45–51)* and hierarchical zeolites with mesoporosity is valuable for the combination of shape selectivity and efficient mass transfer in catalysis. Considerable efforts have been devoted to manufacture mesoporous zeolites by using strategies such as post-synthesis hydrothermal dealumination *(52,53)*, desilication *(54–56)*, recrystallization of the zeolite *(57)*, and assembly of zeolite nanocrystals

Table 2.1 Properties, including advantages and disadvantages, of materials that compete with OMMs

Class of material/ property	Pore size	Uniform porosity	Surface area	Permeability	Thermal stability	Chemical stability	Compositional flexibility	Usage as hard template	Costs
Zeolites	Micro	Very high	High	Low	High	High	Low	Low	Low to medium
Xerogels and aerogels	Meso–macro	Low	Medium	High	Medium	High	Very high	Medium	Low
Metal-organic frameworks	Micro–meso	Very high	Very high	Medium	Medium	Low	High	–	Medium to high
Anodic aluminas	Meso–macro	High	Low	High	Very high	High	Low	Medium	High
OMMs	Micro–meso	High	High	High	High	High	Very high	High	High

(58). The post-treatments result in a decrease of zeolite crystallinity that could affect catalytic properties in many reactions. These treatments also lead to the formation of amorphous alumosilicate fragments inside the meso-pores, which have a negative effect on mass transfer *(59)*. A strategy chosen by Corma *et al.* *(60)* proved to be successful; they reported the preparation of the first member of a family of delaminated zeolites by swelling and exfoli-ating of MCM-22. The material, ITQ-2, has a layered structure made up of sheets with a thickness of ca. 2.5 nm and is characterized by a high external surface area (700 $m^2 g^{-1}$). The catalytic results obtained with these zeolites indicate that the delamination process improves the accessibility of the cat-alytic sites for the reactant without affecting their activity *(61)*.

Alternatively, mesoporosity has been created by synthesis routes involv-ing templates such as carbon black *(62–65)*, carbon nanotubes *(66)*, carbon aerogel *(67, 68)*, monodisperse polystyrene spheres *(69)*, and ordered meso-porous carbon *(70–72)*. The synthesis of hierarchically structured zeolites by confined growth in hard templates is a promising approach for creating or-dered mesoporous structures and controlling mesopore sizes with precisions unachievable by other procedures. In principle, the desired mesopore struc-ture can be produced by manipulating the structure of the hard template *(73, 74)*. However, production costs and the difficulty of large-scale synthesis are still important issues.

Recently, Ryoo and coworkers *(75)* elegantly used the amphiphilic organosilane $[(CH_3O)_3SiC_3H_6N(CH_3)_2C_nH_{2n+1}]Cl$ as a mesopore-directing agent to prepare mesoporous zeolites and aluminum phosphates. Mordenite framework inverted (MFI) zeolite with a mesoporous–microporous hierarchi-cal structure could be prepared with various Si/Al ratios above 14. The ^{27}Al NMR spectra contained a single signal around 57–65 ppm, corresponding to tetrahedral Al sites in crystalline zeolite. No signals attributed to extra-framework Al (octahedral coordination, 0–10 ppm) were observed. The mesopore diameters can be easily controlled in the range of 2–20 nm by changing the molecular structure of the mesopore-directing silanes and the hydrothermal synthesis conditions *(76)*. In catalytic conversion of bulky molecules, such as protection of benzaldehyde with pentaerythritol, condensation of benzaldehyde with 2-hydroxyacetophenone, esterification of benzylalcohol with hexanoic acid, and cracking of branched polyethylene, catalytic activities of mesoporous MFI zeolite prepared by this method were very high in comparison with those of conventional MFI zeolite *(77)*, because of the reduced mass transfer influence.

Another breakthrough was reported by the same research group, namely, the synthesis of 2D MFI zeolite nanosheets by use of a di-quaternary
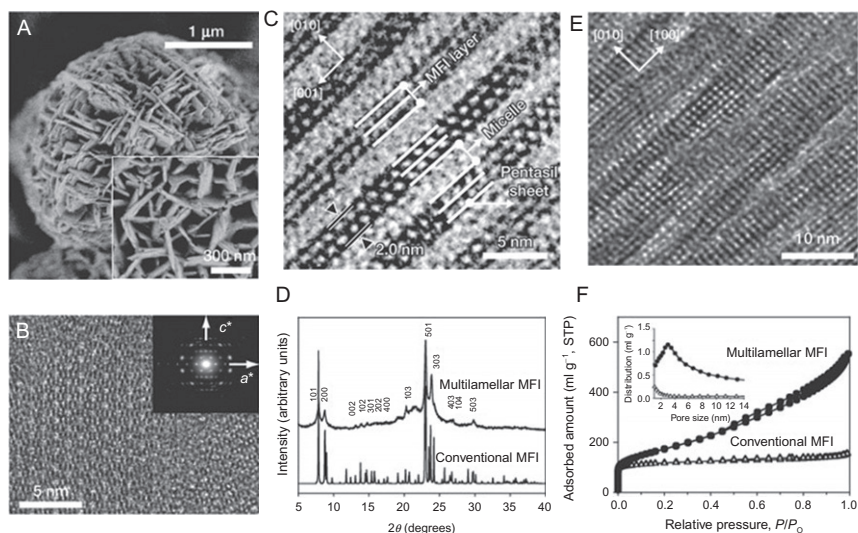
Figure 2.2 As-synthesized MFI nanosheets (A–D); and calcined sample (E, F). (A) SEM image showing that the MFI zeolite has a plate-like morphology with the plates packed and intergrown in three dimensions. (B) TEM and electron diffraction of the basal plane of the plate ([010] incidence of MFI). (C) TEM cross section of the plate showing that each plate is composed of a lamellar stacking of alternating layers of MFI (2 nm) and surfactant micelles (2.8 nm). The MFI layer consists of three pentasil sheets, corresponding to the thickness of a single unit cell along the *b*-axis, with $b = 1.9738$ nm. (D) Powder XRD pattern with only the *h0l* reflections being sufficiently sharp for indexing. The result confirms that the zeolite possesses extended *a*–*c* planes with large coherent domains, while the framework thickness along the *b*-axis is extremely small. (E) TEM image of calcined sample indicating that calcination leads to partial condensation of MFI layers, while the interlayer space (mesoporosity) is still mainly intact. (F) N_2 adsorption–desorption isotherm also confirming the highly mesoporous structure of the calcined sample, with a BET surface area of 520 m^2 g^{-1} *(78)*. *Adapted with permission from Nature Publishing Group.*

ammonium surfactant (Figure 2.2) *(78, 79)*. The catalytic performance of the MFI nanosheets was investigated with large organic molecules as reactants (i.e., cracking of branched polyethylene) so that diffusion of the reactant molecules slows up the reaction. The catalytic activities (normalized to catalyst weight) of the MFI nanosheets were found to be much higher than those of a conventional MFI zeolite, reflecting the transport limitation. Thus, the enhancement in rate was attributed to the large number of acid sites located at the mesopore surface.

The same group also synthesized crystalline mesoporous molecular sieves (MMSs) by using a Gemini-type polyquaternary ammonium surfactant as a soft template; Gemini-type implies that two conventional surfactant molecules are chemically bonded together by a spacer close to the headgroups.

In these MMSs, the mesopores are surrounded by zeolite-like walls, which consist of microporous crystalline alumosilicate frameworks *(80)*. It was established that the crystalline MMSs are promising as acid catalysts for various organic reactions involving bulky molecules, because their catalytic activity is much higher than those of bulk β–zeolite or Al-MCM-41. The superior performance of the MMSs was attributed not just to the facile diffusion of reactants through the mesopores but also to the strong acidity of their crystalline zeolite frameworks.

2.2. Xerogels and aerogels

Xerogels and aerogels can be described as dried gels that retain—at least in part—their porous texture after the drying *(81,82)*. The attractive properties of such porous gels arise from the extraordinary flexibility of the sol–gel processing, which can be combined with various drying techniques that lead to aerogels (supercritical drying) or xerogels (ambient drying) (Figure 2.3). Moreover, gels can be directly synthesized in the desired shape. Xerogels *(83)* and aerogels *(81,84,85)* are probably the closest relatives of OMMs. Their structures and morphologies can be easily controlled in the synthesis and drying process *(86,87)*. Xero- and aerogels have the same kind of disorder in the wall structure as OMMs; they can be synthesized with approximately the same range of compositions; and they have high porosities *(88,89)*. The porosities can, in
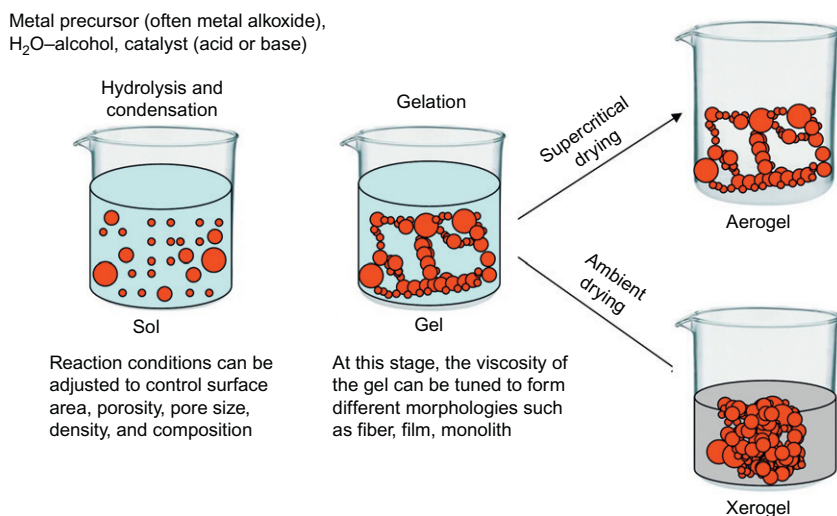

Figure 2.3 Schematic illustration of the steps in the preparation of aerogels and xerogels.

the case of aerogels, reach extreme values, far exceeding those achieved with OMMs. For silica aerogels, porosities exceeding 99% have been reported *(84)*.

Furthermore, some of the xerogels are relatively inexpensive; for example, silica gels sell at approximately the prices of commodity zeolites. In contrast to OMMs, the dried gels typically have relatively broad pore size distributions, and unless they are synthesized as aerogels by supercritical drying, their specific surface areas can often not compete with those of OMMs. Nonetheless, for many of the catalytic applications that are reported for OMMs, xerogels of appropriate composition would probably be equally well suited, unless the application exploits one of the specific advantages of ordered mesoporous solids, such as their concave surface curvature. The curvature distinguishes OMMs from typical gels, which have a predominantly convex surface curvature.

2.3. Metal-organic frameworks

Metal–organic frameworks (MOFs) have expanded the pore sizes of crystalline materials substantially, as discussed in detail in recent reviews *(90–93)*. The term "metal–organic framework" was coined by Yaghi *(94–105)*, who reported some impressive examples. Other researchers have also contributed substantially to the development of this field *(106–114)*. A series of MOF structures is presented in Figure 2.4. Like zeolites, MOFs are characterized by a crystalline arrangement of the atoms comprising the walls. The pore sizes and void volumes of MOFs can be substantially larger than those of zeolites and now extend well into the pore size range associated with OMMs. If solely the pore sizes and pore connectivities are considered, then MOFs are viable alternatives to OMMs with smaller pore sizes, in particular because the synthesis has been successfully scaled up so that bulk quantities of some types of MOF are available at a modest cost *(115,116)*. However, although MOFs are often thermally more stable than expected from their compositions, they still fall short of many OMMs in this respect. Moreover, the chemical stability of MOFs is often lower than that of oxidic OMMs. When surface chemistry and functionality become important, MOFs and OMMs do not compete, but rather complement each other. Although the surfaces of OMMs are in most cases oxidic (if they are not modified by organic groups), the major part of the surface of a MOF is made up of organic molecules, which are linked via metal cations or clusters of metal ions.

2.4. Anodic aluminas

As far as texture and pore structure are concerned, anodic aluminas *(117,118)* come very close to hexagonally OMMs, such as MCM-41 or SBA-15. Anodic aluminas are synthesized by anodic oxidation of metallic
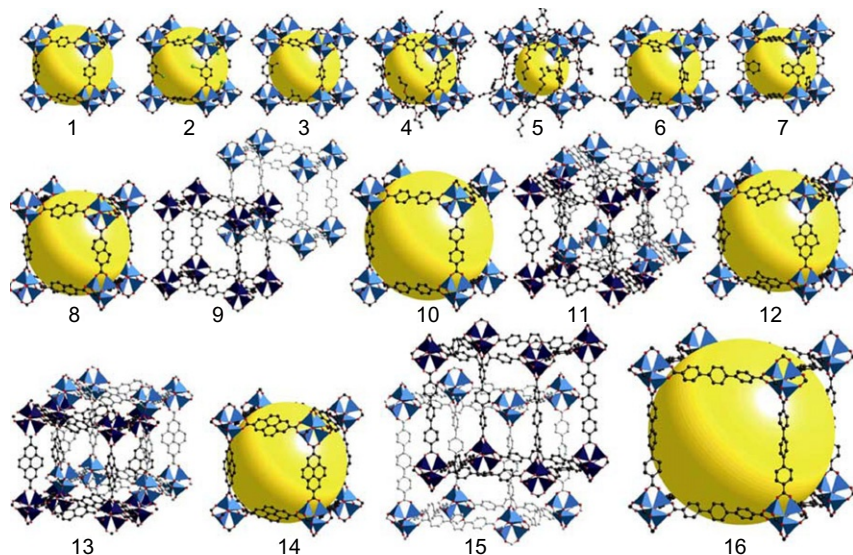
Figure 2.4 A series of 16 isoreticular metal-organic frameworks (IRMOFs); per definition the series comprises materials with the same framework topology (cubic in this case). Each member of the series is prepared by using the appropriate organic linker under solvothermal conditions established for formation of the octahedral secondary building unit (SBU). The linkers differ both in functionality of the pendant groups (IRMOF-1 to -7) and in length (IRMOF-8 to -16). Expanding the length of the linkers can enlarge the internal void space (represented by yellow spheres), but it may also lead to the formation of so-called catenated phases, in which two or more identical frameworks are intergrown (IRMOF-9, -11, -13 and-15) *(100)*. *Adapted with permission from Elsevier.*

aluminum *(119)*. Under some preparation conditions, depending on the current densities and electrolytes, an oxide layer forms that is patterned like a honeycomb. The layer is composed of tubes that are arranged in a hexagonal packing, and the structure of the material strongly resembles the motifs found in MCM–41 or SBA–15 *(120)*. The pore sizes in anodic aluminas overlap the larger pore sizes of OMMs; that is, pore sizes as small as about 7 nm are possible. With respect to an upper limit, anodic aluminas are more flexible than OMMs, and pores with diameters larger than 50 nm can be created. In general, the walls of anodic aluminas are thicker than those of OMMs, and, consequently, porosities and specific surface areas are lower.

In addition to having pore systems that are of similar regularity as those in OMMs, anodic aluminas can be easily synthesized in the form of membranes, that is, with pores oriented in a regular fashion in relation to the macroscopic dimensions of the sample (Figure 2.5). Such membranes, albeit
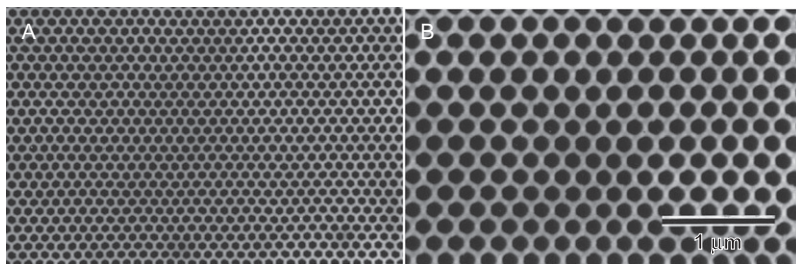
Figure 2.5 SEM images of anodic aluminas with 100 (A) and 200 nm (B) pore diameter. Anodization was conducted in 0.3 M oxalic acid at a temperature of 17 °C to give material (A) or 0.04 M oxalic acid at a temperature of 3 °C to give material (B) *(117)*. *Adapted with permission from American Institute of Physics.*

with a lower degree of order, are commercially available, as the so-called Anodisc filters supplied by Whatman plc. However, the fact that they are typically obtained as films or membranes is probably also the limiting factor in the application of these materials. Because a regular arrangement is obtained only on flat surfaces of aluminum, mass production is difficult, and large quantities, as needed for bulk chemical processing, are not available. Furthermore, the composition is essentially restricted to alumina—a severe limitation, even though alumina is one of the key constituents in many catalysts. In any case, for fundamental studies anodic aluminas may often be more suitable or at least a viable alternative to OMMs.

3. HISTORY AND MATERIALS CHEMISTRY OF OMMs

The first OMMs that were reported consisted mainly of silica. The composition goes back to the original plans of the research groups that discovered OMMs. Kuroda's group *(1)* had attempted to intercalate surfactants into a sheet silicate, whereas the Mobil group *(2,3)* had attempted to produce delaminated layer-structure zeolites by using surfactants. In both cases, the discovery of the ordered mesostructured materials was serendipitous rather than planned.

After finding the first indications of the mesostructure, the researchers optimized the syntheses. The essential ingredients of these initial recipes were a silicon source, a surfactant, and a base, all together in an aqueous solution. Later, various other pathways to form such materials were discovered, which are discussed below. The materials chemistry in the first follow-up publications after the initial discovery was also restricted to the silica basis. Substitution of tetrahedral atoms by titanium, a well-known compositional variant in zeolite chemistry, was soon transferred successfully to OMMs *(121–124)*. Relatively early it became clear that it should be possible to create other framework

compositions *(122)*, and the first success was achieved in 1994 *(125,126)*. In these cases, however, the surfactant template could not be removed.

After the first successful syntheses of porous non–silica materials in the mid–1990s *(127,128)*, the range of compositions was expanded dramatically, in parallel with an increase in the variety of structure types that were synthesized. These developments are covered in reviews *(5,9,12,15–17,19,20,22,24,29,37,39,74,129)*, and only the major developments are highlighted here to facilitate access to the primary literature. Figure 2.6 shows a family tree of OMMs, which traces the major development lines and which serves as a guideline to the following discussion. The tree is rooted in sol–gel science, surfactant chemistry, and zeolite chemistry. At the bottom of the tree are represented two independent developments in the preparation of OMMs. The group of Kuroda *(1)* discovered the folded sheet materials (FSMs), which are obtained by intercalation of
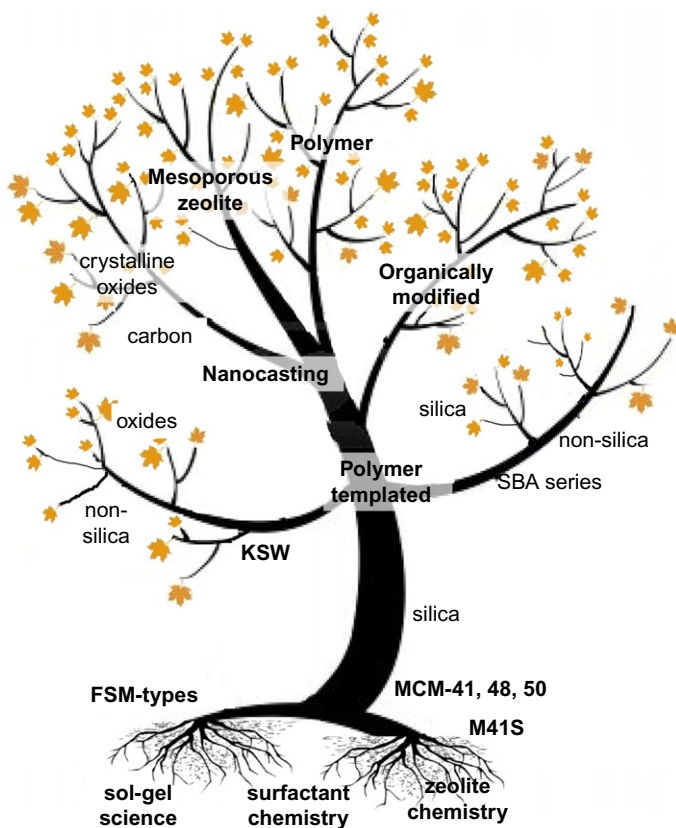

Figure 2.6 Family tree of OMMs.

alkylammonium surfactants such as cetyltrimethylammonium (CTA) into sheet silicates, preferably kanemite. Aging at elevated temperatures then leads to the formation of ordered mesostructured materials that can be converted to porous materials by condensation. Although the similarity between the MCM-41 and the FSM-type or KSW-1 type materials is striking, subtle differences do exist, as was shown in several comparative investigations (130,131).

A more broadly applicable synthesis pathway was independently developed by scientists of the Mobil Oil Corporation (2,3), simultaneous with the work of the Kuroda group. This pathway starts with molecular silicon sources, such as tetraethoxysilane or sodium silicate, or amorphous silica, such as Aerosil®, which are hydrolyzed in the presence of surfactants similar to those used by Kuroda. Condensation of the hydrolysis products in the presence of the surfactant leads to the formation of the ordered mesostructure. This approach evolved from a discovery program conducted within Mobil Oil Corporation to create delaminated zeolitic materials by stabilizing the layers that were formed as intermediates with intercalated guest molecules, such as the surfactants that were used. A good account of the history of the discovery is available (132).

Even in these early investigations it was recognized that the silicas that were obtained had remarkable similarities to known lyotropic phases of surfactants. Therefore, a general mechanism was formulated that involved structure direction by a liquid crystal-like template, possibly assisted by the presence of the silicate species (2,3). This mechanism was subsequently transferred to a variety of syntheses using a range of conditions and various solution species (i.e., surfactants and oxide precursors) (122,126,132–134). Although variants have been discussed, the so-called cooperative assembly mechanism is now the most widely accepted mechanism for the synthesis of OMMs from dissolved molecular precursors under the influence of surfactants.

There has been relatively little development in the field of FSMs (lower left branch in Figure 2.6). Some novel materials were synthesized following the early discoveries (135–137), including the remarkable KSW-2, which consists of a packing of channels with an almost square cross section (137). The properties of the FSMs were analyzed in detail, and the differences from other materials have been highlighted (130,131). The synthesis pathway is rather limited in scope because of the restriction to kanemite and closely related sheet silicates as raw materials (135); moreover, the ordered materials only form within a rather narrow range of synthetic conditions, and thus the properties of the resulting solids can only be controlled within rather narrow

margins. Hence, most researchers in the field of OMMs focused on the M41S class and subsequent developments.

The M41S class of materials (comprising initially the hexagonal MCM-41, the cubic MCM-48, and the lamellar MCM-50) triggered most of the excitement in this research area in the early 1990s. Soon after the initial discovery, other molecular surfactants were explored, which allowed the synthesis of materials with structures different from those of the M41S class *(138,139)*. Very helpful in this context was the concept of the surfactant packing parameter, which had originally been developed to describe the formation of micellar structures in dilute solutions *(140)*. On the basis of geometric arguments, the packing parameter allows the prediction of the type of structure formed with a specific surfactant. After formulation of a more detailed synthesis mechanism of the M41S-type materials *(122)*, it became obvious that non-silica materials should also be accessible through this process.

The first such materials were unstable and could be obtained only in a mesostructured form (and not in a mesoporous form) *(125,126)*. In the first years, replacement of a small fraction of the silicon with aluminum *(2,3)* or titanium *(121–124)* was the maximum deviation from silica that was synthetically attainable. However, only a couple of years later, the first mesoporous non-silica materials, notably the stable first-row transition metal oxides and oxophosphates, were reported *(127,128)*. Various structures and framework compositions are now accessible via this synthesis pathway, as described in numerous reviews *(22,31,40,141,142)*.

The next major advance that led to new classes of materials was the use of neutral, mostly polymeric surfactants. Pinnavaia's group *(143–146)* was the first to use this approach, and several types of mesoporous silica (HMS, MSU-V, MSU-X) were synthesized, which, however, for the most part had more disordered structures than the M41S materials. Attard *et al.* *(147)* used these new surfactants at such high concentrations that lyotropic liquid crystals assembled. The oxides then formed in the aqueous parts of the liquid crystal—that is, a true liquid crystal-templating was realized. Probably the most significant breakthrough in the use of polymeric surfactants was achieved in the groups of Stucky and Chmelka *(148)* with the discovery that triblockcopolymers of the polyethylene oxide–polypropylene oxide–polyethylene oxide (EO–PO–EO) type can be used to synthesize a wide variety of structures with a drastically expanded range of pore sizes. Shortly afterwards, this synthesis was extended to non-silica materials *(149,150)*.

Today, these types of materials, the most prominent one being SBA-15, are moving more and more into the focus of attention as a result of their favorable properties, such as stability and tunability. In particular, the large pore

sizes that are accessible with the triblock copolymer surfactants—in combination with the possibility to create 3D pore networks (as in SBA-16)—are highly attractive *(151–153)*. By use of this triblock copolymer strategy, several types of silica with various morphologies and symmetries such as the FDU (Fudan University) *(154–158)* and KIT (Korea Advanced Institute of Science and Technology) *(159–162)* series were obtained.

Organosilicas are drawn as a separate limb of the family tree (Figure 2.6), although they could also be subsumed under the non-silica materials. These materials are characterized by organic groups that are pendant on the surface of the framework or are incorporated as integral parts of the frameworks, as summarized in several comprehensive reviews *(11,34,36,163–166)*. Although organosilicas are often synthesized by modified versions of the pathways discussed above, they are considered a separate class of materials because of the organic groups, which provide considerable additional flexibility with respect to further alteration. Notable are organosilicas that are synthesized by the hydrolysis and condensation of α,ω-bis(trialkoxysilyl) hydrocarbons *(167–169)*. As hydrocarbon groups, alkyls, alkenyls, or aryls have been used.

During synthesis, the frameworks of these mesostructured materials are assembled in a particular fashion; all silicon atoms have three siloxane bonds to other silicon atoms and one Si—C bond to the bridging hydrocarbon. By using phenylene groups as the bridges, Inagaki *et al. (170)* succeeded for the first time in creating an ordered wall structure. Further functionalization of the organic moieties in the walls, such as sulfonation *(170)*, opens up the possibilities for the synthesis of tailored catalytic materials.

Another limb in the family tree of OMMs includes the nanocasted materials. The nanocasting pathway, which is also referred to as hard templating, was developed by Ryoo *et al. (171)* as an alternative route to cooperative surfactant templating in solution. This strategy is covered in many reviews *(24,73,74,172–177)* and in a book *(178)*. Nanocasting is a highly effective method to fabricate materials that are difficult to synthesize by conventional pathways. A general method for the preparation of ordered nanostructured materials (which may consist of carbon or a metal oxide) is shown in Figure 2.7. Ordered mesostructured materials can be prepared in a three-step procedure. First, a hard (silica) template is synthesized. In the second step, the template is impregnated with a suitable precursor (an organic compound or a metal salt), followed by a thermal treatment under an inert atmosphere or in air. Finally, the mesoporous carbon or metal oxide product is obtained by removal of the silica with dilute HF or NaOH.

The first example of an OMM prepared by the nanocasting process was an ordered mesoporous carbon molecular sieve named CMK-1, which was
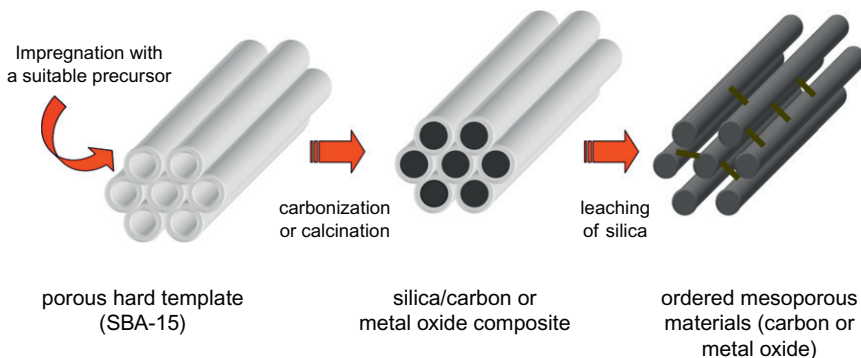
Figure 2.7 General synthesis strategy for the preparation of ordered porous materials via nanocasting *(179)*.

obtained by the use of a silica molecular sieve, MCM-48, as a hard template *(171)*. Sucrose was converted to carbon inside the mesopores of MCM-48 in a mild carbonization process with sulfuric acid as a catalyst. The carbon molecular sieves were then obtained by removal of the silica framework with an aqueous solution of sodium hydroxide. The same group reported hexagonal ordered mesoporous CMK-3 and CMK-5, which were produced by using furfuryl alcohol as carbon precursor and hexagonally ordered mesoporous silica SBA-15 as a hard template *(180)*. CMK-3 has a monomodal pore size distribution, whereas CMK-5 type carbon has a bimodal pore size distribution.

Independent of these findings, the replication of hexagonal mesoporous silica (HMS)-type materials was described *(181)*. A predecessor of the nanocasting procedures was an attempt to replicate the pore structures of zeolites in carbon materials *(182)*. The replication of small parts of the pore systems of ordered mesoporous silicas with noble metals to visualize the connectivity of the pore system is also related to these topics *(183)*.

The nanocasting routes were initially found to be applicable only to the synthesis of carbon mesostructures. Later, the back replication of ordered porous carbons as silica was demonstrated as well *(184, 185)*. In these cases, the carbon mold was removed by combustion. Following this example, several crystalline OMMs including MgO *(186–188)*, boron nitride *(189, 190)*, γ-Al$_2$O$_3$ *(191, 192)*, aluminosilicate *(70, 193)*, CuO *(194)*, ZnO *(195–197)*, Ga$_2$O$_3$, and GaN *(198)* were prepared by using ordered mesoporous carbon as a hard template.

The direct replication of silica to yield nanocasted oxides has also been extensively investigated, and materials with a variety of compositions and morphologies have been reported *(199–221)*. Adjusting the surface

chemistry of the silica precursor can help in achieving successful replication. The surface chemistry has been altered by surface functionalization *(201,222)* or microwave digestion of the silica mold *(199,200)*. Because the nanocasting pathways do not require a specific solution chemistry of the precursors and surfactants, it can be expected that it will become possible to prepare framework compositions that are not accessible by methods relying on surfactants. However, the nanocasting method is limited to precursors that do not react with the silica template and to compounds that can be prepared within the temperature range imposed by the structural stability of the silica template.

Because control of the oxidation states in metal centers is complicated, it is a challenge to fabricate ordered mesoporous metal oxides with metals in lower oxidation states directly by the use of the nanocasting route. One possibility for producing ordered mesostructured metal oxides with metals in lower oxidation states is to reduce other ordered mesoporous metal oxides. The synthesis of cubic ordered mesoporous Fe_3O_4 by reduction of α-Fe_2O_3 with H_2 as a reducing agent was reported by Bruce and coworkers *(223)*. The same group also described the synthesis of Mn_3O_4; the key steps were the preparation of ordered mesoporous Mn_2O_3 and the subsequent reduction to Mn_3O_4 with H_2 as a reducing agent *(224)*. The conversion of mesoporous MnO_2, CuO, and Co_3O_4 to the corresponding oxide structures with the metals in lower oxidation states was demonstrated recently; the reduction was conducted in flowing H_2 diluted with argon (with a molar ratio of 5:95) *(225)*. Shi *et al*. *(211)* prepared ordered mesoporous MoO_2 by using phosphomolybdic acid as a precursor and mesoporous silica KIT–6 as a hard template in an atmosphere of 10% H_2 in argon. The pseudomorphic conversion of ordered mesoporous Co_3O_4 and $5Fe_2O_3 \cdot 9H_2O$ (ferrihydrite) into CoO and Fe_3O_4, respectively, by high-temperature treatment in an alcohol−steam mixture was reported *(226,227)*. In addition to the simple metal oxides, some crystalline spinel–type mixed oxides such as $CoFe_2O_4$ *(228)*, $Co_3O_4/CoFe_2O_4$ *(229)*, $NiFe_2O_4$ *(230)*, and $CuFe_2O_4$ *(231)* were fabricated by nanocasting.

It is even possible to prepare metal nitride and metal sulfide structures by hard or soft templating. Two ammonia nitridation routes were demonstrated by Shi *et al*. *(232)*, who produced CoN and CrN. The first route was direct nitridation (at temperatures of 275–350 °C), which was applied to a mesoporous Co_3O_4 that was a replica of SBA-15 silica obtained by the nanocasting method. The second route, which consists of two steps, was used to synthesize ordered mesoporous CrN nanowire arrays. First, a chromium oxide/silica nanocomposite reacted with ammonia at high

temperatures (750–1000 °C) to form a CrN/silica nanocomposite. Then the silica hard template was eliminated and a self-supporting ordered mesoporous CrN replica was obtained *(232)*.

Braun *et al.* *(233)* were the first to report the synthesis of ordered mesostructured CdS. These materials, which were characterized by a 2D-hexagonal structure, were produced via the precipitation reaction route using the surfactant oligoethylene oxide oleyl ether $[C_nH_{2n+1}(OCH_2CH_2)_m$—$OH]$ as a soft template. CdS was precipitated by flowing H_2S gas over a hexagonally patterned liquid crystal solution that was made of the surfactant and cadmium diacetate or cadmium chloride. By using various templates, the authors produced CdS/surfactant nanocomposites with a lamellar mesophase *(234,235)*. The synthesis of ordered mesostructured ZnS and $Cd_{0.5}Zn_{0.5}S$ was achieved by replacing the cadmium salt by other metal salts *(236)*. Ordered mesostructured CuS was obtained by the cation exchange method using the nanocast CdS as a precursor *(237)*. Shi *et al.* *(238)* demonstrated an atmosphere–assisted high-temperature reductive sulfuration method for the preparation of ordered mesoporous metal sulfides. Highly ordered mesoporous WS_2 and MoS_2 with 2D hexagonal and 3D cubic double gyroid (i.e., a specific infinitely linked, triply periodic minimal surface with space group *Ia3d*) mesostructures were synthesized by using the silicas SBA-15 and KIT-6 as hard templates, phosphotungstic acid (PTA) and phosphomolybdic acid (PMA) as tungsten and molybdenum precursors, and a gas mixture of H_2S and H_2 as a sulfur source. A series of ordered mesoporous metal fluorides including LaF_3, CeF_3, PrF_3, NdF_3, EuF_3, TbF_3, FeF_3, and MnF_2 was also reported; the corresponding metal trifluoroacetates served as precursors in the synthesis *(239)*.

Another breakthrough in the development of ordered mesoporous solids was reported by Liang *et al.* *(240)* and Meng *et al.* *(241,242)*, who synthesized highly ordered mesoporous polymers and carbon frameworks in film and powder forms—these constitute another attractive branch of the tree of OMMs (Figure 2.6). The synthesis involved an organic–organic assembly of triblock copolymers with soluble, low-molecular-weight phenolic resin precursors (resols) that could be produced by an evaporation-induced self-assembly strategy. The family members include mesostructures with lamellar, 2D hexagonal, 3D bicontinuous, and body-centered cubic symmetries, which were obtained by simply varying the phenol/template ratio and the PEO/PPO ratio in the soft template (Figure 2.8). It was hypothesized that the resols favor interaction with hydrophilic PEO blocks in the copolymers; this behavior affects the hydrophilic/hydrophobic ratio in the resol–surfactant mesophase, and in turn the interfacial curvature that is
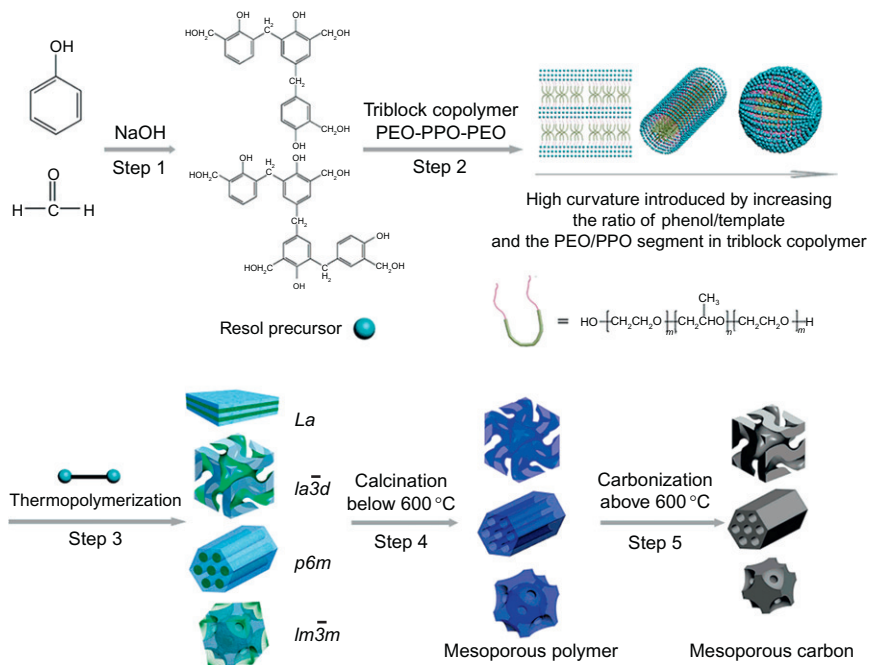
Figure 2.8 Schematic representation of the synthesis of ordered mesoporous polymer resins and carbon frameworks *(241)*. *Adapted with permission from the American Chemical Society.*

responsible for the shape of the micelles that form. The driving force for the organic–organic assembly was attributed to the preferential evaporation of ethanol—used to dissolve the triblock copolymer and the resol precursor—from the ethanol–water solvent mixture. This change in composition induces the organization of the resol–template liquid-crystalline mesophase.

One of the recent developments in the design of OMMs is the preparation of mesoporous crystalline hierarchical zeolite materials *(78)*, which find a place at the top of the tree shown in Figure 2.6.

The preceding discussion shows that various synthetic routes can be used to produce a multitude of framework compositions. It is possible to obtain OMMs in various morphologies. Standard synthesis procedures typically result in the formation of rather fine powders consisting of submicrometer-sized particles. Many catalytic applications require that such powders be compacted into shaped bodies, which is normally not a significant challenge, at least on the laboratory scale. Most OMMs are sufficiently rigid to withstand the pressures that are applied during typical processing conditions, although some loss of pore volume may occur at high pressure during pelletizing *(131,243–245)*. Desplantier-Giscard *et al. (246)* demonstrated

that the mechanical properties of ordered mesoporous silica with a hexagonal structure can be described by formalisms similar to those used to characterize macroscopic honeycomb structures, thus providing a rough guideline to assess mechanical properties.

If one does not want to utilize post-synthetic shaping procedures, which complicate and prolong the synthesis, then the morphologies desired for a catalytic application can be adjusted earlier, even during the formation of the material. A number of techniques are available, and the shapes that can be generated include spheres, hollow spheres *(247–253)*, thin films *(247,254–258)*, fibers *(259–263)*, and tubes *(264–266)*. Recent work on morphology control has focused on the creation of materials with hierarchical macro–mesoporous characteristics, which are often obtained in the form of monoliths *(69,267–271)*. Wang *et al.* *(272)* reported an alternative hard-templating strategy for the synthesis of ordered mesoporous platinum nanoparticles with shape and size control (Figure 2.9). Silica was used as a hard template, and ascorbic acid was employed as the reducing agent at room temperature. Such shape-controlled ordered mesoporous structures have potential for structure–sensitive catalytic reactions, if the shape control extends to the level of the platinum struts.

One of the general (and important) advantages associated with OMMs is the flexibility in the choice of the conditions to make them, in contrast to those needed to make other kinds of porous materials. This flexibility allows the manufacture of numerous porous materials with various compositions, pore topologies, and morphologies. Whereas the synthesis of zeolites is limited to relatively few elements (at least as framework constituents), to a limited number of templates, and to a rather narrow range of conditions, OMMs can be prepared from a large number of elements under a wide range
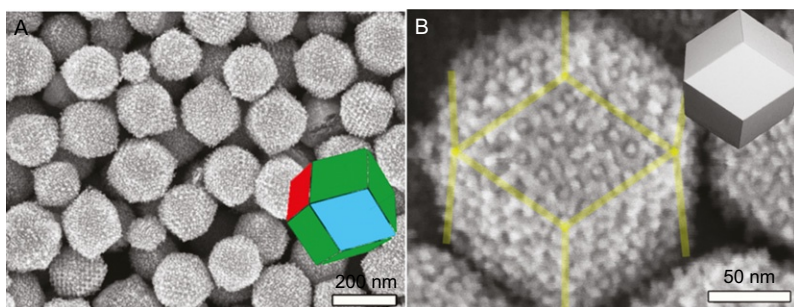

Figure 2.9 (A) Low- and (B) high-magnification SEM images of mesoporous platinum nanoparticles (meso-platinum) prepared with mesoporous silica KIT-6 *(272)*. *Adapted with permission from the American Chemical Society.*

of conditions—including acidic or basic conditions and the use of various cationic, anionic, and non-ionic surfactants with various alkyl chain lengths (and polymers) as soft templates. A given type of material can be synthesized by more than one route, although the resultant properties may not always be identical. By varying the length of the alkyl chains of the template, for example, the pore size of the OMMs can be tuned (in limited size ranges) without difficulty. Other reaction parameters also influence the pore size and can be adjusted for fine-tuning. Alternately, a swelling agent such as 1,3,5-trimethylbenzene (TMB) can be used during the synthesis to enlarge the pores. By adding TMB, the pore size of MCM-41 can be increased up to 10 nm and that of SBA-15 can be increased to 30 nm *(3,149)*. Moreover, the structure and thus the pore topology of an OMM can be changed from 1D lamellar, 2D hexagonal, or quadratic to one of a variety of 3D structures by choice of the synthesis parameters such as pH, temperature, type of surfactant, and composition of the precursor solution *(139,151,273)*. The flexibility of the synthesis allows the production of several types of OMMs with different textural parameters, pore sizes, and morphologies, and all of these properties can significantly affect the catalytic performance of the material *(274,275)*.

Another major advantage of the flexibility of the synthesis is the possibility of making materials in various forms, such as powders, monoliths, shaped bodies, or films. Catalysts in the form of thin films coated onto the surfaces of reactors or structures such as monoliths can be useful for minimizing mass and heat transfer resistance. When bulk silica is used at surfactant solution concentrations exceeding the critical micelle concentration, films of mesophases with hexagonally packed 1D channels can be formed at solid–liquid and liquid–vapor interfaces *(276,277)*. Yang *et al. (254)* reported the synthesis of thin films of ordered mesoporous silica on mica by the following strategy: First, an acidic aqueous solution of the surfactant was prepared. Then a silica source, tetraethyl orthosilicate (TEOS), was added, and the mixture was stirred at room temperature for a few minutes and then brought in contact with the mica substrate. Films of various thicknesses were formed at 80 °C over periods ranging from about an hour to a week. Ogawa *(278,279)* developed a rapid spin-coating procedure for preparation of transparent mesoporous films. Lu *et al. (280)* reported a sol–gel-based dip-coating method for the rapid synthesis of continuous mesoporous thin films on a solid substrate. The formation of mesoporous films of the cubic phase, in which the pores are connected in a 3D network that guarantees the accessibility of the pore space from the film surface, was also demonstrated. Zhao *et al. (255)* prepared continuous mesoporous silica films with

large periodic cage and pore structures by using triblock copolymers and poly-(ethylene oxide) non–ionic surfactants as the structure-directing agents in combination with dip–coating processing. Materials with either continuous channels or with ordered cage arrays were prepared. The films exhibited highly ordered and oriented large periodic mesostructures, and the synthesis could be tuned to give 3D cubic or hexagonal structures with variable pore sizes and porosities.

Non-siliceous materials can also be prepared in the form of thin films. Liang *et al.* *(240)* fabricated an ordered mesoporous carbon film by stepwise self-assembly of a phenolic resin and block copolymers. Grosso *et al.* *(257)* described a process that allows the synthesis of ordered mesoporous crystalline networks and mesostructured nano–island single layers consisting of multiple component metal oxides with various structures. Key elements of this widely applicable and easily controlled process are soft chemistry-based deposition, template-assisted mesostructure growth, and the appropriateness of optimized annealing conditions. Thin films composed of TiO_2 *(281,258)*, Al_2O_3 *(282–284)*, SnO_2 *(285,286)*, Sb–, Nb–, and Ta-doped SnO_2 *(285)*, CeO_2, ZrO_2, and CeO_2–ZrO_2 *(287)* have been reported as well.

The overview presented in this section demonstrates that almost any structure and composition of an OMM that may be desired for catalytic applications can be realized, provided that enough effort is invested. However, there are some obstacles limiting the widespread use of such materials: First, most syntheses are rather expensive, because the surfactant is not easily recovered. However, the costs of the materials are an issue only when the competing materials are inexpensive, as in the case of silica. If the investment in the starting materials for preparation of the oxide is considerable, as in the case of zirconia, the relative cost disadvantage of the OMMs becomes less important, although not negligible. Moreover, on the atomic scale, OMMs are typically not crystalline, but mostly amorphous, which can present a problem for catalytic applications. Crystallization of these materials is difficult if the soft-templating approach is used, because the high surface curvatures are not conducive to the formation of crystalline materials. Moreover, crystallization often occurs only at elevated temperatures when framework atoms become sufficiently mobile. The increased mobility easily leads to collapse of the mesostructure upon crystallization.

Nevertheless, some crystalline mesoporous materials have been made via the nanocasting route by the use of mesoporous silica or carbon as hard templates. Alternatively, crystallization can be accomplished by the following procedure: stabilization of the mesostructure through incorporation of carbon in the pore system, subsequent crystallization by thermal treatment,

and removal of the carbon by combustion *(288)*. Crystalline ternary oxides were synthesized in selected cases by such a pathway *(288,289)*. This approach is discussed further in Section 4.3.

In the next section, catalytic applications of OMMs are presented. The discussion is focused on the effects on catalytic performance that are associated with the structures of the ordered materials.

4. EFFECTS OF MESOSTRUCTURE IN CATALYSIS

OMMs offer a range of catalytic functions, as illustrated in Figure 2.10. Properties of OMMs that influence catalytic activity and selectivity include composition, crystallinity, thermal and chemical stability, surface area, porosity, surface curvature, and surface functionality, including that offered by anchored catalytic components. What differentiates these ordered materials from many other materials as catalysts are the high surface area, the tunable porosity and composition, and the concavity of the surface. Thus, these materials constitute one of the most intensively investigated classes of solid catalysts in the preceding two decades.

OMMs offer intrinsic catalytic functionalities themselves, and, alternatively, they can be used as supports for catalytic species such as metal or metal
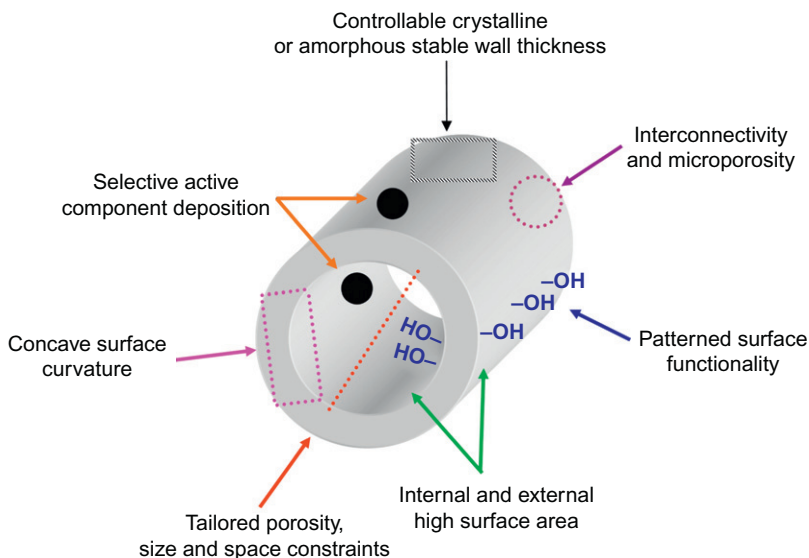

Figure 2.10 Properties of OMMs that can lead to exceptional catalytic performance in various reactions.

oxide particles. OMMs have been investigated as acid–base and redox catalysts. For redox catalysis, non-silica materials with intrinsic redox functions are available, but more often, the silica matrix is used to incorporate redox-active ions, such as titanium. Several of these functions may be combined in one material to create a multifunctional catalyst. Thus, OMMs are in principle suitable for almost any type of catalytic reaction.

However, for such materials to be of commercial interest, they have to provide a benefit that less expensive and less complex materials do not offer. This prerequisite strongly restricts the types of catalytic transformations for which the effort and expense of preparing ordered mesoporous catalysts are worthwhile. It is clear that mesoporous materials do indeed provide specific properties that are difficult to realize in other classes of catalytic materials, but in a number of the reported investigations, it is not made clear how such properties are exploited to enhance the catalytic performance. Often several effects contributing to the catalytic properties have remained unresolved.

Notwithstanding these limitations, we attempt here to highlight specific benefits of OMMs as catalysts. We emphasize that the resolution of specific effects of the catalyst is often difficult when several effects are important.

4.1. High surface area

OMMs often have high internal surface areas. When interpreting the values of surface areas quoted from the literature, one should keep in mind that the standard algorithms to determine surface areas from N_2 adsorption data are often not well suited to OMMs, because the possible presence of micropores can induce capillary condensation in the pressure range typically used to determine Brunauer–Emmett–Teller (BET) surface areas. The limitations of the BET method and approaches to overcoming them are discussed elsewhere *(290–295)*.

Because the OMMs are typically rather expensive, even when they are produced on an industrial scale, one has to evaluate how significant the potential advantage of high surface area may be. Pure-silica materials and aluminosilicates have to compete with their amorphous or zeolite counterparts in catalytic applications. MCM-41-type materials typically have surface areas of approximately $1000 \text{ m}^2 \text{ g}^{-1}$. However, precipitated amorphous silica and alumosilicates or silica xerogels can be prepared with surface areas close to that of MCM-41, and their syntheses are appreciably easier and less expensive than that of MCM-41 *(296)*. Thus, in most cases the advantage of the high surface area of an ordered mesoporous silica is outweighed by the lower

cost of disordered silicas, and so large-scale catalytic applications of the ordered materials are for the most part excluded. Nonetheless, there are reported cases in which the high surface area seems to be sufficiently beneficial to make the materials attractive, and some of these reports will be discussed below. The situation is slightly different for ordered mesoporous aluminosilicates and related materials that are acid catalysts. The advantage of high surface area in terms of catalytic activity (provided that mass transfer limitations are not dominant) is often not of primary importance in typical acid-catalyzed reactions. Rather, the benefits of smaller pores in zeolites are manifested in the catalyst selectivity; many applications of zeolites as catalysts involve shape selectivity.

The development of novel catalysts for oxidation of SO_2 to SO_3 is a case in which the combination of high surface area with defined porosity was exploited *(297)*. The conventional catalyst for this reaction is V_2O_5/SiO_2, which is typically modified by addition of an alkali metal compound. However, the vanadium catalyst is limited with respect to the SO_2 feed concentration, which may not exceed approximately 10 vol%, because at higher SO_2 concentration the balance between V(V) and V(IV) becomes unfavorable. The high activity of the vanadia materials results from the fact that the active phase is present as a melt under reaction conditions, so that the entire volume of the alkali vanadate melt is available to effect conversion. The vanadia catalysts are not able to handle the high SO_2 concentrations that are present in feedstreams from smelters that use pure O_2 (instead of air). Thus, alternative catalysts are required for such feeds. Screening experiments revealed that catalysts containing iron were promising for this application. To achieve a sufficient activity of the catalyst, a high surface area support was needed, because the iron-containing phase, in contrast to the vanadia, does not melt under process conditions. Thus, a high surface area of the iron species is required. Iron-modified MCM-41-type materials were found to be effective in this process, because the iron nanoparticles were highly dispersed and stabilized on the high surface area OMMs. Irrespective of the mode of incorporation of iron into the catalyst (incipient wetness impregnation, ion exchange, or direct synthesis), the MCM-41-supported catalysts were generally superior to those made from commercial silica with a surface area of about 170 $m^2 g^{-1}$. The advantages of the ordered silica mesostructure probably arise from the high surface area for dispersion of the active iron oxide or iron sulfate species and from the hindrance to agglomeration of the iron species present on the support surface. The long-term stability of the material was remarkable, with only little catalyst deactivation observed over periods

of several weeks in a flow reactor at temperatures exceeding 700 °C. The capability of various OMMs to stabilize highly dispersed iron oxide species was also demonstrated in the work of Fröba's group, who investigated the state of iron oxide particles in various mesoporous silica *(298,299)* and carbon *(300,301)* materials.

The activity of iron–modified MCM-41 and HMS materials as catalysts for the benzylation of benzene with benzyl chloride was also attributed to the high surface areas and the resulting high dispersions of the iron species *(302)*. In this case, the iron was introduced during synthesis, and the authors proposed that it was transported to the intrachannel surfaces during calcination and present in the form of highly dispersed clusters *(303)*. A similar investigation essentially confirmed these results *(304)*. Sun *et al.* *(305)* used iron-modified SBA-15 for the same reaction. They prepared highly dispersed iron oxide nanoclusters in the well-ordered mesoporous channels of SBA-15. The material was tested in the benzylation of benzene by benzyl chloride, and it was found that the catalyst activated the reactants at relatively low temperatures, such as 40 °C. Furthermore, the catalyst could be regenerated. The outstanding catalytic performance was attributed to the active sites provided by the iron oxide nanoclusters, the high surface area, and the open pore channels for access of the reactants to the catalytic sites.

These and other investigations show that the high-silica surface areas can be expected to result in high activities of the catalysts per unit mass. However, the lack of comparisons of the catalyst performance with the performance of other mesoporous silicas and zeolites makes it difficult to assess the advantages that might be attributed to the ordered mesoporous support.

Gallium–modified MCM-41 is another material that was tested for the benzylation reaction *(306)*. The best-performing catalysts were those for which there were indications of a highly dispersed Ga_2O_3 species, and the high activity and selectivity can probably be attributed to the high surface area of MCM-41. The authors compared the performance of their catalysts with that of a Ga_2O_3/SiO_2 sample, which was characterized by low activity and selectivity. However, no further properties of this catalyst were specified.

A systematic investigation was presented by Li *et al.* *(307)*, who compared fumed SiO_2, MCM-41, and SBA-15 as supports of ruthenium and nickel particles as catalysts for ammonia decomposition. The catalysts incorporating ordered mesoporous supports were found to be more active than those with ordinary silica supports. The higher activity was attributed to the higher surface area and the porosity of the ordered mesoporous supports, which allows high dispersion of the nanoparticles in the silica matrix.

It was concluded that the type of support and the preparation methodology can have a considerable effect on metal dispersion and thus the performance of the catalyst. However, which of the support properties, the surface area or the confining pore system that allows high dispersion of the nanoparticles, was more significant remains unclear. Similar effects were observed in other cases; a higher catalytic activity (per unit mass) of a Ru/SBA-15 catalyst than a low-surface-area Ru/SiO$_2$ was demonstrated for Fischer–Tropsch synthesis *(308)* and hydrogenation of nitrobenzene *(309)*.

Landau *et al.* *(310)* demonstrated an unequivocal effect of the high surface area of OMMs. They investigated the alkylation of phenol with methanol on alumina-coated wide-pore MCM-41 and compared this type of catalyst with a precipitated alumina reference catalyst. The surface functionality of each catalyst was found to be essentially identical, but the alumina-coated MCM-41 with its higher surface area was 2.3 times more active (per unit mass of catalyst) in the alkylation reaction. However, the activity did not scale linearly with surface area, implying that other factors, possibly associated with the pore structures and mass transfer, contributed as well.

An effect of the surface area was also observed in the Prins condensation of β-pinene and formaldehyde to give nopol. In the presence of a MCM-41 catalyst, a conversion of 61% was reached, whereas a silica gel gave only a 37% conversion under similar conditions *(311)*. Although the surface area of the silica gel was not given, the average pore size of 16 nm suggests that it had an appreciably lower surface area than MCM-41. The authors attributed the higher conversion in the structured catalyst to a better accessibility of the sites, but because the average pore diameter of the silica was 16 nm, it was suggested that the mass transfer was less restricted in the gel than in the MCM-41, which has a pore diameter of 2 nm, although the presence of quite small pores in the gel could lead to the opposite inference. It is thus plausible that the higher surface area is the explanation for the relatively high activity of the structured mesoporous catalyst. Another key result emerging from this investigation is that the catalytic activity was substantially increased by grafting tin species onto the MCM-41, resulting in a conversion close to 100% under the same conditions. (The amorphous silica was not modified with tin.)

In oxidative dehydrogenation (ODH) of propane to propylene on silica-supported vanadia catalysts, ordered mesoporous silicas have a clear advantage over other supports because of the high dispersion of vanadium species that can be achieved *(312)*. Isolated vanadyl species have been suggested to be the active sites for this reaction. Higher surface area supports should allow higher vanadia loadings while maintaining isolated species. Incorporation of

the vanadium species is possible via direct synthesis from vanadium-containing reaction mixtures or by impregnation of a preformed silica. SBA–15 was found to be particularly well suited as a catalyst support, with propylene yields exceeding 30% *(313,314)*. In earlier investigations, MCM–41 and MCM–48 were also found to be suitable supports of catalysts for the oxidative dehydrogenation of alkanes (ethane, propane, and isobutane) because of their high surface areas *(315–318)*, but they are inferior to the SBA–15 type materials. In all these investigations it was found to be necessary to avoid the formation of extended vanadia species; this observation confirms the importance of a high dispersion of the catalyst and therefore the importance of a high surface area of the support.

Partial oxidation of methane is another catalytic reaction that evidently reflects the benefit of a high dispersion of active vanadium species on a silica support *(319,320)*. The results of several investigations demonstrate the high activities of catalysts incorporating ordered mesoporous high–surface–area silica supports. Berndt *et al. (321)* found relatively high productivities for formaldehyde and methanol in the reaction catalyzed by a V-MCM–41 containing 2.8 wt% vanadium. A catalyst supported on SBA–15 was later shown to have a 30% higher formaldehyde productivity *(322)*. Similar findings were reported in another investigation of the partial oxidation of methane to formaldehyde. Ordered hexagonal mesoporous pure-silica SBA–15 was used as a support to generate highly dispersed vanadium–containing catalysts, VO_x/SBA–15 *(323)*. Catalytic activity data indicated that isolated surface vanadium species, which were predominant at vanadium coverages below the monolayer value, were found to be more active and selective for formaldehyde formation than agglomerated vanadium oxide species. A high formaldehyde space–time yield (STY) of about $2.4 \text{ kg kg}_{cat}^{-1} \text{ h}^{-1}$ was achieved with the most active VO_x/SBA–15 catalyst (3.85 wt% V) at a temperature of 618 °C, which is much higher than the maximum productivity of about $1.3 \text{ kg kg}_{cat}^{-1} \text{ h}^{-1}$ reported for conventional VO_x/SiO_2 catalysts. It was concluded that the mesoporous pure-silica SBA–15 is a good support for dispersing vanadium oxide, because the high surface area implies that the monolayer capacity is reached at a higher vanadium loading (ca. 4 wt% V) than on amorphous silica. The maximum STY of formaldehyde obtained in this work was similar to the value of $2.2 \text{ kg}_{cat} \text{ kg}^{-1} \text{ h}^{-1}$ reported for VO_x/MCM–41 *(321)*. In summary, these results demonstrate that it is advantageous to use high–surface–area siliceous mesoporous materials to support vanadium oxo species for the partial oxidation of methane; the situation is similar to that observed for the ODH reaction.

A molybdenum-containing material (8.8 wt% Mo/SBA-1) was also catalytically active for the partial oxidation of methane *(324)*.

Catalysts for the oxidation of methanol with niobium species as the active component also benefit from the high dispersion and isolation of the catalytic species that can be achieved on ordered mesoporous silica *(325)*. A niobate-containing catalyst synthesized by direct incorporation of 3.5 wt% niobium on MCM-41 was found to have a higher activity than catalysts prepared with Cab-O-SIL® silica having a surface area of $330 \text{ m}^2 \text{ g}^{-1}$. Normalized to the number of niobium atoms in the sample, a 1 wt% Nb_2O_5/SiO_2 catalyst exhibited a slightly higher activity than the 3.5 wt% Nb/MCM-41 sample, but at niobia loadings of 10 wt%, the normalized activity of Nb_2O_5/SiO_2 dropped strongly, probably because of the low number of isolated niobate units that can be accommodated at these loadings on the Cab-O-SIL® silica. Similarly, the advantage of a high support surface area and thus a niobium-rich SBA-15-supported catalyst was observed in the oxidation of methanol and in the epoxidation of cyclohexene *(326)*.

Although the high surface area of ordered mesoporous structures does not present a particular advantage in the case of silica and alumosilicates, because other forms of the supports with nearly the same surface areas are available, the advantage of the high surface areas of the ordered supports can be significant for materials with compositions that do not lend themselves to synthesis in forms with high surface areas. However, the specific surface areas of ordered mesoporous forms of most non-silica oxides are substantially lower than those of silicas. This difference is related to the higher framework density of most non-silica materials compared with silica. If a silica with a wall density of 2.2 g cm^{-3} had a surface area of $1000 \text{ m}^2 \text{ g}^{-1}$, a material with the identical texture (pore size, wall thickness, and topology) made of TiO_2 (with a density of 4.3 g cm^{-3}) or of ZrO_2 (with a density of 5.7 g cm^{-3}) would have a specific surface area of only 510 or $390 \text{ m}^2 \text{ g}^{-1}$, respectively. In any case it is usually more difficult to produce non-silica materials with high surface areas than silica materials.

One of the most commonly applied materials in catalysis is alumina, in its various polymorphs. Not much is known about catalysis by ordered mesoporous aluminas. One reason for the lack of information is the ready availability of high-surface-area aluminas made with conventional syntheses *(327)*. Another reason is the difficulty of producing ordered mesoporous alumina by surfactant-assisted assembly or by nanocasting. Although some success with such syntheses has recently been achieved *(146,150,328,329–333)*, the textural properties are not far superior to those

that can be obtained by conventional syntheses, such as the thermal decomposition of boehmite. Moreover, for most of the catalytic applications, γ-alumina is the desired phase, but surfactant-directed processes typically result in the formation of amorphous walls. The synthesis of ordered mesoporous γ-alumina has recently been reported to occur as a result of soft templating *(334)* and nanocasting *(192,335)*. Surprisingly, the mesostructure of the alumina prepared by soft templating was found to be stable at temperatures as high as 1000 °C—and this stability can be highly beneficial in high-temperature catalytic reactions *(334)*. Moreover, the average pore diameter of the alumina could be tuned in the range 3–7 nm, which in prospect could allow size-selective catalysis. The mesostructured alumina was doped with ruthenium and used as a catalyst for the selective hydrogenation of acetone, D-glucose, and D-(+)-cellobiose and size-selectivity was observed for these variously sized molecules. However, the OMM did not have a catalytic activity superior to that of commercially available γ-Al_2O_3.

Although alumina is one of the most commonly used oxides in catalysis, the aluminas created by surfactant-assisted pathways have so far been tested only in a few catalytic applications. Alumina-coated silica was tested for the alkylation of phenol with methanol *(310)*, and alumina was tested as a support for a rhenium catalyst for olefin metathesis *(336)*, platinum–doped alumina was tested for CO oxidation *(337)*, and an alumina-tungstophosphoric acid composite was tested for selective conversion of isopropanol to dehydrated and dehydrogenated products *(338)*. In an early paper, a mesoporous alumina synthesized by the route developed by Vaudry *et al. (339)* was used. This route does not seem to correspond to a true liquid crystal-templating, because no dependence of the pore size on the surfactant was observed. Nevertheless, the route allows the synthesis of alumina with a high specific surface area, and indeed a high activity of the mesoporous alumina was observed. Catalysts prepared with the mesoporous alumina by impregnation with ammonium perrhenate had higher catalytic activities (related to mass) in the metathesis of 7-hexadecene to 7-tetradecene and 9-octadecene than catalysts synthesized via the same pathway, but with commercial γ-alumina as the support *(336)*. Analysis of the rhenium species did not indicate any difference between the two catalysts; thus, the higher activity of the former is attributed to the high surface area of the mesoporous catalyst (564 $m^2\,g^{-1}$), which is much greater than that of the reference sample (166 $m^2\,g^{-1}$).

In summary, the advantage of the high surface area is significant for non-silica oxides other than alumina, and therefore these materials have been tested in various applications, mostly as catalyst supports, for reactions

benefiting from the high surface area and for photochemical reactions, which also benefit from high surface areas. For example, the high surface area of mesoporous CeO_2 and ZrO_2 supports for palladium was exploited in the hydrogenation of phenol, with cyclohexanone being the main product (340). The mesostructured supports exhibit rather high surface areas, exceeding $200 \text{ m}^2 \text{ g}^{-1}$. In comparison with commercial supports, which, however, had different compositions, the mesostructured materials performed appreciably better, evidently because of the high palladium dispersions made possible by the high support surface areas.

Several materials incorporating mesostructured titania were investigated as catalysts and photocatalysts (341–349). Perkas et al. (350) found somewhat better performance of Fe_2O_3 supported on mesostructured titania for cyclohexane oxidation than of catalysts supported on pyrogenic titania P25. The catalyst supported on mesoporous titania gave a conversion of 25.8%, whereas the catalyst supported on P25 gave a conversion of only 21.3% under comparable conditions. The difference in surface areas of the two materials was more than enough to explain the differences in conversion, and so it was inferred that additional effects influenced the catalyst performance. The Fe_2O_3 was deposited on the supports by the ultrasound method, which had been used by Gedanken et al. (351) to synthesize various OMMs. Yoshitake et al. (352) investigated mesoporous titania with a surface area of up to $1000 \text{ m}^2 \text{ g}^{-1}$ (although the analysis of textural data may be influenced by the presence of micropores) as a support for vanadium species in the oxidation of propylene (mainly to give the oxidation products CO and CO_2), and they compared the results with those obtained with a catalyst on a titania support with a surface area of about $50 \text{ m}^2 \text{ g}^{-1}$. The catalyst on the mesoporous support had a significantly higher activity than that on the conventional support, and the activity roughly scaled with the surface areas of the materials.

Several photocatalytic conversions on catalysts consisting of mesoporous semiconducting oxides were investigated. We emphasize that typically the defect density of ordered mesoporous oxides is higher than that of crystalline bulk oxides. Defects may lead to the formation of electron or hole traps, thus resulting in reduced quantum efficiencies in photocatalysis. The low quantum efficiency of mesoporous titania and of niobia in the oxidative dehydrogenation of 2-propanol to acetone was attributed to this effect (353). Some success was achieved with a mesoporous titania film in the photocatalytic oxidation of NO to NO_2—this material was better than a film prepared by the sol–gel route without surfactant (354). However, the characterization

of the samples was not sufficient to demonstrate the formation of an ordered mesostructure; only a higher porosity (relative to that of the sol–gel prepared film) was demonstrated.

High surface area is a key property of ordered mesoporous semiconductors used for solar energy conversion. Group-5 transition metal oxides show promising activities in photocatalytic water splitting. Ordered mesoporous tantalum oxide loaded with 4 wt% NiO was characterized by a productivity of 150 μmol h^{-1} for H$_2$ and 73 μmol h^{-1} for O$_2$, exceeding by 50% the water splitting activity of crystalline bulk Ta$_2$O$_5$ loaded with NiO (1.0 wt%) *(355)*. The high activity was attributed to the thinness of the walls and the correspondingly rapid electron migration. The same group reported water splitting activity for an unmodified magnesium–tantalum mesoporous mixed oxide prepared with the aid of the surfactant Pluronic® P-123 *(356)*, but the activity was lower than that of the NiO-modified samples. Ordered mesoporous Ta$_3$N$_5$ with crystalline wall structures was prepared from an amorphous mesoporous Ta$_2$O$_5$ by nitridation at 800 °C in flowing NH$_3$ *(357)*. The BET surface area, pore diameter, and wall thickness of the mesoporous Ta$_3$N$_5$ were approximately 100 m^2 g^{-1}, 4 nm, and 2 nm, respectively. It was found that mesoporous Ta$_3$N$_5$ loaded with platinum nanoparticles was active for photocatalytic H$_2$ evolution from an aqueous methanol solution under visible light (i.e., light at wavelengths longer than 420 nm). The photocatalytic activity of mesoporous Ta$_3$N$_5$ was three times higher than that of conventional bulk Ta$_3$N$_5$ under the same reaction conditions, and the difference was attributed to the high surface area and the thin, crystalline pore walls that enabled efficient charge transfer of photoexcited electrons and holes to active sites on the surface.

A metal-free polymeric photocatalyst with high surface area, ordered mesoporous C$_3$N$_4$, for H$_2$ production from water under visible light was described by Wang *et al.* *(358)*. Although the estimated quantum efficiency of the platinum-modified C$_3$N$_4$ catalyst was relatively low (approximately 0.1% with irradiation at wavelengths of 420–460 nm), the results provide new insights for finding alternative high-surface-area materials for solar energy conversion. Such functional materials could consist of thermally and oxidation-stable polymeric organic semiconductor structures, which are cheap and easily accessible.

A benefit of a high surface area was also claimed in several dye degradation experiments; although in such investigations, it is difficult to unambiguously attribute the properties to a high specific surface area. For example, it was found that crystalline ordered mesoporous BiVO$_4$, which was prepared

by nanocasting with KIT-6 silica as a hard template, exhibited superior photocatalytic performance (relative to conventional bulk $BiVO_4$) in the photochemical degradation of methylene blue and in the photocatalytic oxidation of NO in air under visible-light irradiation. The higher catalytic activity was ascribed to the small particle size and high surface area of the ordered mesoporous $BiVO_4$ *(208)*.

An intriguing application of ordered mesoporous niobium oxide *(359)* is the activation of N_2. When a reduced sample of such a niobia reacted with bistoluene niobium to coat the support with niobium, nitride species formed *(360)*. Niobia has rarely been prepared in the form of high–surface-area materials, apart from samples prepared by complex pathways, such as synthesis by supercritical drying. Such samples have textural properties akin to those observed for OMMs. *(361,362)*. Similar behavior was observed in tin(IV) phosphates synthesized by Serre *et al.* *(363)*, who obtained such materials in the hexagonal as well as in the cubic form. These samples were catalytically active for the reduction of NO by C_2H_4 in the presence of O_2. The hexagonal material was superior to the cubic one. The reason for the difference is not obvious, but it may be related to a different coordination state and an increased number of surface tin species in the hexagonal samples.

There have also been attempts to synthesize ordered mesoporous vanadyl pyrophosphate (VPO)–type catalysts for the oxidation of *n*–butane to maleic anhydride *(364)*. The nature of the active sites of these catalysts is not known, although numerous studies have been devoted to the subject *(365)*. The OMM with a high surface area did indeed show an appreciable selectivity to maleic anhydride that decreases with increasing conversion; however, its activity was significantly lower than that of the conventional VPO–type catalyst. This deficiency was attributed to the amorphous nature of the mesoporous catalyst, although this property would not be expected to be conducive of good selectivity.

A recent investigation into the synthesis of ordered mesoporous Co_3O_4 by the group of one of the authors *(366)* demonstrates the importance of the materials design strategy, which can be used to tune morphology, porosity, and surface area. A series of Co_3O_4 samples was prepared by nanocasting with KIT-6 (cubic ordered silica) as a hard template, and the resulting materials were tested as catalysts for CO oxidation. Textural parameters of the hard template play an important role in determining the structure of the nanocast materials. Depending on the type of hard template and its textural parameters, porosity, surface area, and particle size of the mesoporous Co_3O_4 can be controlled to a certain extent. Cubic ordered mesoporous silica (KIT-6) has two mesoporous

channel systems that are connected to one another through micropores. This mesostructured silica is characterized by a low-angle XRD pattern that shows the (211) and (220) reflections. If the interconnectivity between the two meso-pore channel systems of the silica hard template via the micropores is high enough, nanocast metal oxides possess a perfect replica structure with a symmetry identical to that of the parent—and thus show the same reflections as the parent template. However, if KIT-6 prepared at a lower aging temperature (normally below 60 °C) is used as hard template, the result is a decreased degree of interconnectivity between the two mesopore systems of the gyroid structure. In this case, a replica with lower symmetry is formed, and the low-angle XRD patterns of the nanocast materials show an additional (110) reflection *(204)*. As is evident from the SEM images shown in Figure 2.11, Co_3O_4-40, which was fabricated from KIT-6 aged at 40 °C, has more open uncoupled sub-frameworks, whereas Co_3O_4-100 and Co_3O_4-135, obtained from KIT-6 aged at 100 and 135 °C, have coupled frameworks. Parent material that is aged at a high temperature has a dense structure and contains a high fraction of
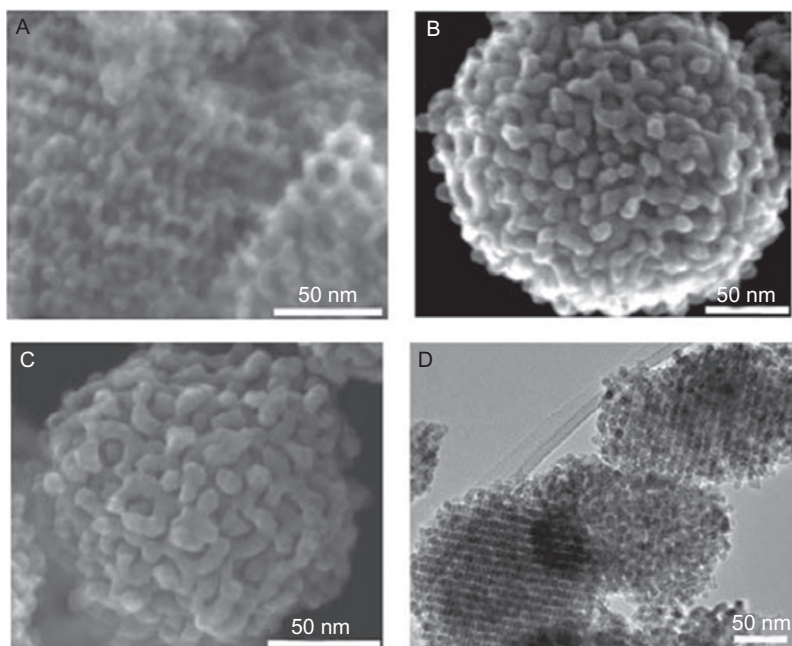

Figure 2.11 High-resolution SEM images of Co_3O_4 that was nanocast from KIT-6 at 40 °C (A), 100 °C (B), and 135 °C (C) aging temperature; (D) shows a TEM image of Co_3O_4-100 (from KIT-6 template aged at 100 °C) after catalytic testing *(366)*. *Adapted with permission from the Royal Society of Chemistry.*
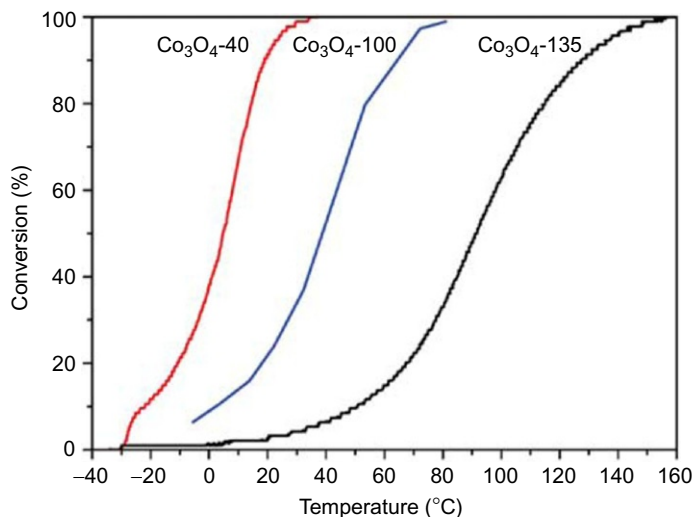
Figure 2.12 CO oxidation catalyzed by cubic ordered mesoporous Co_3O_4 *(366)*. *Adapted with permission from the Royal Society of Chemistry.*

micropores connecting the two mesopore systems. The surface areas of the nanocast Co_3O_4-40, Co_3O_4-100, and Co_3O_4-135 materials were 153, 114, and 70 m^2 g^{-1}, respectively. The activity was evidently dependent on the textural properties of the samples, with the best performance achieved for the material with the highest surface area, as shown in Figure 2.12. Co_3O_4 with a high surface area was sufficiently active to convert 100% of the CO to CO_2 at about room temperature under the conditions of the experiments. The light-off temperature (read at 50% conversion and thus termed T_{50}) of CO increased with decreasing surface area of the ordered mesoporous Co_3O_4. T_{50} for Co_3O_4-40 was 4 °C, whereas for Co_3O_4-100 and Co_3O_4-135 it was 38 and 91 °C, respectively. Normalized to surface area, the performance of the high-surface-area samples was still substantially better, which indicates that mass transfer limitations associated with the narrower pores in the samples Co_3O_4-100 and Co_3O_4-135 had an additional negative impact on the catalytic performance.

These results show the relevance of the design strategy for the properties of the catalysts. By changing one parameter—the aging temperature of the hard template—it was possible to tune the textural parameters, crystallite size, pore size, geometry, and morphology of nanocast Co_3O_4, all of which influence the catalytic performance.

Besides the aforementioned powder forms of OMMs, thin-film morphologies have also shown superior catalytic activities relative to those of other

forms of the same material, simply as a result of their high surface areas. For example, Pan *et al.* *(348)* demonstrated the preparation of a cubic ordered mesoporous TiO_2 film, which was sometimes loaded with 4 mol% WO_3. In the photocatalytic decomposition of 2-propanol in the presence of vapor–phase reactants, the WO_3-loaded material had a 2.2 times higher catalytic activity than the mesoporous TiO_2 itself and a 6.1 times higher activity than an unloaded nonporous TiO_2 film. The superior catalytic activity of the mesoporous over the nonporous TiO_2 was attributed to its higher surface area and the porosity of the material, and the activity enhancement resulting from the WO_3 doping was ascribed to an increase in surface acidity. Ordered mesoporous composite thin films consisting of rutile TiO_2 nanocrystals with amorphous Ta_2O_5 were reported by Wu *et al.* *(367)*. These authors used evaporation-induced self-assembly, followed by heat treatment at about 800 °C. It was found that incorporation of specific amounts of Ta_2O_5 (20 mol %) into the mesoporous TiO_2 film, together with the unique mesoporous structure itself, increased the onset temperature for crystallization, which became high enough to lead to rutile formation from the amorphous titania precursor. The formation and retention of the ordered mesoporous structure was found to be favored by a block copolymer template, which stabilizes the mesostructure of the amorphous mixed oxides before crystallization. The resulting materials were highly active in the photodegradation of rhodamine B in water under illumination by UV light. The synthesis of the ordered mesoporous thin films was extended to other types of oxide such as Bi_2O_3 and $NaTaO_3$.

Brezesinski *et al.* *(368)* reported the synthesis of ordered mesoporous Bi_2O_3 by co-assembly of hydrated bismuth nitrate with a diblock copolymer. The advantage of the mesoporous thin-film morphology became evident in the photodegradation of rhodamine B. The templated Bi_2O_3 films showed a much higher photocatalytic activity than conventional Bi_2O_3 films, which was attributed to their high surface areas and high phase purity. Recently, the fabrication of ordered mesoporous $NaTaO_3$ thin films with both 3D honeycomb and nanopillar-like structures was demonstrated by the same research group, who used sol–gel templating with a novel amphiphilic diblock copolymer as the structure-directing agent *(369)*. The catalytic activity of the material was investigated in the photodegradation of methylene blue, and superior activity was observed relative to that of the non-templated thin films of the same initial composition. Likewise, this enhancement of activity was ascribed to high surface area and also to porosity, which has a substantial effect on the surface density of the catalyst and influences the reaction kinetics and mass transfer, and hence the overall performance.

4.2. Tailored porosity

The possibility of tailoring porosity, in particular to synthesize materials with pore diameters exceeding those of zeolites, while maintaining (some of) the catalytic properties, is probably the characteristic of OMMs that leads to the widest range of applications in catalysis. OMMs thus allow processing of molecules with sizes exceeding those of zeolite pores. Many of the transformations investigated have therefore been selected to emulate the reactions catalyzed by acidic zeolites or titanium silicalite (TS-1). This section, addressing these points, is divided into acid–base catalysis and redox catalysis.

4.2.1 Acid–base catalysis—Introduction of suitable functionality

The acidic properties of alumosilicate OMMs are quite similar to those of amorphous alumosilicates. This similarity was recognized soon after the first description of MCM-41 *(370,371)*. Many different pathways for aluminum incorporation have been investigated, and other trivalent elements such as boron, gallium, and iron have also been incorporated into the walls. Although the fraction of tetrahedrally and octahedrally coordinated heteroatoms varies and depends on the synthetic pathways, not much difference from amorphous silica matrices has been observed with respect to the acid strengths of the sites *(17)*. This result is as expected, because the local configurations of the atoms in the walls of MCM-41 and related materials essentially correspond to those found in amorphous gels *(372)*. The essentially amorphous nature of the walls is also responsible for the limited hydrothermal stability of ordered mesoporous alumosilicates and silicas *(373–376)*. Several methods have been developed to increase the hydrothermal stability of the materials as well as to introduce sites with higher acid strength.

The low hydrothermal stability was the first problem that was tackled in the earlier stages of research on OMMs. Some success was achieved by grafting aluminum onto the pore surfaces and in this way protecting the labile siloxane bond against hydrolytic attack *(377,378)*. Another possibility is the protection of the wall by making it hydrophobic, possibly by treatment with various organosilyl compounds, which are grafted onto the walls *(379)*. Increasing the structural order of the material, for example by the addition of inorganic salts during the synthesis, was also found to be helpful in improving the hydrothermal stability *(380)*. A simple, effective method is to increase the wall thickness, for example, by making SBA-15 instead of MCM-41. However, thicker walls typically imply a reduced surface area and, therefore, this option may not always be the best.

Most zeolites have much higher hydrothermal stabilities than ordered mesoporous alumosilicates. Therefore, many attempts have been made to induce partial conversion of the walls to zeolitic structures or to cover the walls with zeolitic species. In addition to the expected increase in hydrothermal stability, zeolitic moieties should also introduce the desired strong acidity. The first strategies relied on the use of template mixtures, comprising templates inducing the formation of zeolitic structures such as tetra-alkylammonium ions with short-chain alkyl groups and others that favor the formation of OMMs, such as CTA ions. However, the resulting products were not the desired composites, but rather two phase systems, with separate macroscopic domains consisting of either mesoporous material or zeolitic material *(381)*.

Furthermore, post-synthesis recrystallization of the walls was attempted by employing as–prepared MCM–41 instead of a conventional silica source in a regular zeolite synthesis gel under mild conditions *(382)*. However, the first real success was achieved when the opposite approach was taken, that is, a zeolite precursor gel was first treated under mild conditions to initiate nucleation of small zeolitic entities without further growth and then a surfactant template was added *(58,383–386)*. It is difficult to demonstrate the incorporation of zeolitic units into the walls of mesoporous materials, because the thinness of the walls allows only for a small size of the zeolite units, thus hindering their detection by diffraction experiments. Indications of zeolite species in a bulk sample can also arise from macroscopically separated domains, as was reported *(381)*. However, there is circumstantial evidence that indicates that the wall structure of the samples has at least been altered; specifically the hydrothermal stabilities are substantially improved and the samples have higher activities in reactions catalyzed by strong acid sites.

An alternative to this approach is the coating of preformed ordered mesoporous silica with zeolite fragments *(387–389)*. Such coatings also appear to substantially improve the stability of the materials, because they can be heated in steam to 800 °C without substantial structural degradation. In addition, strong acidic Brønsted and Lewis sites are detected by IR spectroscopic analysis of adsorbed pyridine.

Heteropolyacids are strong acids with the disadvantage of having low-surface areas in their solid forms. Therefore, they are well suited to being supported on high-surface-area materials such as ordered mesoporous silica. Several investigations have been devoted to this topic *(390–396)*. The resulting supported catalysts have increased numbers of accessible acid sites relative to the bulk forms of the acid, although in most cases the dispersion does not seem to

have been optimized. Leaching of the heteropolyacid can be a problem, depending on the solvent and the conditions of the reaction. A two-step procedure applied to support $Cs_xH_{(3-x)}PW_{12}O_{10}$ appears to deliver optimal results with respect to leaching stability and dispersion of the catalysts *(396)*.

Acidic sites with limited thermal stability can be created by functionalization of the silica surface with organic acid groups. Thiol groups are easily grafted to the surface of silica by treatment with 3-mercaptopropyltrialkoxysilanes, and subsequently the thiol group can be readily oxidized to a sulfonic acid group *(397–403)*. Alternatively, incorporation of the functional silane during the synthesis by co–condensation and subsequent oxidation is also possible *(404–406)*, and an alternative is direct co–condensation with 2-(4-chlorosulfonylphenoxy)-ethyltrimethoxy silane, which avoids the additional oxidation step and directly results in an arenesulfonic acid–modified material *(407)*.

Carboxylic acid groups on the supports can be obtained by using 3-cyanopropyltetraalkoxysilane and subsequent hydrolysis of the nitrile group. Thus, a modified material was synthesized by co–condensation of the cyanopropylsilane and TEOS in the presence of P–123. Simultaneous with the removal of the block polymer surfactant with sulfuric acid *(408)*, the nitrile groups in the material are converted to carboxylic acid groups *(409,410)*. The strongest acidic sites can be generated by modification of ordered mesoporous silica by perfluoroalkylsulfonic groups, leading to acidic sites of the same type as those present in Nafion® resin, as reported by Alvaro *et al.* *(411,412)*. The acidic group is grafted to the surface by reaction of the silica with 1,2,2-trifluoro-2-hydroxy-1-trifluoromethylethane sulfonic acid sultone for 6 h under reflux conditions in the presence of dry toluene (Figure 2.13). The resultant acid catalysts showed high activity for acylation of anisole *(413)*, alkylation of isobutylene and 1–butene *(414)*, esterification of carboxylic acids, Friedel–Crafts acylation *(412)*, and α–methylstyrene dimerization *(415)*.
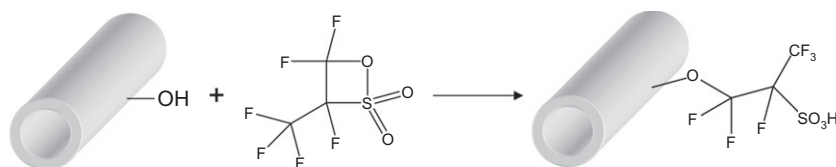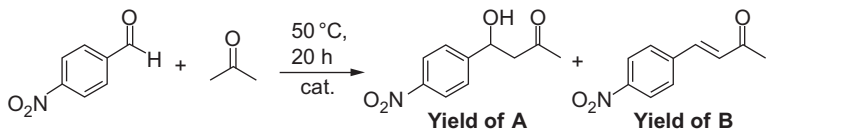

Figure 2.13 Surface functionalization of MCM-41 or SBA-15 silicas with 1,2,2-trifluoro-2-hydroxy-1-trifluoromethylethane sulfonic acid sultone to give sulfonic acid groups of the same type as those present in Nafion® resin anchored to the silanol groups with perfluoroalkyl tethers *(411)*. *Adapted with permission from the Royal Society of Chemistry.*
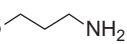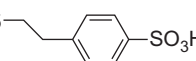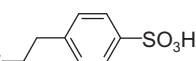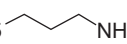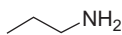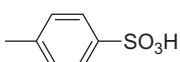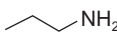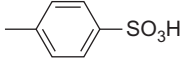
Basic groups can be introduced by deposition of basic oxides or by grafting of organic molecules with basic groups. Kloetstra *et al. (416,417)* prepared basic catalysts by depositing species such as Na^+, Cs^+, or lanthanum salts in the pores of MCM-41. The resulting materials were catalytically active for Knoevenagel condensation and Michael addition reactions. The more frequently applied approach is the grafting of basic organic molecules; this approach was introduced by Brunel and coworkers *(163,418–420)*. Particularly flexible appears to be the proposed two-step method, whereby first a chloropropyl group is grafted to the silica surface; then the chlorine atom is replaced by an amine group *(420–422)*. By this method, complex amines (for which no functionalized silanes are available) can be anchored to the surface. Introduction of basic groups (amines) by co-condensation is also possible, as was first described by Macquarrie and coworkers *(423,424)*.

A mixture of acidic and basic sites can also be attached to the silica structure to prepare bifunctionalized mesoporous catalysts. Sulfonic acid and propylamine groups were incorporated in SBA-15 in a one-pot synthesis using poly(ethylene glycol)–*block*-poly(propylene glycol)–*block*-poly(ethylene glycol) (P-123), HCl, H_2O, tetraethoxysilane, 2-(4-chlorosulfonylphenyl)ethyltrimethoxysilane, and 3-aminopropyltrimethoxysilane, as described by Zeidan *et al. (406)*. The immobilized catalysts were tested in the aldol condensation of 4-nitrobenzaldehyde with acetone, which resulted in aldol addition and condensation products. The catalytic data characterizing various catalysts are presented in Table 2.2.

As shown in Table 2.2, a conversion of 62% was obtained when SBA-15 functionalized with both sulfonic acid and amine groups was used (Entry 1), whereas SBA-15 functionalized only with a sulfonic acid or an amine group produced a considerably lower conversion (Entries 2 and 3). A physical mixture of acid-functionalized SBA-15 and amine-functionalized SBA-15 gave an intermediate conversion, which was significantly lower than that observed with the bifunctionalized acid–base catalyst (Entry 4). The support alone effected no conversion (Entry 5). It was also found that the homogeneous analogues of the sulfonic acid and the amine did not convert the starting materials into products, as these functionalities apparently neutralized each other and precipitated out of the reaction mixture (Entry 6). The individual soluble acidic and basic analogues gave low conversions (Entries 7 and 8), much lower than the acid–base bifunctional catalyst supported on SBA-15. It was concluded that the high porosity of the ordered mesoporous silica permits facile immobilization of functional groups. These groups cannot coexist in solution as active catalytic sites because they

Table 2.2 Conversion and product yields obtained in the aldol reaction between 4-nitrobenzaldehyde and acetone in the presence of various molecular and supported catalysts with sulfonic acid or amine groups, or combinations thereof, achieved by mixing or by co-functionalization *(406)*

Entry	Catalyst (10 mol %)	Yield of A (%)	Yield of B (%)	Conv. (%)[a]
1	SBA-15⌇NH$_2$ / SBA-15⌇SO$_3$H	45	17	62
2	SBA-15⌇SO$_3$H	8	8	16
3	SBA-15⌇NH$_2$	25	8	33
4	SBA–15–A/SBA–15–B[b]	30	14	44
5	SBA–15	0	0	0
6	⌇NH$_2$ + ⌇SO$_3$H	0	0	0
7	⌇NH$_2$	3	5	8
8	⌇SO$_3$H	3	1	4

[a]Total conversion. Yields determined by ^{1}H NMR spectroscopic analysis with THF as an internal standard.
[b]1:1 mixture of sulfonic acid-functionalized SBA-15 (SBA-15-A) and amine-functionalized SBA-15 (SBA-15-B).
Adapted with permission from Wiley.

neutralize each other, and only the supported catalyst facilitates the reaction. The high surface area of the porous material allows the simultaneous anchoring of the acidic and basic functional groups with sufficient separation to prevent their neutralizing each other.

Mesoporous organosilica materials containing acidic and basic functional groups in separate locations—in the pores and integrated into the silica

walls—were synthesized by modifying the organic groups in the pore walls of the silica, which had been prepared by co-condensation of an acid precursor, TEOS, and *t*-butoxycarbonyl (Boc)–protected aminopropyltriethoxysilane as a basic precursor in the presence of a block copolymer template (Figure 2.14) *(425)*. The sulfonic acid groups were generated in the pore wall by converting disulfide bridges to thiol groups, and then oxidizing them with hydrogen peroxide, followed by treatment with dilute sulfuric acid. Subsequently, the protecting group, added to ensure that the functionality of the aminopropyl group was not altered during the chemical treatment of the ordered mesoporous silica, was removed by thermal treatment in vacuum to obtain basic NH_2 groups in the pores. The accessibility of the amino groups in this material was confirmed by reaction with acrylamide. The results showed that the self-assembly synthesis of mesoporous organosilicas with framework and surface groups, followed by suitable chemical transformations, is a promising approach towards the creation of nanostructures with opposing functionality in close proximity
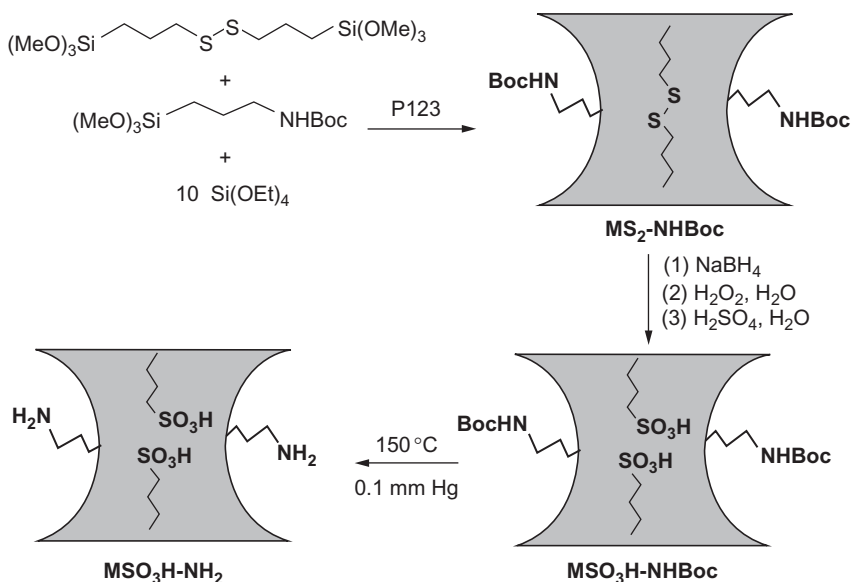
Figure 2.14 Preparation of bifunctional ordered mesoporous organosilica. Disulfide units are attached to the organic moieties that are part of the wall, while NHBoc functional groups are anchored to the surface of the silica matrix. The reduction of disulfide units is achieved by $NaBH_4$ treatment, the sulfonic acid groups are then formed by oxidation of the thiol groups. The amino groups are obtained by thermal decomposition of NHBoc *(425)*. *Adapted with permission from the American Chemical Society.*

to each other. No catalytic data were presented, but this bifunctional material with acidic and basic groups may find application in transformations requiring acid and base catalysis in sequence.

4.2.1.1 Petroleum refinery catalysis and petrochemical conversions

The relatively large pore sizes of OMMs should provide advantages over the classical zeolite catalysts for conversions involving large molecules. However, the limited hydrothermal stability of the mesoporous materials is a serious obstacle under the harsh practical conditions of petroleum refinery processes. Nevertheless, a first commercial application of an OMM has been reported *(132)*, although details were not disclosed. There are reports stating that the problem of hydrothermal instability has been solved for this material *(426)*. Pilot-plant synthesis—on the scale of 600 kg—and commercial application of MCM-41 in fluidized-bed (fluid) catalytic cracking of hydrocarbons were reported by Da *et al. (427)*. The acidic sites of the mesoporous materials were suitable for cracking of the larger molecules present in the feedstock, and in comparison with a commercial catalyst, increases of 1.85 and 3.47%, respectively, in the yields of diesel fuel and lighter oil were observed.

The acidic sites of unmodified OMMs are of moderate strength. Hence, it is expected (and was observed) that for small molecules such as hexane, heptane, tetralin, or decalin, the cracking activity of MCM-41-type materials is substantially lower than that of 12-membered ring zeolites, such as USY or zeolite β *(372,428–432)*, because the small molecules fit into the pores of the zeolites and therefore the higher acid strength of the zeolites comes to bear. The lower strength of the acidic sites in ordered mesoporous alumosilicates can be advantageous if oligomerization products of short-chain olefins (e.g., hexenes) are the target and zeolites such as USY catalyze undesired cracking reactions *(429)*.

For the conversion of bulkier molecules, however, the larger pores of OMMs can be an advantage. Asphaltenes *(433)* or palm oil *(434)* were cracked at significant rates in reactions catalyzed by ordered mesoporous alumosilicates, although in the case of palm oil, HZSM-5 still performed better than any of the mesoporous materials. In asphaltene cracking (Figure 2.15) on iron-modified mesoporous SBA-15-type silica, a clear dependence of the activity on pore size was observed. The asphaltene conversion increased almost linearly with increasing pore size up to a diameter of 12 nm and reached 65% *(433)*. This trend was tentatively attributed to better access of the asphaltenes to the sites in the larger pore material.
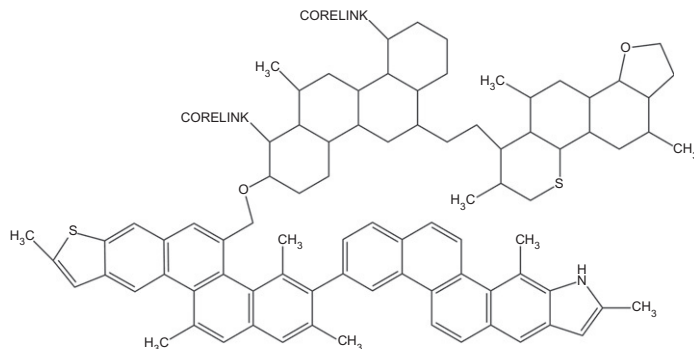
Figure 2.15 Structural model of one of the common asphaltenes (heavy Canadian asphaltene), consisting of aromatic and aliphatic hydrocarbon units and heteroatoms including N, S, and O *(435)*.

Asphaltenes can be so large that they cannot fully enter the pores of catalysts with pore diameters less than 10 nm, and, therefore, use of large-pore catalyst supports is beneficial. The good performance of a heteropolyacid $(H_3PW_{12}O_{40})$–loaded MCM-41 catalyst with a pore diameter of about 2.6 nm in the cracking of 1,3,5-triisopropylbenzene was attributed to the better accessibility of the pores compared to those of zeolites *(394)*. However, at heteropolyacid loadings exceeding 20–25 wt%, the structure of the MCM-41 collapsed, and the activity declined with increasing amounts of heteropolyacid incorporated. The stability of the material at high loadings could to some extent be improved by fluorination. Heteropolyacid loadings of 50 wt% in such materials were achieved without deterioration of the silica structure *(436)*. In the synthesis of methyl *tert*-butyl ether, such a catalyst reached an activity comparable to that of a commercial Amberlyst-15 (sulfonic acid) resin catalyst.

In many oligomerization reactions, large pores in combination with the moderate acidity are also beneficial. Butene oligomerization was carried out with high selectivity to branched oligomers, and little deactivation occurred relative to that observed with zeolites or amorphous alumosilicate catalysts, on which strongly adsorbed residues formed *(437)*. There are several other reports of the oligomerization of small olefins, but clear advantages of structured catalysts over other catalysts, such as amorphous alumosilicates, were not observed *(429, 430)*.

There are not many reports demonstrating a true advantage of the ordered mesopore structures over other materials for acid-catalyzed reactions with potential refinery applications. In contrast, promising activities of

transition metal–modified ordered mesoporous silicas in hydrotreating reactions have been observed. The function of the silica is mainly to disperse and stabilize the sulfidic phases of the supported catalysts formed under reaction conditions; these applications are discussed in Section 4.5.

4.2.1.2 Bulk, intermediate, and fine chemicals syntheses

One of the first demonstrations of the beneficial combination of mild acidity and the pore system of MCM-41 was reported by Climent et al. (438). Jasminaldeyde is synthesized by aldol condensation of heptanal and benzaldehyde. Because of the facile self-condensation of heptanal, this compound normally has to be added slowly to a semibatch reactor during the reaction, resulting in long reaction times and secondary reactions of reagents and initial products. This limitation was circumvented by first conducting an acetalization reaction of heptanal with methanol. After the addition of benzaldehyde, the acetal was slowly hydrolyzed on the mildly acidic MCM-41, and the heptanal that formed reacted in an aldol condensation with benzaldehyde. With this procedure, a low concentration of free heptanal could be maintained during the whole course of the reaction. By-products were formed only in minor amounts, because the uniform channels of the MCM-41 catalyst allowed rapid transport of the product out of the pore system, such that secondary reactions were avoided to a large extent.

Alkylation reactions of aromatic molecules involving bulky reactants and products are difficult to perform on zeolite catalysts because of the restricted pore access. For such reactions, the larger pores of OMMs can be highly advantageous, provided that the acid site strength is sufficiently high. Climent et al. (439) investigated the suitability of OMMs for the first step of acetalization. This reaction does not require strong acidity, and therefore the weak to medium-strength acidic sites of MCM-41 and related solids are sufficient. In a comparative study of the activity of MCM-41 and several zeolites for the acetalization of various aldehydes and trimethyl orthoformate, it was observed that zeolite β and zeolite Y were superior to the mesoporous material with respect to activity, but they deactivated more rapidly. Siliceous and aluminum–containing MCM-41 were observed to have similar activities, which suggests that the silanol groups are the sites of the reaction.

An example of the advantageous combination of mild acidity and an open pore system for rapid mass transfer was reported by Liu et al. (440), who investigated the alkylation of diphenylamine with α-methylstyrene, which results in the formation of the antioxidants mono- and dicumenyldiphenylamine.

Various catalysts incorporating mesostructured alumosilicates (Al–MCM–41, Al–HMS, and Al–MSU–G) performed substantially better than a commercial acid-treated clay catalyst or heteropolyacids supported on OMMs. The superior performance of the alumosilicates was attributed to (a) the medium acid strength, which is sufficient to catalyze the desired alkylation but not the undesired dimerization of methylstyrene and (b) unimpeded diffusion of the reactants to the catalytic sites. The low susceptibility to deactivation was associated with the regularity of the pore system, which was presumed to limit pore plugging by high–molecular–weight side products.

Many other investigations have been devoted to Friedel–Crafts alkylation reactions with various reactants, either on alumosilicate OMMs or siliceous samples into which other components, such as zirconia, gallium species, or others, had been introduced to create acidic sites. These heteroelement-containing systems are discussed below in the section on control of active phase dispersion. With respect to the investigations concerning alumosilicates, the discussion is focused on those cases in which the OMMs exhibited verifiable advantages over other materials. A more comprehensive coverage of the literature of alkylation reactions is available (17).

An early example of the use of MCM–41 for a Friedel–Crafts alkylation demonstrated the advantage of the large pores (441). The activity of Al-MCM–41 with a pore diameter of 3 nm in the alkylation of 2,4-di-*tert*-butylphenol with cinnamyl alcohol was more than an order of magnitude higher than that achieved with zeolite Y, and the difference was attributed to diffusion limitations experienced by reactant and/or product molecules in the zeolite pores. The final product of the reaction is dihydrobenzopyran, which is formed after intramolecular ring closure. A mesoporous ultra-stabilized Y zeolite exhibited somewhat higher activity than the untreated zeolite, but it was still inferior to the MCM–41 catalyst. The performance of the OMM could also not be reached with a soluble catalyst, diluted sulfuric acid, or an amorphous alumosilicate.

For reactions involving extremely bulky molecules, shape selectivity may be expected when the mesopores are in the lower size range. Such behavior was observed for the alkylation of benzene with 1-alkenes, by either varying the catalyst pore size or by varying the size of the olefin (from C_6 to C_{16}). With 1-octene as the reactant, the selectivity for the mono-alkylated product increased with decreasing pore size of the MCM–41, as shown by the data in Table 2.3. When AlCl$_3$-grafted MCM–41 with a pore diameter of about 3.3 nm was used as a catalyst, the selectivity to mono- and

Table 2.3 Conversions and selectivities in the alkylation of benzene with 1-octene catalyzed by AlCl$_3$ supported on MCM-41 materials with various pore sizes *(442)*

Catalyst	1-Octene conv. (%)	Selectivity to monoalkylated benzene (%)	Selectivity to dialkylated benzene (%)
AlCl$_x$/MCM–41 [18]	100	75.2	24.8
AlCl$_x$/MCM–41 [16]	100	79.7	20.3
AlCl$_x$/MCM–41 [14]	100	83.3	16.7
AlCl$_x$/MCM–41 [12]	100	84.2	15.8
AlCl$_x$/MCM–41 [10]	100	89.7	11.3
AlCl$_x$/ZSM–5	5	78.2	21.8

The numbers 10–18 in brackets indicate the carbon chain lengths of the surfactants used in the synthesis of the mesoporous materials; resulting pore sizes range from 2.2 to 3.9 nm. Ten millimoles of 1-octene was added dropwise at room temperature over a period of 30 min to a vessel containing 1.65 g (20 mmol) of benzene and 0.1 g of the catalyst.
Adapted with permission from Elsevier.

dialkylated products increased considerably with increasing chain length of the olefin *(442)* (Table 2.4).

Another example demonstrating a strong influence of the pore size of the OMM on the selectivity is the product distribution found in the alkylation of 4-*tert*-butylphenol with styrene *(443)*. In this reaction, both the mono-alkylated and the dialkylated products (2-(1-phenylethyl)-4-*tert*-butylphenol and 2,6-bis-(1-phenylethyl)-4-*tert*-butylphenol, respectively) are bulky. The reaction was carried out on heteropolyacid-loaded meso-porous silicas with pore diameters of 1.8, 3, and 10 nm. At a conversion of 90%, the catalyst with 3-nm-diameter pores exhibited by far the highest selectivity for the monoalkylation product, and this result was interpreted as a case of transition state shape selectivity, whereby the formation of the dialkylation product was restricted by the pores.

An apparent shape selectivity effect was observed in the methylation of 2-naphthol to form 2-methoxynaphtalene *(444)*. An Al-MCM-41 catalyst with a pore diameter of 4 nm produced higher selectivities to the desired product than Al-MCM-41 with 6.4- or 8-nm-diameter pores. However, naphthalenes are relatively small molecules, and therefore one would not ex-pect shape-selective properties of the catalyst with pores having a diameter of 4 nm. Indeed, this material had not only the highest selectivity, but also the highest activity for the O-methylation reaction, probably because of its

Table 2.4 Selectivities for the alkylation of benzene with 1-alkenes in the reactions catalyzed in solution (by AlCl$_3$) and on the solid consisting of AlCl$_3$ supported on MCM-41 *(442)*

Alkene	Catalyst[a]	Selectivity toward alkylbenzenes[b]		
		Mono[c]	Di	Tri
1-Hexene	Homog.	58.6	31.1	10.3
1-Hexene	Heterog.	79.9	20.1	–
1-Octene	Homog.	66.0	24.3	9.7
1-Octene	Heterog.	79.7	20.3	–
1-Decene	Homog.	68.5	22.5	9.0
1-Decene	Heterog.	91.1	8.9	–
1-Dodecene	Homog.	72.5	27.5	–[d]
1-Dodecene	Heterog.	96.2	3.8	–
1-Tetradecene	Homog.	70.1	29.9	–[d]
1-Tetradecene	Heterog.	98.5	1.5	–
1-Hexadecene	Homog.	77.5	22.5	–[d]
1-Hexadecene	Heterog.	>99.0	<1.0	–

[a]Homog.: homogeneous catalysis with AlCl$_3$ (0.15 mmol); Heterog.: AlCl$_x$ MCM-41 *(16)* (0.1 g of catalyst containing 0.15 mmol of AlCl$_x$).
[b]Determined by GC analysis of the product mixture.
[c]Exclusively linear alkyl benzenes.
[d]Nonvolatile product, not analyzed by GC.
10 mM of the respective alkene was added dropwise at room temperature over a period of 30 min to a vessel containing 1.65 g (20 mmol) of benzene and 0.1 g of the catalyst.
Adapted with permission from Elsevier.

relatively high density of active sites. The longer residence times in the pores relative to those characterizing the larger-pored catalysts might explain the greater occurrence of the undesired side reactions.

Even if no shape selectivity effects are exploited, acid–catalyzed reactions involving bulky molecules may be advantageous on OMMs. Bisphenol A, an important raw material in the synthesis of polymers, is a rather bulky molecule and is manufactured by the acid–catalyzed condensation of acetone and phenol. Although it can be synthesized with zeolite catalysts *(445)*, conversions on such catalysts were found to be inferior to those achieved with the porous sulfonic acid resin Amberlyst 15, probably because of diffusion limitations in the narrow zeolite channels or exclusion of the bisphenol A from the channel system. Heteropolyacids loaded onto MCM-41 were found to

be active for this reaction *(446)*. The best results obtained with modified silicas were reported for sulfonated MCM–41 and MCM–48 *(447)*. The catalysts were prepared by post–synthesis functionalization of the silica materials with 3-MPTS and subsequent oxidation to form sulfonic acid groups with H_2O_2. Catalysts with a medium loading of sulfur (approximately 1 meq g^{-1}) performed best and were almost as active as the sulfonic acid resin Amberlite 120 with a slightly superior selectivity to the desired p,p'-bisphenol A. Higher sulfur loadings were possible, but the catalysts were less active because in these cases not all the sulfur species could be oxidized to give sulfonic acid groups; it is probable that dimerization to give the disulfide, which is difficult to oxidize, had occurred.

A combination of the effect of high surface area and suitable surface polarity can promote the performance of the catalyst in this reaction even further. A sulfonic acid–functionalized CMK–5 ordered mesoporous carbon, CMK–5-SO_3H showed a phenol conversion of 8.9% with high selectivity of 84.0% to p,p'-bisphenol. Both conversion and selectivity for CMK–5-SO_3H were much higher than those obtained with sulfonated ethylene-bridged periodic mesoporous organosilica (EPMOpropyl-SO_3H) and sulfonated SBA–15 (SBA–15-CH_2CH_2aryl-SO_3H) under identical conditions *(448)*. Even more suitable for the reaction was a sulfonic acid–modified ordered mesoporous polymer comprising a phenolic resin *(449)*. In both cases, the improved performance was attributed to the lower surface polarity of the catalyst relative to the silica materials and the resulting favored adsorption of the reactants and exclusion of water.

For the synthesis of bisphenol F, which is the condensation product of phenol and formaldehyde, MCM–41 modified by post–synthesis with aluminum isopropoxide was found to have a high activity *(450)*. This catalyst was found to be superior to zeolite β, and its superiority was attributed to the fact that the reaction is catalyzed by acidic sites of medium strength; hence, the strongly acidic sites in zeolite β offered no additional benefit. Moreover, the larger pores of MCM–41 may contribute to the improved productivity. Like the zeolite, amorphous alumosilicate is characterized by a much lower activity than the MCM–41 catalyst, a point that was not addressed by the authors.

Superior performance of an MCM–41 catalyst relative to zeolite β was also observed in the cyclization of racemic citronellal to isopulegols *(451)*. Although both catalysts showed similar initial activities, the deactivation of zeolite β was much more rapid than that of the mesoporous catalyst. On both catalysts substantial amounts of organic matter accumulated during the reaction, and these caused the deactivation. It appears that the larger

pores of the MCM-41 can tolerate greater amounts of deposits than the zeolite before the pore system becomes inaccessible. When enantiopure (+)-citronellal was used as the reactant, the performance of the catalysts was comparable. The cause of the deactivation was therefore inferred not to be the reagent or the desired product, but most likely an impurity in the racemic citronellal.

SBA–15 modified with arenesulfonic acid was found to be highly active in Friedel–Crafts acylations with acetic anhydride as the acylating agent and anisole or 2-methoxynaphthalene as reactants *(407)*. The grafted arenesulfonic acid sites were more active than *p*-toluenesulfonic acid in the homogeneous reaction (as judged from the TONs, i.e., the number of molecules converted to product per catalytic site within a fixed reaction time—which can be interpreted as a measure of the average rate during the reaction time) and also more active than the sites on Nafion[®], although Nafion[®] overall was the best catalyst (per unit mass basis) as a result of its high density of acidic sites. However, the comparison of the materials may not reflect differences in intrinsic activity because of possible deactivation of the catalysts during the progress of the reaction in addition to possible mass transfer effects.

Motivated by the excellent catalytic properties of Nafion[®] for many reactions, researchers attempted to create "Nafion[®]-type" MCM-41 or SBA-15, that is, mesoporous silicas functionalized with the same type of groups as those present in Nafion[®]. These materials were characterized by high activities in the esterification reaction between ethanol and octanoic acid *(411)*. The catalysts comprising OMMs were superior to composites of Nafion[®] and amorphous silica; per site, the rate on the OMMs was about an order of magnitude higher. Mesoporous MCM-41 silica with Nafion[®]-type sites also showed high activity and selectivity for long-chain carboxylic acid esterification with ethanol and high-molecular-weight alcohols, with nearly 100% selectivity at conversions of more than 95% *(412)*. Furthermore, acylation of anisole was carried out with good conversion and high selectivity for the desired *para*-isomer, but deactivation by diaryl carbocations limited the reusability of the catalyst.

For both reactions, the new Nafion[®]/MCM-41 catalysts exhibited significantly higher activity than any of the previously reported hybrid inorganic–organic acid catalysts. The reason for this dramatic improvement in activity is unclear. An MCM-41/Nafion[®] composite prepared from tetraethoxysilane and Nafion gel solution with CTA surfactant was found to be a highly selective catalyst for α-methylstyrene dimerization to the corresponding

acyclic dimer *(415)*. As expected, MCM–41 itself (i.e., the silica material without Nafion® resin or any metals) showed no activity for this dimerization. The perfluorosulfonic acid Nafion® resin was supported on mesostructured SBA–15 materials by means of impregnation, whereby the resin content could be varied *(413)*. The optimal loading in a Nafion®/SBA–15 material was ca. 13 wt% Nafion®; this sample showed the best catalytic performance at a temperature of 150 °C and an equimolar ratio of anisole to acetic anhydride. The catalytic activity of this material was superior to those of other perfluorosulfonic acid-containing catalysts, such as the Nafion®-SAC-13 or the SFS material, which is prepared by reactive grafting of perfluoroalkylsulfonic acid precursors onto SBA–15 mesoporous silica. The local reaction environment created by the nearly complete filling of the mesopore system with acidic resin might be at the root of the improved performance.

An obvious effect of the pore size was observed by Hu *et al.* *(452)*, who investigated the isomerization of 1-heptene on MMS-supported vanadium catalysts (V–MCM–41, V–SBA–15 and V–TUD–1) with various pore structures and pore sizes, which were prepared by a post-synthesis grafting method using atomic layer deposition. The catalytic results showed a noteworthy effect of both pore structure and pore size on the catalytic performance in 1-heptene double bond isomerization. Larger pore materials effected higher conversions and produced lower *cis*-heptenes/*trans*-heptenes ratios. V–TUD–1, a mesoporous material with a 3D pore structure, gave a higher 2-heptene/3-heptene ratio than the 2D-structured V–MCM–41 and V–SBA–15. The highest conversion was achieved with the V–SBA–15 catalyst. It was found that higher vanadium content in SBA–15 resulted in a higher conversion, a lower 2-heptene/3-heptene ratio and a lower *cis*-heptenes/*trans*-heptenes ratio, while it led to a slight decrease in isomer selectivity. Catalyst stability tests indicated that V–SBA–15 exhibits the lowest deactivation rate and the least coke formation, which was ascribed to its having the largest pore diameter among this set of samples.

Considering the work that has been done regarding the application of OMMs in acid-catalyzed reactions, one infers that in specific cases such solids can be more suitable than other materials. However, it is necessary—as in the case of zeolites—to carefully tune the properties of the material to the desired application. In many cases, it is not clear from the reported data whether the optimum has been reached, be it with catalysts made from OMMs or from other types of solids.

Only a few cases of the use of MCM–41 and related materials in base-catalyzed reactions, such as Knoevenagel condensations, Michael additions,

or etherification reactions, have been described *(417,418,453–456)*. With respect to base catalysis, it is even more questionable than in the case of acid catalysis whether OMMs offer advantages, because a wide variety of other possible catalysts are available, and certainly not all of them have been tested as references. It is obvious that appropriately modified OMMs, for example Cs^+-exchanged forms, can be used in base-catalyzed reactions, but at present it seems that the potential for application is limited.

The strategy for grafting basic organic molecules to the pore walls may be considered as somewhat different from the approaches described here, and this topic is discussed in Section 4.2.1. One interesting concept to produce basic sites, however, is additionally mentioned in the present context, although no supramolecular templating is realized to create materials with narrow pore size distribution: Siliconimidonitrides can be synthesized in a porous form with narrow pore size distributions *(457,458)*. These materials are basic—as are materials obtained by nitridation of silica with ammonia at high temperatures—but more strongly basic sites can be generated by incorporation of alkali metals. Such materials are highly basic, catalyze double bond isomerization and side chain alkylation of aromatic molecules, and show shape-selective properties *(458)*. Regarding base-catalyzed reactions in general, it is emphasized that many of these reactions produce water, which can hydrolyze the basic sites and reduce the base strength.

4.2.2 Redox catalysis

Epoxidation reactions are among the most challenging reactions in catalysis. It was therefore considered a significant advance when it was discovered that TS-1, a titanosilicate with the MFI structure *(459)*, catalyzes the direct epoxidation of propene with H_2O_2 *(460)*. However, TS-1 suffers from the pore size limit of the MFI-structure, that is, molecules with a size exceeding roughly 0.55 nm cannot enter the pore system, so that the catalyst has a low activity for conversion of such molecules. For example, cyclohexene is not epoxidized by TS-1 *(461)*. Moreover, TS-1 cannot be used in combination with the more bulky *tert*-butyl hydroperoxide as an oxidant, and therefore, attention has been focused on the development of titanium-substituted, larger pore zeolites as epoxidation catalysts *(462,463)*. Some progress was made with the introduction of Ti-β zeolite *(463–466)*. Nevertheless, there is still strong interest in active and selective epoxidation catalysts with larger pore sizes.

Thus, titanium-modified MCM-41 was described relatively soon after the discovery of the parent material MCM-41 by two groups *(121,123)*. Corma *et al.* *(123)* reported a titanium-modified MCM-41 material with

a pore diameter of 2 nm, in which the titanium was incorporated in the silica framework. This catalyst selectively oxidized olefins and cycloolefins to give epoxides at low temperatures. Ti–MCM–41 samples showed a lower intrinsic activity and lower consumption of H_2O_2 for olefin oxidation than either Ti-β or Ti–silicalite. Ti–MCM–41 (synthesized in the absence of aluminum and consisting only of Si, O, and Ti) exhibited a high selectivity for the production of epoxides. For the oxidation of larger organic molecules, for example alpha–terpineol, which experience diffusion limitations even in large–pore zeolites such as Ti-β, the ordered mesoporous Ti–MCM–41 catalyst showed much better catalytic activity than the zeolites *(467)*.

Tanev *et al.* *(121)* described a soft–templating approach for the preparation of mesoporous silica–based molecular sieves partly substituted with titanium (designated Ti-HMS) by using a mixture of $Si(OC_2H_5)_4$ and Ti (iso–$OC_3H_7)_4$ as starting precursors and dodecylamine as a soft template. These materials exhibited high catalytic activity and selectivity in the oxidation of 2,6 *tert*–butyl phenol (DTBP) to the corresponding quinine and in the conversion of benzene to phenol. However, whereas TS-1, Ti-HMS, and Ti–MCM–41 were all effective catalysts for the direct hydroxylation of benzene, 2,6-DTBP could not be oxidized by TS-1 because of its small pores. Ti-HMS and Ti–MCM–41 redox catalysts, on the other hand, gave high conversions, which demonstrated the importance of mesoporosity in effecting the oxidation of the larger substrates.

Mandache *et al.* *(468)* investigated the epoxidation of a series of dibenzocycloalkenes with hydrogen peroxide on Ti-substituted MCM-41 and SBA-15 silica to evaluate the effects of the catalyst texture on both activity and selectivity to the epoxide. It was found that Ti-SBA-15 with 1.5 mol% Ti performed better than MCM-41 with the same titanium loading because of the SBA's larger pore size and the resulting facile diffusion of the dibenzocycloalkenes.

The large diameters of the pores of OMMs and the easy access to the interior surface facilitate further functionalization with various organic groups and metal complexes. Lin *et al.* *(469)* described how the titanium center can be activated by visible light when it is part of an oxo–bridged moiety covalently anchored to the pore surface of MCM-41. Metal-to-metal charge transfer (MMCT) is possible in such Ti–O–M moieties, with M = Cu(I) or Sn(II). In Ti-Sn(II)-MCM-41, the metal-to-metal electron transfer (from Sn^{2+} to Ti^{4+}) upon visible-light excitation was demonstrated by the EPR signal of Ti^{3+} at cryogenic temperatures. Activation of titanium centers by MMCT excitation of heterodinuclear moieties anchored to mesoporous silica

surfaces offers new opportunities for catalysis of demanding photochemical transformations previously limited to induction by UV light.

With their wide range of metal oxidation states and redox potentials, MMCT units can serve as tunable single photon and single electron pumps that drive catalytic reactions *(617)*. The aforementioned research group extended its work to an oxygen–producing photocatalytic unit anchored to MCM-41 mesoporous silica; this unit consisted of a single framework Cr (VI) center as a visible light-absorbing electron pump, coupled to an iridium oxide nanocluster *(470)*. Figure 2.16 shows the amount of O_2 evolved from an aqueous solution that was either free of $Na_2S_2O_8$ electron acceptor or contained it at a concentration of 0.01 M. No O_2 evolution was observed (i) in the dark, (ii) under illumination of Cr–MCM-41 that was free of Ir_xO_y, or (iii) under illumination of Ir_xO_y-MCM-41 that was free of chromium; these results demonstrate that water oxidation was driven by charge transfer-excited Cr(VI)–O coupled to iridium oxide clusters. These types of covalently anchored metal centers can serve as charge-transfer chromophores; they facilitate the use of visible light-induced charge transfer and allow variation of the redox potential by choice of various donor or acceptor metal combinations *(471)*.
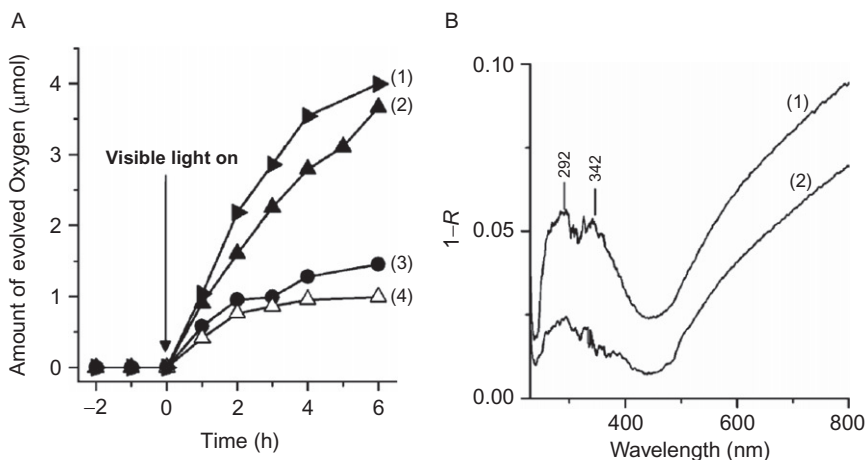

Figure 2.16 (A) Photochemical O_2 evolution from aqueous suspensions of Ir_xO_y-Cr-MCM-41 with Cr/Si ratios of (1), 0.01; (2), 0.02; and (3), 0.05 in the presence of 0.01 M $S_2O_8^{2-}$; (4) results of the experiment (Cr/Si ratio $=0.02$) in the absence of $S_2O_8^{2-}$; (B) Diffuse reflectance UV spectra of dehydrated Ir_xO_y-Cr-MCM-41(Cr/Si ratio $=0.02$) pellet after 6 h of O_2 evolution. (1) with and (2) without $S_2O_8^{2-}$ added. Experiments were conducted at a pH of 5.4 (buffer: KH_2PO_4 (1.1×10^{-2} M) and $Na_2B_4O_7$ (4.4×10^{-4} M)) *(470)*. *Adapted with permission from the American Chemical Society.*

Recently, immobilization of a chiral Mn(III) salen complex on modified mesoporous supports (MCM-41 and SBA-15) was reported *(472)*. The complex was attached to the surface by a covalent grafting method using 3-aminopropyltriethoxysilane as a reactive surface modifier. The supported catalysts showed higher chiral induction (ee, 68–71%) for enantioselective epoxidation of styrene and 4-chlorostyrene with aqueous NaOCl (12%) as an oxidant in presence of pyridine N-oxide (PyNO) as an axial base than their soluble counterpart (ee, 48%). The SBA–15-supported catalyst was found to be more active than an MCM-41-supported catalyst, and the difference was attributed to the larger pore diameter of the former. A promising strategy was described by Karimi *et al. (473)*, who functionalized SBA-15 with a bipyridylamide ligand, followed by complexation with Pd(OAc)$_2$ to afford the corresponding immobilized palladium catalyst shown in Figure 2.17. The TEM image of the catalyst, shown in Figure 2.17, does not give indications of any palladium particles inside the channels of the SBA-15 silica, suggesting that the palladium was molecularly dispersed. The palladium-containing catalyst was tested for the aerobic oxidation of various alcohols. The catalyst showed remarkable activity for the selective oxidation of various types of allylic alcohols by producing the corresponding α,β-unsaturated carbonyl compounds in excellent yields. The oxidation of primary aliphatic alcohols under the same conditions gave the corresponding esters in excellent yields, whereas the oxidation of secondary aliphatic alcohols gave only moderate yields of the corresponding ketones. Thus, this synthetic method demonstrated the benefit of a combination of an organic ligand and ordered mesoporous channels, resulting in a synergistic effect between the two
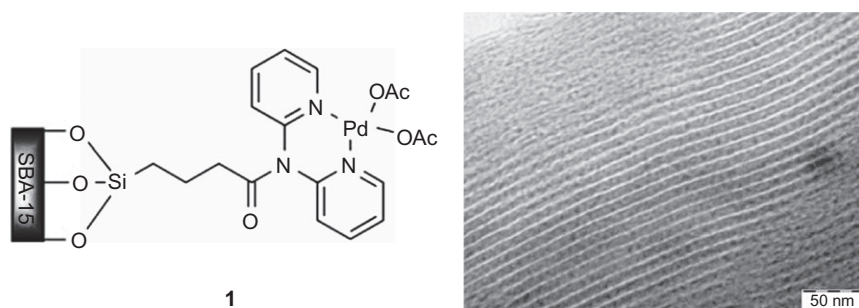

Figure 2.17 Structure (1) and TEM images of Pd-SBA-15 catalyst with the metal complex anchored perpendicularly to the ordered channels of the mesoporous silica *(474)*. The scheme suggests the mode of anchoring of the palladium complex on the internal and external surface of the silica. The TEM image shows the uniform structure of the OMMs without any indication for nanoparticle formation. *Adapted with permission from Wiley.*

components: enhancement of activity, prevention of the agglomeration of palladium species, and generation of a durable catalyst reflecting the advantages of the porosity and the structure of the silica support.

The examples discussed above represent only a small fraction of the literature of redox catalysis on OMMs. By doping a suitable OMM with an active component (such as metal nanoparticles), the application of this type of material as a catalyst can be extended to almost any type of redox reactions. However, in most cases, it is not clear whether the pore system and the tailored porosity of OMMs are the cause of better performance or other characteristics of the catalysts are responsible.

4.3. Crystallinity and structure stability

One of the greatest advantages of zeolites over ordered mesoporous silica is probably their crystallinity and structural stability, which play a critical role in many catalytic reactions. The amorphous state of most of the as-made mesoporous oxides, especially of the non-silica materials, limits their catalytic performance because of relatively poor thermal and mechanical stabilities. In contrast, crystalline materials have much better stabilities and commonly have superior catalytic properties, which originate from their more homogeneous surface and bulk structures or the presence of defined lattice defects. Higher crystallinity in solids might also provide higher photocatalytic activity, because photo-excited electron–hole pairs can be transferred to the surface at a higher rate, which reduces the recombination rate of the electron and the hole (473).

The crystal structure and the crystallinity of OMMs can be controlled to a certain extent by varying the synthetic pathway. When soft-templating methods are used to prepare OMMs, the product is usually an amorphous material because of the low decomposition temperature of the template and the tendency of many oxides and oxyhydrates to first precipitate as amorphous solids. In contrast, hard-templating pathways are more suitable for the formation of crystalline OMMs. Alternatively, some post-treatments are described that allow crystallization of initially amorphous materials, prepared by using a soft-templating method, without loss of the mesostructure. An example was reported by Katou *et al.* (475). First, a hexagonally ordered mesoporous niobium–tantalum (Nb:Ta ∼ 1:1) mixed oxide with a non-crystalline wall was synthesized with P-123 as a soft template. Subsequently, the strategy presented in Figure 2.18 was pursued (288). The pores of the OMM were filled with furfuryl alcohol that was later polymerized and carbonized. Filling the
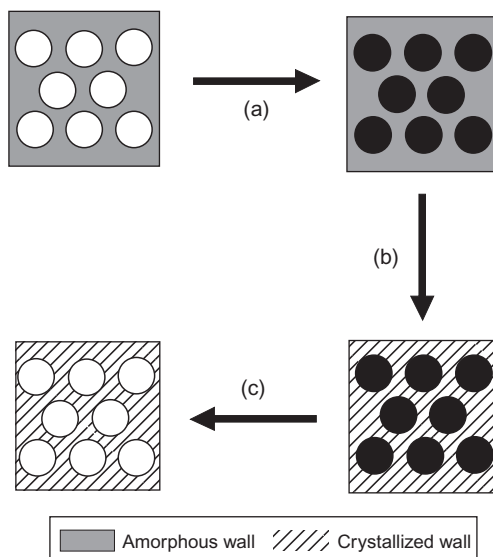
| Amorphous wall | ///// Crystallized wall |

Figure 2.18 Schematic illustration of the synthesis of mesoporous niobium–tantalum oxide with 2D hexagonally ordered mesoporous structure and crystalline walls. (a) Accumulation of polymerized furfuryl alcohol and subsequent carbonization at 550 °C in vacuum. (b) Crystallization of walls at 650 °C in a helium atmosphere. (c) Removal of carbon by calcination at 500 °C in air *(288)*. *Adapted with permission from Wiley.*

pores of an OMMs increases its thermal stability. Thus, during a high-temperature treatment step, the amorphous walls were transformed to crystalline walls without destruction of the mesostructure. By removal of the carbon, crystalline ordered mesoporous niobium–tantalum oxide was obtained.

The preparation and crystallization of mesoporous Ta_2O_5 by reinforcement of the amorphous mesoporous framework with SiO_2 was described by Noda *et al.* *(476)*. The crystallized sample was shown to be an efficient photocatalyst for overall water splitting under UV light irradiation with NiO_x, RuO_2, or $Rh_{2-y}Cr_yO_3$ as a co-catalyst. Following crystallization, the photocatalytic activity of the NiO_x-loaded semiconductor mesoporous Ta_2O_5 was improved by nearly an order of magnitude relative to that of the amorphous form. This higher catalytic activity was attributed to efficient transfer of excited electrons and holes from the interior of the material to the exterior surface of the catalyst through the thin-walled crystalline phase *(473)*.

The surface properties of hexagonally ordered mesoporous Nb_2O_5 with amorphous and crystalline walls were characterized with water adsorption–desorption isotherms and IR spectroscopy *(477)*. The surface

of the amorphous sample was found to be hydrophilic, and the surface OH groups were acidic. In the case of crystalline mesoporous Nb_2O_5, the OH groups were non-acidic and the pores were less hydrophilic. The effects of the different surface properties were compared in the oxidation of cyclohexene by aqueous H_2O_2 in various co-solvents. A high selectivity of 95% for 1,2-epoxycyclohexane was obtained in methanol as the solvent at 40 °C when crystalline mesoporous Nb_2O_5 was the catalyst and the conversion was 12%. In contrast, amorphous mesoporous Nb_2O_5 showed a moderate selectivity of 68% for 1,2-cyclohexanediol in acetonitrile as the solvent at 60 °C at a conversion of 22%. The differences between amorphous and crystalline materials with regard to the selectivity for oxidation of cyclohexene in the respective solvents were ascribed to the different acidic properties of the surface OH groups and the differing degrees of hydrophilicity of the materials brought about by crystallization.

Highly crystalline, mesoporous anatase thin films on various substrates such as quartz and fluorine-doped tin oxide (FTO) were synthesized by using carbon inclusion to stabilize the framework during thermal crystallization in an approach resembling that introduced by Tang *et al.* (349). Amorphous TiO_2 was prepared by using P-123 as soft template, which was either removed by calcination at 300 °C for 2 h or left in the precursor as an additional carbon source. The samples were designated as $C-TiO_2$ and $C-P-123-TiO_2$, respectively. Furfuryl alcohol was allowed to diffuse into the mesoporous or the mesostructured TiO_2 films as either the sole carbon precursor or a second carbon precursor. Subsequent carbonization and crystallization of the titania walls was carried out under vacuum at various temperatures. Finally, the carbon was burned in air and a mesoporous material with crystalline titania walls was obtained. Control samples, for which the carbon stabilization was omitted, were prepared at each temperature as well. The TiO_2 thin films were characterized as photoanodes by measuring the zero-bias photocurrent for water photolysis using a xenon lamp in the temperature range of 400–600 °C. It is known that the crystal phase, crystallinity, particle size, surface states, and surface area affect the photocatalytic properties. As shown in Figure 2.19, at low calcination temperatures of 400 °C, at which crystallization-induced stresses were not sufficient to destroy the mesoporous framework, all $C-TiO_2$, $C-P-123-TiO_2$, and further control samples were characterized by comparable photocatalytic activities. Significant differences arose after calcination at higher temperatures. The highest of all the efficiencies was 2.5%, observed for $C-TiO_2$ after calcination at 500 °C. This value is 4 times higher than that characterizing a control sample that had comparable crystallinity, and it is
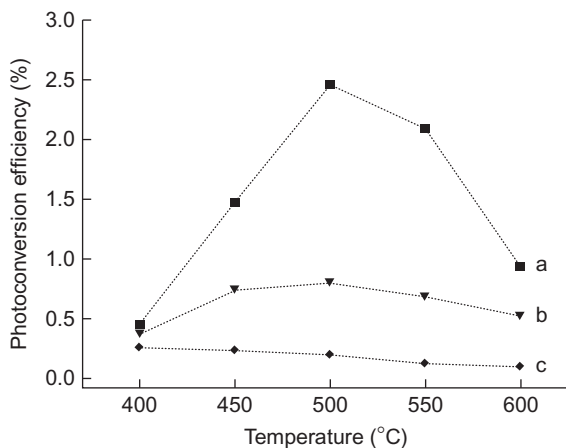
Figure 2.19 Effect of calcination temperature on photoconversion efficiencies of (a) C–TiO$_2$, (b) control, and (c) C–P-123–TiO$_2$ samples at zero-bias and illumination of 40 mW cm^{-2} *(349). Adapted with permission from the Royal Society of Chemistry.*

10 times higher than that of a sample with a similar pore structure, C–P-123–TiO$_2$. These results demonstrate the combined advantages of mesostructural ordering and crystallinity for the photocatalytic properties of TiO$_2$; the main effect can be ascribed to the large accessible surface area in the ordered sample. Efficiencies of both C–TiO$_2$ and the control samples increased with increasing calcination temperature up to 500 °C and declined after treatment at higher temperatures. This behavior is consistent with the trend of the crystallinity; as the crystalline fraction in the material increases with increasing temperature, the photocatalytic properties are first improved (because good crystallinity facilities charge transfer), but then the mesopore system eventually collapses as a result of poor thermal stability. Significantly lower values were observed for C–P-123–TiO$_2$, primarily because of the amorphous nature of the framework.

Ismail *et al. (478)* reported that palladium-doped hexagonally ordered mesoporous TiO$_2$ is characterized by 2.5 times higher HCHO formation rate in the photooxidation of CH$_3$OH than palladium photo-deposited on commercial Sachtleben Hombikat UV-100. The key to this success was attributed to Pd/TiO$_2$ networks with ordered mesopores, which provide channels for fast transport of the methanol molecules. The highest photocatalytic activity for the oxidation of methanol (Figure 2.20) was achieved with TiO$_2$ that has high crystallinity as a result of high-temperature calcination. These data also reflect the good charge carrier transport properties that are provided by highly crystalline anatase.
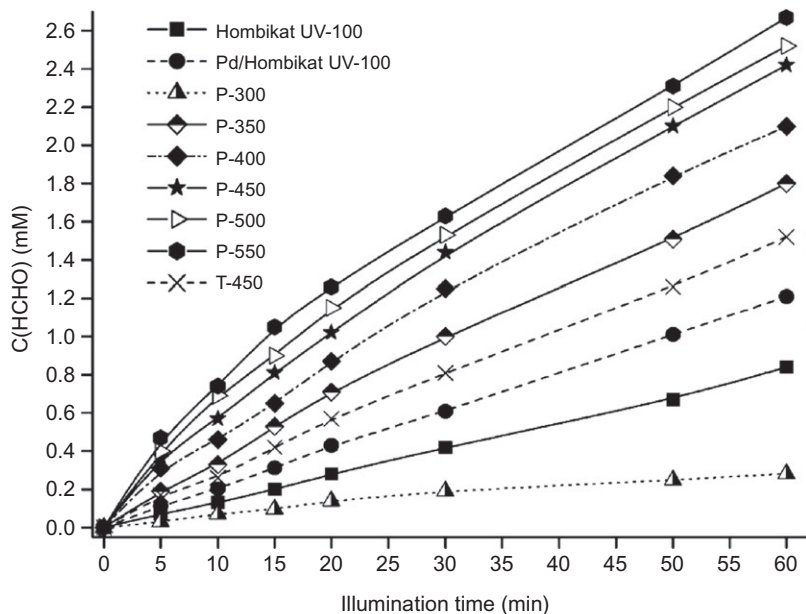
Figure 2.20 HCHO concentration during photooxidation of methanol on mesostructured Pd/TiO$_2$ calcined at temperatures of 300, 350, 400, 450, 500, and 550 °C and Pd/Hombikat UV-100 photocatalysts as a function of illumination time *(478)*. Data characterizing palladium-free reference samples Hombikat UV-100 and mesostructured TiO$_2$ ("T-450") are also shown. *Adapted with permission from the American Chemical Society.*

In summary, all of these findings suggest that the crystallinity of OMMs, which can be controlled to some extent because of the flexible synthesis conditions, plays a critical role in determining catalytic properties of these materials, especially in photocatalytic processes.

4.4. Concave surfaces

For applications in catalysis, the surface chemistry of OMMs is of particular interest. One attribute that may influence the surface properties is the geometry. In general, three types of geometry can be encountered; they are convex surfaces (e.g., those of the spherical particles of fumed silica), concave surfaces (e.g., those of the cylindrical pores of porous silicas such as MCM-41 or SBA-15), and planar surfaces (e.g., those of silicon wafers, glass plates, or quartz crystals), as shown in Figure 2.21 *(479)*. These are idealized pictures; in most materials, various types of surface geometry may be present at the same time. For example, in silica gel there are convex surfaces
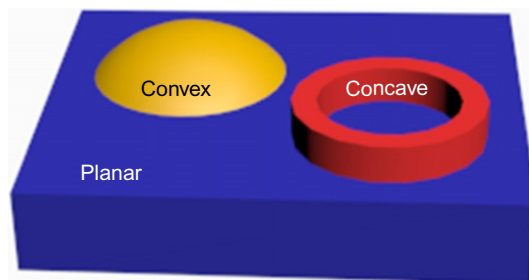
Figure 2.21 Prototypical surface geometries of materials: planar (faces of block), convex (top of spherical cap), and concave (inside of ring).

characterizing the spherical particles, which are the main building blocks of the gels, and concave surfaces in the neck regions, where the spherical particles are connected to each other. OMMs are somewhat exceptional in this respect, because their well-defined mesostructures often lead to a predominance of only one type of surface geometry. Whereas curvatures on the macroscopic scale are not expected to have consequences for catalytic reactions because of the much smaller dimension of a typical active site, the geometry of surfaces on the nanometer size scale may influence the reactivity of surface sites.

The geometry on the nanometer scale affects the spacing between supported moieties, which can, for example, be individual tethered organic species or the interlinked units in polyoxometallates. Depending on the curvature, the packing of these active moieties may vary, which will affect the interaction between active species and support, or between the attached active units.

Buchanan and coworkers *(480,481)* investigated the effect of pore confinement and molecular orientation on mesoporous MCM–41 (with two different pore diameters: 1.6 and 2.8 nm) and on nonporous Cab-O-SIL$^{®}$ silica—which has a convex surface curvature—for hydrogen transfer in the free-radical pyrolysis of 1,3-diphenylpropane (DPP). Two-component mixtures of DPP and 3-fluorene (3–FL) or 2-fluorene (2–FL) were anchored to the surface of the MCM–41 and Cab-O-SIL$^{®}$ silica, as illustrated in Figure 2.22. The difference between 2–FL and 3–Fl spacers in the catalysis, which requires hydrogen transfer, is striking. The catalytic data indicate that the reaction rate was slightly enhanced by a factor of 1.1 in the MCM–41 (2.8 nm pore diameter) compared with the rate on Cab-O-SIL$^{®}$ for the combination DPP and 2–FL. A small further rate increase was observed in the smaller pores of MCM–41 (1.6 nm pore diameter). However, when
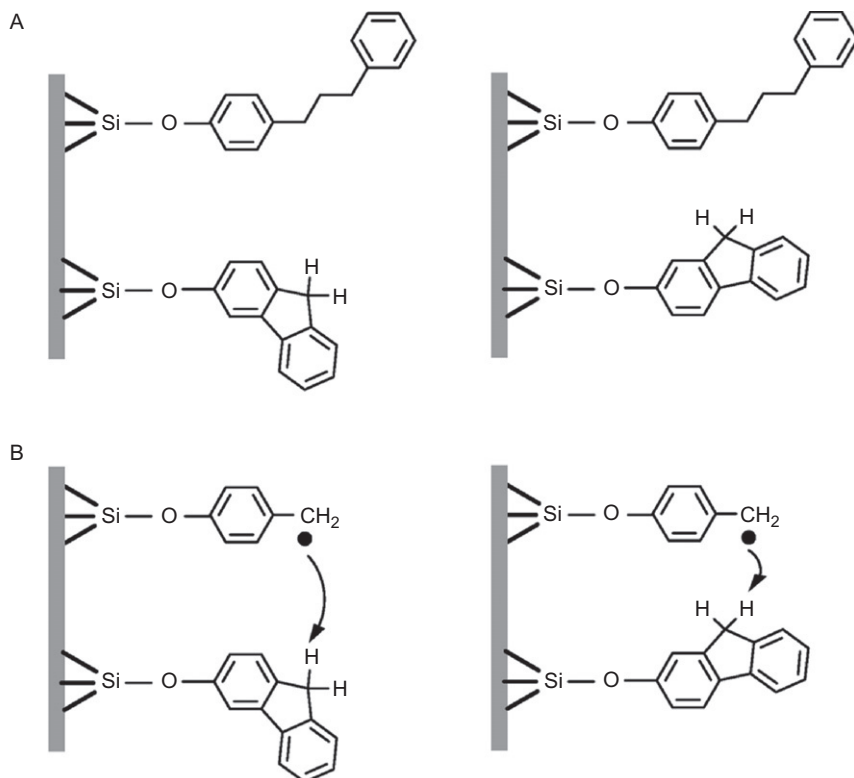
Figure 2.22 (A) Adjacent location of reactant 1,3-diphenylpropane and hydrogen acceptor 3-fluorene (left) and 2-fluorene (right) spacer molecules in the confines of a pore of MCM-41. (B) Key hydrogen transfer step requiring adequate molecular orientation *(480)*. *Adapted with permission from the American Chemical Society.*

DPP and 3–FL were combined, the reaction rate increased by a factor of 2.21 for the MCM–41 with 2.8–nm pore diameter and by a factor of 3.27 for the 1.6–nm pore diameter relative to the values characterizing the Cab-O-SIL® support. The superior catalytic activity was attributed to the concave surface curvature of the MCM–41, which facilitates the orientation of the spacer group and allows the hydrogen transfer *(482)*.

A post–synthesis grafting method with 3–aminopropyltriethoxysilane (3–APTES) was used for the functionalization of silica gel and ordered mesoporous silica materials (SBA–15 and MCM–41). Vanadyl cations were immobilized on the surfaces via the amino groups, and the resulting materials were used as catalysts for the oxidation of cyclohexane in the liquid phase *(483)*. Catalytic activity and metal–leaching investigations showed that catalysts made by immobilizing vanadium on mesoporous solids were more

active and stable than a silica gel–supported vanadium catalyst and a framework–substituted V–MCM-41 catalyst. The higher activity and stability of the immobilized vanadium catalysts were attributed to the isolation of the active metal sites, as well as to the spatial restrictions caused by the concave silica surfaces of the mesoporous solids, as contrasted to the convex silica surfaces of the silica gel sample *(483)*.

The anchoring of chiral organometallic complex catalysts in the pores of OMMs may lead to noteworthy changes of the catalytic properties of the complexes as a result of additional restrictions brought about by the pores. If the pore size distribution is narrow, all the anchored species should experience approximately similar restrictions. Because the reactant interacts with both the pore walls and the chiral directing group, the interaction is distinctly different from that experienced if the chiral catalyst were free, as in a homogeneous reaction *(484)*. Figure 2.23 shows an example of the promotion of enantioselectivity resulting from the tethering of an asymmetric catalyst to a concave surface *(485)*. When the hydrogenation of (E)-α phenylcinnamic acid was performed with the same complex (Rh^{I}-(S)-(−)-2-amino-methyl-1-ethyl pyrrolidine) tethered either to a concave or to a convex silica support, the differences in catalytic results, mainly in terms of enantioselectivity, are remarkable. Indeed, the chiral induction, causing *ee*
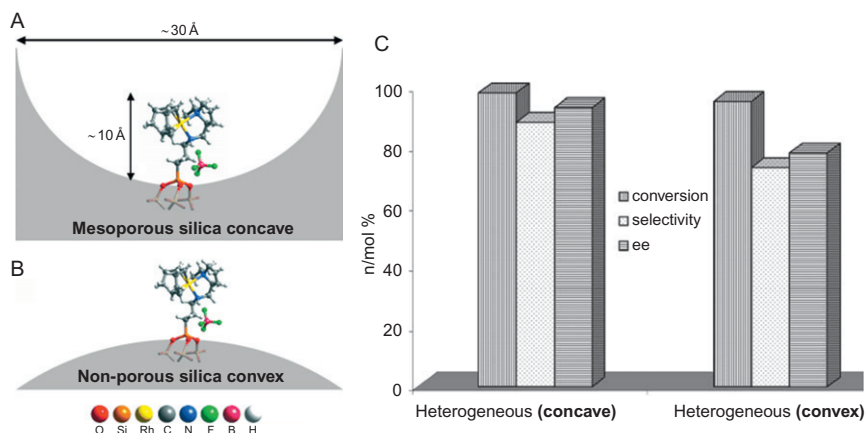
Figure 2.23 Graphical model (to scale) showing the constraints of the catalyst anchored to (A) MCM-41 (concave) and (B) Cab-O-SIL® silica (convex) surfaces. Enantioselectivity is higher for a given anchored chiral organometallic catalyst (in this case [Rh(1,5-cyclooctadiene) (1R,2R)-(+)-1,2-diphenylethylenediamine]BF$_4$) when it is attached to a concave rather than to a convex silica surface (C) *(485,486)*. *Adapted with permission from Wiley, Springer.*

values higher than 95%, is maximized when the complex is anchored to the concave silica surface, and when there is a close interaction between the re-actant and the chiral moiety as well as between the reactant and the pore walls. To attain this effect, both the concave pore geometry and a well-adapted pore size are required.

4.5. Control of active phase dispersion and morphology by pore and space constraints

One of the properties unique to OMMs is their uniform and tunable pore size distribution, which allows the homogenous dispersion of an active phase in this matrix. The resulting solid can be used as a catalyst for a variety of reactions. With the aid of the pore constraints of OMMs, the particle size of a supported active phase can be controlled in a straightforward manner. As discussed in the preceding section, the concave surfaces of OMMs may also play an important role in deposition and confinement of nanoparticles. Nanoparticles that are deposited on concave surfaces are expected to be thermally more stable than those on flat or convex surfaces because they have a larger interface with the support than the latter.

Immediately after the discovery of the hexagonally OMMs MCM-41 and MCM-48, these materials were mainly investigated as catalysts for acid-catalyzed or oxidation reactions. However, after a short time, MCM-41 and related materials started to attract attention as support materials. This interest was based on their high thermal stability (up to 1000 °C), porosity, narrow pore size distribution, and high surface area (up to 1500 $m^2\,g^{-1}$). The most widely used method for the introduction of metal oxides (which are commonly used as precursors of supported metals) into mesoporous solids is wet impregnation with a solution of a thermally unstable precursor salt. During drying and calcination, oxide particles are formed in the host structure. An alternative method applied for dispersion of a second phase in the silica structure involves the use of organometallic precursors that react as bases and therefore can be grafted onto the surface of the silica. The protons of the silanol groups, which are normally present in abundance on the internal surface area of the ordered mesoporous host, are substituted by a fragment of the organometallic precursor. The grafting procedure itself typically results in molecularly dispersed species, but calcination often leads to formation of oxide particles in the pore system of the host material. Although the dispersion of the metal oxide is generally high and mainly determined by the area density of silanol groups, often only lower loadings of the catalytic species are attained, which is a disadvantage of this method in

comparison with wet impregnation. Moreover, many of the precursors are moisture and air sensitive, and one has to work under dry, air-free conditions. Furthermore, grafting procedures typically involve more complex and expensive precursor species than impregnations. Further possibilities for incorporation of active components into mesoporous structures are solid state exchange or loading via the gas phase with a volatile precursor and subsequent calcination (CVD and ALD).

Corma et al. (487) reported one of the first examples of the use of MCM-41 as a support. They investigated the performance of nickel–molybdenum sulfide ("Ni–Mo") supported on MCM-41 alumosilicate for mild hydrotreating of a vacuum gas oil. The catalyst supported on MCM-41 performed better than those supported on amorphous silica or zeolite USY, and the advantage was attributed to the higher surface area and higher thermal stability of the catalyst, as well as the presence of uniform pores in the mesopore range that allow a fine and homogeneous dispersion of the Ni–Mo sulfide nanoparticles.

In a similar investigation by the same group, platinum nanoparticles were deposited in a MCM-41 silica matrix and tested for the catalytic hydrogenation of aromatics in diesel fuels. It was shown that MCM-41 materials with very high surface area and a regular arrangement of uniform mesopores are excellent supports for highly dispersed platinum catalysts. These catalysts exhibited, as did those supported on mesoporous amorphous silica–alumina, much better catalytic activity for the hydrogenation of naphthalene at moderate temperatures than conventional platinum catalysts with supports such as commercial amorphous silica–alumina, silica, γ-alumina, and zeolite USY (488).

Precise and controllable material preparation and thorough characterization leading to an understanding of the interactions between the host and the catalytically active component are expected to facilitate the optimal exploitation of the unique properties of OMMs. In an early attempt to develop an understanding of how the preparation variables affect the structure of a catalyst consisting of metal nanoparticles in a structured mesoporous solid, Junges et al. (489) investigated platinum supported on MCM-41. They prepared the catalysts by various methods, including (a) direct introduction of a platinum precursor during the synthesis of the MCM-41; (b) incipient wetness impregnation; and (c) ion exchange. The catalytic activities of the materials were determined for low-temperature CO oxidation. The achievable platinum loadings were found to depend on the preparation method and the precursor (a neutral or a charged platinum complex). Ion exchange resulted in a maximum platinum loading of approximately 1 wt%, but when

platinum was introduced in the synthesis gel, about 80% of the precursor $[Pt(NH_3)_2Cl_2]$ was incorporated in the catalyst. When $[Pt(NH_3)_4]^{2+}$ was used as a precursor, 30–50% incorporation was achieved. The incorporation of $[PtCl_6]^{2-}$ was dependent on the amount used: for high target loadings of approximately 5 wt%, about 50% of the platinum was incorporated, whereas when the target loading was 1 wt%, only 15% of the platinum was incorporated. The platinum particle sizes were found to depend on the preparation method. When the platinum was incorporated directly in the synthesis gel, the average platinum particle diameter (determined by XRD line broadening) was about 6 nm. TEM images showed that smaller (4-nm diameter) nanoparticles were located in the MCM-41 pores and larger ones on the external surfaces or at defects of the MCM-41 particles. The average particle diameters of the platinum crystallites prepared from the charged platinum precursors were greater than these, up to about 10 nm. The nanoparticles in the samples prepared by ion exchange were also about 10 nm in diameter. The incipient wetness impregnation resulted in a bimodal platinum nanoparticle size distribution, with large platinum particles (with diameters of about 20 nm) present along with nanoparticles having diameters of only about 2 nm. The distribution of the particle sizes was tuned by changing the platinum loading: At platinum loadings exceeding 4 wt%, the number of 2-nm-diameter particles per unit volume was almost independent of the loading, but as the platinum loading increased, the fraction of large particles located outside the mesopores increased. But when the loading was reduced to 2 wt%, the number of smaller nanoparticles per unit volume decreased as well, although larger particles still existed even at these relatively low loadings.

As shown in Figure 2.24, the least active of these catalysts were the ones synthesized by ion exchange, corresponding to the relatively large average platinum particle size. These catalysts gave CO conversions of 50% at about 127 °C ("T_{50}") with deviations of only about ±5 °C reflecting the variations in the conditions of the ion exchange. The catalysts obtained by incorporation of the platinum species via the synthesis gel were characterized by a value of T_{50} of about 102 °C, again with only small deviations within this group. However, the temperatures required for 50% conversion with the catalysts prepared from the neutral platinum complexes were found to be lower by about 5 K relative to the values observed when the charged species were used in the catalyst preparation, again in agreement with the platinum particles sizes. The best performance was achieved with the catalysts prepared by the incipient wetness method, with T_{50} being as low as 87 °C.
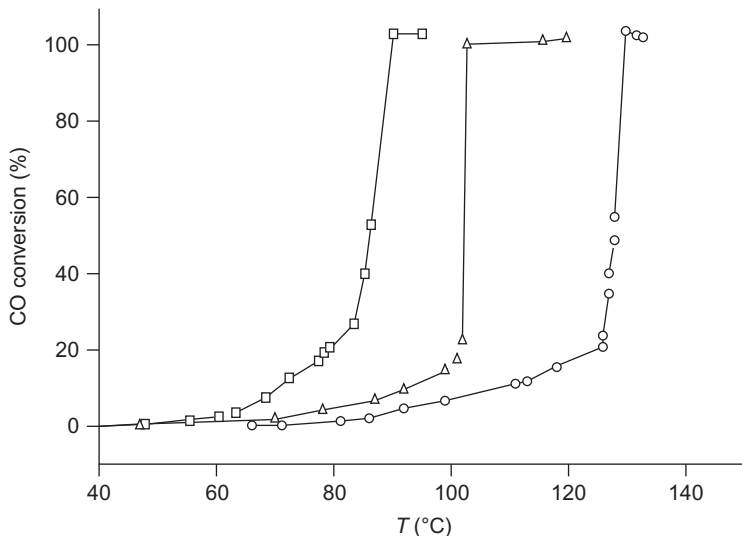
Figure 2.24 Catalytic activity of platinum supported on MCM-41 for CO conversion; the catalysts were prepared by the incipient wetness method (□), ion exchange (△), and incorporation of the precursor during the synthesis of the MCM-41 support (○) *(489)*. *Adapted with permission from the Royal Society of Chemistry.*

The high activity was attributed to the small platinum nanoparticles (with diameters of approximately 2 nm) that were incorporated in the pores of the MCM–41 support.

This investigation highlights the importance of the strategy for incorporation of the nanoparticles into the silica matrix. The preparation method affects the loading and dispersion of the active phase, both of which influence the catalyst performance. In a later investigation by the same group *(490)*, preformed metal colloids were loaded onto OMMs by various methods. The colloids were incorporated in the pores and retained their small sizes.

At the end of the 1990s, researchers made substantial efforts to design and apply modified mesoporous MCM-41 with active species attached to the framework *via* host–guest interactions, and they created materials characterized by isolated and uniform catalyst sites on the inner walls of the pores. Mehnert and Ying *(491)* reported the synthesis of palladium catalysts supported on MCM-41; the catalysts were synthesized by vapor deposition of a volatile palladium complex onto the interior walls of the porous framework, followed by reduction. The resulting solid was investigated as a catalyst for Heck reactions, and it had high activity and selectivity. The grafting

process used in the catalyst synthesis, which had the aim of coating the internal surfaces of the pores with a highly dispersed metal was found to be strongly dependent on the properties of the volatile metal complex and the reaction conditions. The grafting of palladium onto degassed silica–based MCM–41 was carried out by sublimation of the volatile organometallic complex $[Pd(\eta\text{-}C_5H_5)(\eta\text{-}C_3H_5)]$ under vacuum through a bed of the porous support. Following the deposition of the palladium complex on the interior pore surface, the palladium was reduced in flowing H_2, producing an air-stable, black powder. The palladium content was controlled between 10 and 30 wt% by changing the mass of the volatile complex relative to the mass of MCM–41. The supported palladium catalysts were found to catalyze the Heck carbon–carbon coupling reaction of aryl halides, and the activity of the catalyst was greater than that of commercial Pd/Al_2O_3, Pd/SiO_2, and $Pd/$carbon (each containing about 10 wt% palladium). This new class of Heck catalyst is characterized by high activity, facile synthesis, and high stability. The high volatility of the precursor, the high surface area of the support, and the accessibility of the interior pore space all favor a uniform distribution of discrete metal complexes in the catalyst (without cluster formation).

The reduction of air pollutants is one of the most rapidly increasing applications in catalysis. The reduction of NO_x is a particularly important reaction, because NO is present in the effluent streams from power plants, waste incinerators, and diesel and lean-burn automotive engines. Various transition-metal-containing MCM–41 catalysts were shown to be competitive with transition-metal-containing microporous molecular sieves as catalysts for the reduction of NO_x with hydrocarbons. Schiesser *et al.* (492) reported the loading of MCM–41 with rhodium, cobalt, or platinum nanoparticles by incipient wetness impregnation with aqueous solutions of $Rh(NO_3)_3$, $Co(NO_3)_2$, or $PtCl_4$. After the incorporation of the metal, each catalyst was calcined in air at 550 °C for 3 h to obtain the corresponding metal or metal oxide nanoparticles, the size of which was limited by the pore size of the silica matrix. It was found that platinum supported on siliceous MCM–41 was the most active catalyst, even more active than a corresponding catalyst with a dense metal oxide support. The superiority of the Pt/MCM–41 catalyst might be related to the uniform porosity and pore size distribution of the support, which favors a high dispersion of the metal nanoparticles.

Researchers have devoted significant effort to CO oxidation catalyzed by gold, and this reaction is frequently considered to be a model for investigations of metal–support interactions or it is used to illustrate the high activities

of gold–containing catalysts. Gold nanoparticles on oxide supports are among the most attractive catalysts for low-temperature CO oxidation *(493–496)*. Space and size constraints of OMMs can facilitate the preparation of uniform gold nanoparticles by affecting their size and dispersion. The synthesis of an active gold catalyst with approximately 4.5 nm particle diameter dispersed on SBA-15 was reported by Yang *et al. (497)*, who used the following deposition strategy. The surface of SBA-15 was functionalized with positively charged groups by using *N*-trimethoxysilylpropyl-*N,N,N*-trimethylammonium chloride, and then $[AuCl_4]^-$ species were incorporated into the channel system by ion exchange. Reduction with $NaBH_4$ gave highly dispersed gold nanoparticles in the channels of the mesoporous silica. A CO oxidation rate of $2.7 \times 10^{-4} \text{mmol g}_{cat}^{-1} \text{s}^{-1}$ was observed. The catalyst had a higher activity than any other Au/SiO_2 material made by a solution technique—these have almost no activity at room temperature. It was concluded that because the gold particles were essentially isolated from the support by the organic coating of the channels, metal–support interaction is highly improbable as an explanation of the high catalytic activity of the gold. The results indicate that OMMs can be used as hosts and that a specific interaction between gold and the support is not necessary for the generation of highly active gold catalysts. Following this investigation, other gold nanoparticles with various sizes supported on OMMs that show high catalytic activities in CO oxidation were reported *(498–506)*.

With growing worldwide demand for petroleum products, significant attention has been given to upgrading heavy and residual oils to middle distillates. The potential of ordered mesoporous silica-supported Co–Mo catalysts for the hydrodesulfurization (HDS) of petroleum residues was investigated by Reddy *et al. (507)*. Mesoporous MCM-41 with a SiO_2/Al_2O_3 ratio of about 41 was impregnated with $Co(NO_3)_2 \cdot 6H_2O$ and $(NH_4)_6Mo_7O_{24}$, followed by calcination and sulfidation. The catalytic results obtained with these solids were not as good as those obtained with commercial sulfided $Co–Mo/Al_2O_3$. The lack in performance was attributed to the small pore diameter of MCM-41 (2.8 nm), which is not large enough for allowing facile access of bulky molecules such as asphaltenes.

After the discovery of SBA-15, which has larger pores than MCM-41, conversion of larger molecules became possible. A variety of nanoparticles were incorporated into mesoporous SBA-15 silica *(314,508–524)*. Rioux *et al. (525)* supported platinum on SBA-15 and investigated the effect of the platinum particle size in room-temperature ethylene hydrogenation and ethane hydrogenolysis. They synthesized platinum nanoparticles with

diameters in the range of 1.7–7.1 nm by alcohol reduction methods and in-corporated them into mesoporous SBA-15 silica with a 9 nm pore diameter using a low-power sonication. The pore size of the SBA-15 restricted the growth of the platinum particles. After drying, calcination and reduction in H_2, surfactant-free platinum nanoparticles on the mesoporous silica were obtained, as shown in Figure 2.25. The catalytic data characterizing ethylene hydrogenation indicate that the reaction is structure-insensitive with particle diameters between 1.7 and 3.6 nm. The hydrogenolysis of ethane on

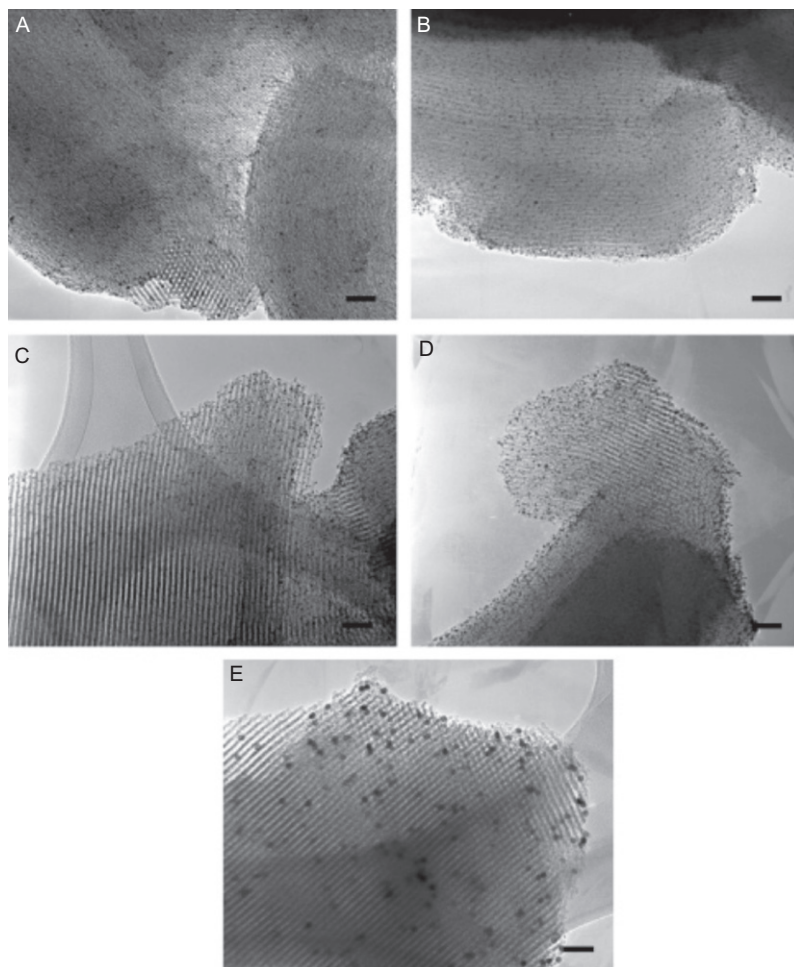**Figure 2.25** TEM images of Pt(X)/SBA-15 catalysts with the particle diameter (nm) X be-ing: (A) 1.7, (B) 2.6, (C) 2.9, (D) 3.6, and (E) 7.1. The scale bars are 20 nm long *(525)*. *Adapted with permission from the American Chemical Society.*

platinum particles with diameters ranging from 1.7 to 7.1 nm was found to be weakly structure-sensitive, with smaller particles exhibiting higher specific activities. Turnover rates for ethane hydrogenolysis were enhanced with increasing metal dispersion, suggesting that coordinatively unsaturated metal atoms, present in small particles, are more active for hydrogenolysis than the low-index planes that dominate in large particles. The catalysts showed excellent thermal stability, which is probably ascribable to the confining pore system.

The synthesis method used for these catalysts is generally applicable. Thus, various metal–support combinations can be realized and used to investigate correlations of activity and selectivity with structure and size. Thus, the same research group *(509)* reported monodisperse rhodium and platinum nanoparticles as small as ~ 1 nm in diameter that were synthesized from precursors stabilized with a fourth-generation polyaminoamide (PAMAM) dendrimer (a hyperbranched polymer) in aqueous solution and then immobilized by deposition on a high-surface-area SBA-15 mesoporous support. The catalytic activities of the SBA-15-supported rhodium and platinum nanoparticles for ethylene hydrogenation were investigated. Catalysts were active without removal of the dendrimer cap, but reached their highest activities only after reduction in H_2 at a moderate temperature (150 °C). The high surface area and uniform porosity of the silica support facilitate the preparation of nanoparticles with uniform dispersions and preserve the small particle through treatments at elevated temperatures, and these are significant benefits for further catalytic investigations involving small nanoparticles.

In Fischer–Tropsch catalysis, the size of the metal particles influences their performance *(526)*. It thus comes as no surprise that researchers have tried to exploit the confining pore system of OMMs to control the particle size of typical Fischer–Tropsch catalysts, with most efforts directed towards cobalt. Khodakov *et al. (524)* evaluated the effect of the mesoporosity of several silica supports, including SBA-15 and MCM-41, on the activity and selectivity of catalysts for this reaction. They found that cobalt particle size and reducibility were strongly dependent on the pore diameter of the support. Smaller pore sizes resulted in smaller cobalt oxide nanoparticles, which were more difficult to reduce than larger ones. Catalytic activity and C_{5+} selectivity increased with increasing support pore diameter. The catalytic activity of SBA-15-supported cobalt was 5–10 times greater than that of MCM-41-supported cobalt with the same cobalt loading *(527)*, commensurate with the larger pore size of the SBA-15.

Another investigation of the effect of pore size on the performance of Fischer–Tropsch catalysts was reported by Xiong et al. *(528)*. They prepared Co/SBA-15 (with 30 wt% cobalt) by incipient wetness impregnation using a series of SBA-15 silicas with various pore sizes. After reduction, cobalt particles were found to be distributed on both the exterior and interior surfaces of the support. In comparison with the catalysts with smaller pores, larger pore catalysts had more adsorption sites for CO (both terminally and bridge-bonded CO). SBA-15 with larger pores induced the formation of larger cobalt clusters with lower dispersion and better reducibility than supports with smaller pores, and they also adsorbed more CO. With increasing pore size of SBA-15, the CO conversion first increased and then decreased, in line with the maximum of activity at intermediate cobalt particle sizes reported in many investigations. The catalysts with larger cobalt clusters were more selective for products with 5 or more carbon atoms; this result corresponds to the observations of Khodakov et al. *(524)*.

Besides metal nanoparticles, metal oxides such as Fe_2O_3 *(529)*, CeO_2 *(530)*, Ga_2O_3 *(531)*, In_2O_3 *(531)*, Cu_2O *(532)*, and WO_3 *(533)* were supported on ordered mesoporous silica. The formation of the mixed oxide $CsLaO_2$ in MCM-41 and its behavior as a basic catalyst for the Knoevenagel addition of enolates to benzaldehyde were investigated by Kloetstra et al. *(417)* soon after the discovery of OMMs.

A basic catalyst, CaO supported on mesoporous SBA-15 silica, was reported by Albuquerque et al. *(511)*. This material catalyzed the transesterification of vegetable oils with high conversions when the reactants were sunflower oil (95%, 5 h reaction time) or castor oil (65%, 1 h). The OMM-supported catalyst had a higher activity than a commercial CaO catalyst, and no leaching of the active phase was detected. Li et al. *(534)* supported MgO on various ordered mesoporous silicas (MCM-41, KIT-6, and SBA-15) by wet impregnation and *in situ* coating using magnesium acetate and magnesium nitrate as precursor salts. Among the catalysts tested in the transesterification of blended vegetable oil with ethanol to produce biodiesel, MgO-impregnated SBA-15 showed the highest activity by achieving a conversion of 96% within 5 h. Although the effect of the type of host material was questionable in this investigation because of the different textural properties, the catalytic activity appears to be related to the surface magnesium concentration, which can be easily tuned for a single host material by varying the loading method. The type of precursor salt that was used did not affect the catalytic activity.

Nguyen et al. *(535)* prepared a series of mesoporous silica-supported $LaCoO_3$ perovskites with various La–Co oxide contents (from 10 to

50 wt%) by impregnation of ordered mesoporous silica with a mixed lanthanum–cobalt citrate complex and subsequent calcination. During calcination at 600 °C, highly dispersed $LaCoO_3$ perovskite formed inside the pore channels of the mesoporous silica. The catalytic activities of the materials were tested for the total oxidation of methane, and a much higher catalytic activity and resistance to sulfur poisoning of the supported materials was observed relative to those of bulk $LaCoO_3$ perovskites.

Vanadium is one of the most widely used active components in industrial oxidation catalysts. Vanadium oxide nanoparticles with various crystal structures have been incorporated into ordered mesoporous silica for a range of catalytic reactions, such as oxidative dehydrogenation of ethane [536], propane [313,314,537], butane [538], and ethylbenzene (the latter giving styrene) [539], and the partial oxidation of methane to give formaldehyde [322,540,541]. Li *et al.* [542] prepared VPO catalysts that consisted of mainly crystallized $(VO)_2P_2O_7$ on SBA-15, MCM-41, and fumed SiO_2 by using a deposition–precipitation method. It was observed that the highest VPO dispersion was achieved on the SBA-15 sample, whereas the lowest VPO dispersion was obtained on the nonporous fumed SiO_2 sample. In general, all VPO catalysts supported on all silicas were characterized by high activities for partial oxidation of butane to maleic anhydride. The group of this author [543,544] demonstrated that the morphology of dispersed oxides depends strongly on the nature of the supported phase. Whereas zirconia is obtained in the form of small particles, the growth of which is confined by the pores, it is possible to obtain rare-earth metal oxides with very high dispersions by supporting them on the ordered mesoporous silica SBA-15. It was proposed that the rare-earth oxides spread to form a monolayer. Only after completion of the monolayer do nanoparticles form, in coexistence with the monolayer. This approach is quite versatile and would probably work for most of the rare-earth oxides and mixtures thereof, and thus there are routes to a wide range of materials with variable surface properties, which might be interesting for various catalytic reactions.

Iron–modified OMMs (Fe_2O_3/MCM-41) showed superior performance over iron supported on conventional silica in the oxidation of sulfur dioxide [544]. There are a number of reports about OMM-supported catalysts incorporating iron oxides, with high catalytic activities observed for various reactions such as selective reduction of NO [545], Friedel–Crafts alkylations [546], methanol decomposition [275], epoxidation of propylene [547,548], oxidation of sulfides to sulfoxides [549], hydroxylation of benzene [550], and decomposition of ammonia [551].

Jiao and Frei prepared Co_3O_4 *(552)* and manganese oxide *(553)* clusters in mesoporous SBA-15 silica by simple wet impregnation and subsequent temperature treatment. The catalytic activity of the materials was investigated in solar water splitting by using $[Ru^{2+}(bpy)_3]$/persulfate as a dye sensitizer under visible-light irradiation. Nanosized Co_3O_4, clusters exhibited 65-fold better catalytic activities than bulk, micro-sized Co_3O_4, and the difference was attributed to the large number of active sites that were available in the former catalyst because of the high surface area of the clusters, which in turn was brought about by the pore and space constraints of the silica support. A series of manganese oxides with different crystal structures was prepared by varying the calcination temperature of a MnO_x/KIT-6 composite in the range of 400–900 °C, and it was found that all nanostructured manganese oxide clusters supported on mesoporous silica KIT-6 were effective catalysts for O_2 evolution from water, as shown in Figure 2.26 *(553,554)*.

The following turnover frequencies (per manganese oxide nanocluster) were reported: 630 s^{-1} for MnO_x/KIT-6 calcined at 400 °C; 1210 s^{-1} for that calcined at 500 °C; 3330 s^{-1} for that calcined at 600 °C; 1260 s^{-1} for that calcined at 700 °C; 1590 s^{-1} for that calcined at 800 °C; and 1830 s^{-1} for that calcined at 900 °C. The material prepared by calcination

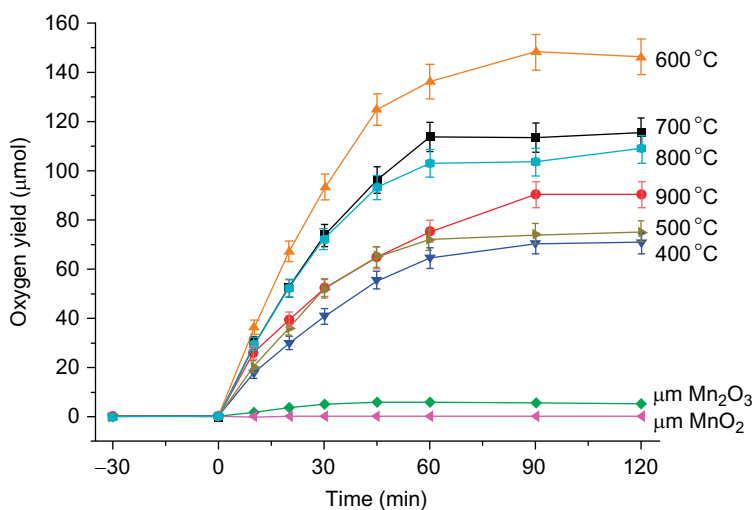**Figure 2.26** O_2 evolution obtained during photocatalytic water splitting in aqueous suspensions (40 mL) of various manganese oxides with $Ru^{2+}(bpy)_3$–persulfate as a visible-light sensitizer. MnO_x/KIT-6 samples were calcined at the temperatures indicated; bulk manganese references samples consisted of micrometer-sized particles *(553)*. *Adapted with permission from the Royal Society of Chemistry.*

at 600 °C, which had a high content of Mn_2O_3, had the highest activity. The results of this investigation show that there are benefits of OMMs in addition to the uniform dispersion of the active component that can typically be achieved. Pore and space constraints can help control a material's composition such as oxide stoichiometry and its crystal structure by preventing aggregation and crystallite growth.

Metal oxides and sulfides have also been incorporated as active components into ordered mesoporous structures for use in a variety of catalytic reactions. Many reports concern HDS *(507,522,555–571)*, which is a widely used industrial process to remove sulfur from natural gas and petroleum. For example, Huirache-Acuna *et al. (558)* prepared an HDS catalyst by immobilization of a ternary cobalt–molybdenum–tungsten oxide on phosphate-loaded mesoporous SBA-15 and SBA-16. The effects of support morphology (SBA-15 vs. SBA-16) and of support modification with variable amounts of phosphorus were investigated. The sulfided catalysts were tested for the HDS of dibenzothiophene (DBT) at 350 °C and 3.1 MPa. It was found that independent of the support, the presence of phosphorus inhibited the HDS activity. Indeed, the catalytic properties were not influenced by the support structure (SBA-15 or SBA-16). In terms of the reaction rate constants, CoMoW/SBA-15 and CoMoW/SBA-16 catalysts were both found to be more active than a commercial $CoMo/Al_2O_3$ catalyst incorporating a small amount of phosphorus.

Vradman *et al. (522)* reported the preparation of layered nanoslabs of a WS_2 phase in the channels of SBA-15 at loadings up to 60 wt%; this phase was characterized by a well-defined hexagonal crystalline structure, an average slab length of 3.6 nm, and a stacking number of 3.2. Sonication of a slurry containing SBA-15 in a $W(CO)_6$-sulfur-diphenylmethane solution resulted in an amorphous WS_2 phase inside the mesopores of the host. The amorphous phase was subsequently transformed into hexagonal, crystalline WS_2 by sulfidation with 1.5% dimethyl disulfide in toluene in flowing H_2 at 320 °C and 5.4 MPa. In addition, nickel was introduced into the WS_2/SBA-15 composite by impregnation from an aqueous solution of nickel acetate. Incorporation of the nickel in the material up to a Ni/W ratio of 0.4 increased the catalytic activity. In the HDS of DBT and in the hydrogenation of toluene, the activity of the optimized Ni–W–S/SBA-15 catalyst was 1.4 and 7.3 times higher, respectively, than that of a sulfided commercial Co–Mo/Al_2O_3 catalyst.

The idea of using the confining pore system to restrict the growth of a second material and thus to retain a high dispersion even under severe

reaction conditions can be extended to a complete filling of the entire pore system, followed by removal of the matrix. This method allows the preparation of various ordered mesoporous replica materials that are not easy to produce by the soft-templating method. Joo *et al.* *(180)* described a general strategy for the synthesis of highly ordered, rigid arrays of nanoporous carbons, termed CMK-5, by using ordered mesoporous silica as template; these nanocarbons have uniform and tunable pore diameters. After the preparation of the SBA-15, the pore volume of the SBA-15 was filled with furfuryl alcohol ($C_5H_6O_2$) by the incipient wetness technique, and the resulting material was heated for 3 h to 80 °C to induce acid-catalyzed polymerization of the furfuryl alcohol. In this way, the pore walls of the silica were coated with a layer of polymer. Subsequently, the polymerized furfuryl alcohol was converted to carbon inside the SBA-15 template by pyrolysis under vacuum at a maximum temperature of 1100 °C. Finally, the silica template was removed with HF or aqueous NaOH solution. When used as a support, the resulting material affords a high dispersion of platinum nanoparticles, exceeding that obtained on other common microporous carbon materials (such as carbon black, charcoal, and activated carbon fibers). It was observed that the cluster size increases with the metal loading, but the extent of the increase is much smaller than for conventional porous carbons. Even when the platinum loading was increased to match that of carbon (i.e., 50% of the total weight was platinum), the platinum clusters were characterized by a narrow particle size distribution centered around a diameter of 2.5 nm, as shown in Figure 2.27. This exceptional dispersion strikingly illustrates the confining effect of the pores of the ordered mesoporous carbon. In contrast, when other porous carbons, such as carbon black, activated charcoal, and activated carbon fiber, were used, the equivalent experiments resulted in the formation of much larger platinum particles with a wide distribution of diameters ranging up to 30 nm. The high dispersion of the metal clusters incorporated in CMK-5 led to a promising electrocatalytic activity for O_2 reduction, which was attributed to the small size and uniform dispersion of the platinum nanoparticles in the mesoporous carbon, which constrains the growth of the metal particles with its confining pore system.

Following this work, several reports were published regarding the advantages of ordered mesoporous carbon materials for applications in electrocatalysis *(572–584)* and in other fields. Lu *et al.* *(585)* supported palladium on ordered mesoporous carbon (Pd-OMC) and obtained highly temperature-stable and uniformly dispersed palladium clusters with a diameter of 1 nm that were embedded in the carbon walls. After incorporation of
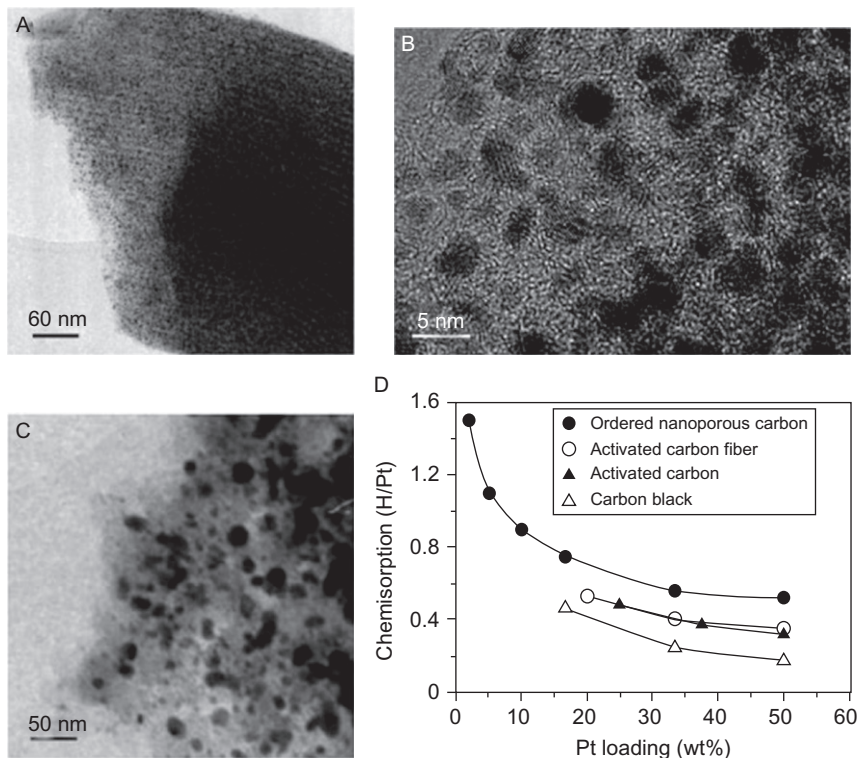
Figure 2.27 (A and B) TEM images of ordered mesoporous carbon with a specific surface area of 2000 $m^2 g^{-1}$; (C) TEM image of carbon black (Vulcan XC-72). (D) Hydrogen chemisorption data (the average number of H atoms chemisorbed per Pt atom) for various kinds of carbons supporting platinum: ordered nanoporous carbon (solid circles), carbon black (open triangles), activated carbon (Darco KB, BET surface area $= 1500\ m^2 g^{-1}$) (solid triangles), and activated carbon fiber (Osaka ACF A-15, BET surface area $= 1500\ m^2 g^{-1}$ (open circles) *(180). Adapted with permission from Nature Publishing Group.*

polyacrylonitrile (PAN) into the pore system of SBA–15, the cross–linking of PAN molecules was improved by oxidation. When the composite was immersed into an aqueous solution of $Pd(NO_3)_2$, it adsorbed palladium cations, because of the presence of the nitrogen functionalities. Subsequent pyrolysis of the composite under argon and silica leaching resulted in a palladium–doped ordered mesoporous carbon. The palladium particles were not located in the mesopores, but rather in the micropores present in the walls—thus the particles were limited to extremely small sizes.

The catalytic activity of Pd-OMC was tested for alcohol (specifically benzyl alcohol, 1-phenylethanol, and cinnamyl alcohol) oxidation to

produce the corresponding aldehydes, with supercritical CO_2 as the reaction medium. The catalytic data indicate that the selectivity to the aldehyde was in all cases higher than 99%. No acid was detected in the product, confirming that the alcohol was selectively converted to aldehyde. This synthetic pathway, which exploits the pore constraints of the silica template to create a Pd-OMC catalyst with near atomic dispersion of the metal with a high level of control, thus resulted in catalysts with excellent properties for the oxidation of alcohols. It should be possible to generalize this synthetic approach and distribute other noble metal species in carbon walls with a high dispersion, while keeping the mesopores clear of any blocking species.

A range of carbon precursors can be used to prepare ordered mesoporous carbon by the nanocasting route. When a carbon source that contains metal centers is used as a precursor, ordered mesoporous carbons that are doped with metal nanoparticles can be obtained in one step. Recently, we demonstrated the synthesis of an ordered mesoporous carbon containing highly dispersed copper–sulfur particles in the carbon framework. A nanocasting route, involving the use of SBA-15 as the template and copper(II) phthalocyanine–tetrasulfonic acid tetrasodium salt (denoted as PcS) as the single precursor was used *(586)*. Below a pyrolysis temperature of 600 °C, the PcS molecules were stable, however, at higher pyrolysis temperatures, the PcS molecules decomposed to give carbon and copper–sulfur compounds in the carbon framework, or large copper particles, depending on the conditions. The specific surface areas of the resultant carbons could be tuned in the range of 530–980 $m^2\ g^{-1}$, and the pore volumes could be tuned in the range of 0.5–1.2 $cm^3\ g^{-1}$. Using phthalocyanine as carbon precursor, it is possible to directly prepare nanocast carbon containing highly dispersed metal nanoparticles in its skeleton. Following this work, graphitic ordered mesoporous carbon materials were synthesized by a pseudo–solid state method, employing metal (nickel, cobalt, iron) phthalocyanines and SBA-15 *(587)*. The synthesis strategy is straightforward; metal phthalocyanine and mesoporous SBA-15 silica were ground together in a 1:1 mass ratio. Then the powders were heated to 900 °C in a tube furnace in flowing argon, and the resultant carbon–silica composites were treated with HF solution to remove the silica. As shown in Figure 2.28, the resulting ordered mesoporous carbon has a highly ordered pore structure, and the embedded nanoparticles are highly dispersed, as a result of the ordered structure and the pore constraints of the parent silica template.

Similar to powder morphologies, thin-film morphologies can also be used as hosts for the incorporation of nanoparticles, which provide
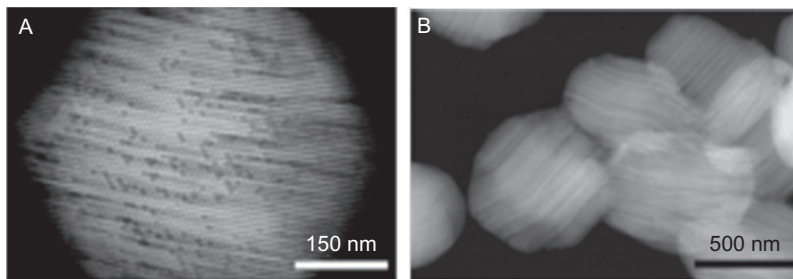
Figure 2.28 TEM images of (A) the (110) plane and (B) the (001) plane of a nanoporous carbon with embedded nickel species, CMK-3-NiPc *(587)*. *Adapted with permission from Wiley.*

additional functionality. Ismail *et al*. *(588)* grew cubic ordered mesoporous TiO_2 on a conductive FTO (fluorine–doped SnO_2) by layer–by–layer deposition using a dip–coating procedure. After calcination, the TiO_2 was decorated with platinum nanoparticles by an electrochemical deposition technique. The catalytic properties of the final material were tested in the photooxidation of acetaldehyde with gas–phase reactants. The pristine ordered mesoporous TiO_2 and the Pt/TiO_2 nanocomposites exhibited significantly higher photocatalytic activity than commercial Pilkington Activ^{TM} glass and dense TiO_2 films, which were used as references. The platinum deposition significantly enhanced the catalytic activity of TiO_2. Silver–doped TiO_2 was also prepared by a one–pot route, with P–123 triblock polymer used as the structure–directing and reducing agent and with $AgNO_3$ and titanium(IV) tetraethoxide used as precursors. Conversion of Ag^+ to Ag^0 took place by *in situ* heat–induced reduction during or through the oxidation of the template at 400 °C, simultaneously with the controlled polymerization of the TiO_2 framework *(589)*. The catalytic activity of the ordered mesoporous Ag/TiO_2 films was evaluated in the photocatalytic degradation of 2–chlorophenol as a model reaction. It was found that the ordered mesoporous Ag/TiO_2 films had an eight times higher activity than the nonporous commercial photocatalyst Pilkington Activ^{TM}.

4.6. Patterned arrangement of surface functionalities

Another potentially useful property of OMMs is the patterned arrangement of surface functionalities. Such patterning can be present in the as–made material; or it can be introduced by co–condensation during the template–directed synthesis of the mesoporous materials; or it can be introduced by post–synthetic grafting methods using the silanol groups on the external

or internal surface of the mesoporous silica. There are reports that the surface of as-prepared ordered mesoporous silica is inhomogeneous, consisting of hydrophobic and hydrophilic patches *(590)*, which react differently in grafting reactions with functional silanes *(591)*. It was claimed that it is predominantly the hydrophobic parts of MCM-41 that react with silanes, that is, siloxane bonds are opened on the hydrophobic patches. However, this effect does not seem to have been exploited for specific catalytic functions of OMMs, although such a patterned arrangement of functionalities could be used to direct the orientation of molecules with respect to the surface.

The view most often expressed in the literature is that functionalization by grafting typically involves reaction of the surface silanol groups (Si—OH) with silane coupling agents such as silyl chlorides (R_3Si—Cl), silyl alkoxides (R_3Si—OR), and disilazanes (R_3Si—NH—SiR_3), and results in siloxane linkages (Si—O—SiR_3) to the internal and/or external surface of the mesoporous silica. The most evident advantage of the grafting method is good preservation of the mesostructure during this post-modification *(592)*. However, grafting has some limitations: attachment of a layer of functional groups to the pore surface can result in a reduced pore size and pore volume, and the number of functional groups that can be grafted (and thus the loading) is limited by the density of reactive surface silanols. It is also still difficult to control the loading and the uniformity of the functional groups, although methods have been developed for better control of loading and improved homogeneity of the loading *(593)*.

Grafted functional groups are also occasionally ineffective because of partial cross-linking of the functional groups with the silica-surface silanol groups. An alternative to grafting is co-condensation. Key to this method are silane precursors that may contain various functional groups and are introduced during the synthesis of the mesoporous silica. After hydrolysis, condensation, and polycondensation reactions, a hybrid silica containing the functional groups of the silane precursor is obtained. More detailed information regarding the functionalization of OMMs is presented in a recent review by Athens *et al*. *(594)*.

However, in most cases no patterned arrangement of the functionalities is achieved by this method; rather, a statistical distribution of grafted groups, or a gradient from the outside to the inside of the particle is obtained. So far, such deliberately created inhomogeneous distributions do not seem to have been used for catalytic purposes.

Inagaki *et al*. *(170)* demonstrated the synthesis of a material with a truly patterned—and ordered—arrangement of surface functionalities; these

authors prepared an ordered benzene–silica hybrid material that had a hexagonal array of mesoporous and crystal-like walls. The hybrid material was synthesized by using a benzene-bridged organosilane monomer (1,4-bis (triethoxysilyl)-benzene), which was added to an aqueous solution of alkyltrimethylammonium surfactant containing sodium hydroxide, and kept at 95 °C for about 20 h. The benzene–silica hybrid material was obtained by collecting the white precipitate and removing surfactant by solvent extraction. These types of material have a patterned arrangement of surface functionalities. The silica moieties provide hydrophilic surface patches, while the sections exposing the benzene rings have hydrophobic surface functionality. The surface of the hybrid material was even sulfonated with preservation of both the meso- and molecular-scale ordered structures. Such structures, with periodically arranged hydrophobic–hydrophilic sections, could allow structural orientation of active components incorporated in the pores, which might improve the selectivity and activity in various catalytic reactions and enhance the opto–electrical efficiency of doped molecules, nanoparticles, and clusters.

Mesoporous silicas modified with sulfonic acid groups, either by the one-pot or by the grafting method, have shown superior catalytic activities in the hydrolysis of sucrose and starch in comparison with conventional catalysts such as Amberlyst-15, Nafion–silica, and HZSM-5 (595). A series of periodic mesoporous organosilicas with differently patterned surfaces was reported by Corma et al. (596). The materials were obtained by varying the relative concentrations of TEOS and a silylated carbapalladacycle complex, which formed part of the walls of the hybrid material. Catalytic activities of these periodic mesoporous organosilica materials for a Suzuki cross-coupling reaction were found to be much higher than that of a related amorphous silica catalyst containing the same complex. However, other than in this example, this interesting feature of ordered materials, that is, a surface patterned with organic moieties of organosilanes, does not seem to have been exploited for catalysis.

Mbaraka et al. (597) reported the further functionalization of organosulfonic acid-functionalized mesoporous silica with various hydrophobic organic groups, such as methyl, ethyl, and phenyl groups, to obtain a multifunctional mesostructured catalyst. Both post-synthesis grafting and one-step cocondensation techniques were used to introduce the hydrophobic organic groups, with the techniques being elaborate enough to preferentially modify the external or internal surfaces, respectively. The resultant materials were tested for the esterification of fatty acids with methanol to produce

methyl esters, which is a step in the production of biodiesel. It was found that incorporation of hydrophobic groups in the organic–inorganic hybrid acid catalyst enhanced the catalytic performance. The performance was also strongly dependent on the method of incorporation and on the size of the hydrophobic organic groups.

The results of the investigation demonstrate the potential for designing the environment of a catalytic site at the molecular level by the use of organic–inorganic mesoporous materials, whereby functionalization could be achieved at will on either the external or the internal surface of ordered mesoporous silica.

In addition to silanes and organic groups, various hetero elements can be grafted onto the silica surface. For instance, Jarupatrakorn *et al. (598)* demonstrated a molecular-precursor approach targeted at grafting site-isolated titanium species onto the support materials (Figure 2.29). The resulting solids had high activity and selectivity as epoxidation catalysts. The tris(*tert*-butoxy)siloxy titanium complexes $Ti[OSi(O^tBu)_3]_4$, $(^iPrO)Ti[OSi(O^tBu)_3]_3$, and $(^tBuO)_3TiOSi(O^tBu)_3$ were allowed to react with the hydroxyl groups of amorphous Aerosil® or mesoporous MCM-41 or SBA-15 with the concomitant loss of HO^tBu and/or $HOSi(O^tBu)_3$, thus producing titanium species on the silica surfaces. It was found that the titanium species were mainly present in isolated, tetrahedral coordination environments. Increasing the number of silane ligands in the molecular precursor not only decreased the amount of titanium that was grafted, but it also improved the catalytic activity and selectivity for the epoxidation of cyclohexene with cumene hydroperoxide as an oxidant. Moreover, the high-surface-area mesoporous silicas (MCM-41 and SBA-15) were found to be more effective than amorphous silica as supports for these catalysts.

With respect to the patterned arrangement of surface functionalities, the dual pore system of SBA-15, which has hexagonally arranged cylindrical mesopores with micropores within the walls, is highly attractive.
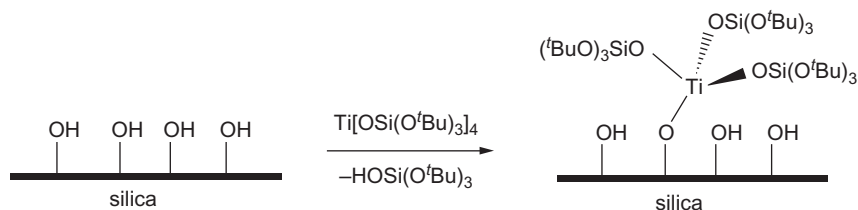

Figure 2.29 A scheme for the grafting of titanium species onto the surface of porous silica *(598)*. *Adapted with permission from the American Chemical Society.*

The triblock copolymer template P-123 that is used to obtain an ordered mesoporous structure can be removed by calcination, microwave digestion, or extraction by solvents or supercritical fluids, which generates both pore types at the same time. However, making both the micropores and mesopores accessible in one step prevents independent modification of the different pores. It is therefore highly desirable to open the two types of pores in independent steps, making it possible to also functionalize them independently.

For example, the mesopore surface could be made hydrophobic with the micropores kept hydrophilic, or mesopores could be functionalized with an acidic functional group and micropores with a basic group. Such an approach could provide multifunctional acid–base catalysts. Independently controlled accessibility to the two pore systems could also provide pathways for selective deposition of organic or inorganic guest species in either one of the two pore systems.

A method for selective removal of the template from either the micro- or the mesopores is controlled ether cleavage of the block polymer template *(408,599)*. The mesopores are first opened by partial decomposition of the template by ether cleavage catalyzed by sulfuric acid under precisely controlled conditions. The poly(ethylene oxide) chains embedded in the pore walls, which are less accessible to the acid, can be decomposed subsequently by gentle thermal treatment in air to create micropores. Furthermore, because the entire process is based on reactions at low temperatures, the resulting SBA-15 has larger mesopores, a greater micropore volume, and a higher hydroxyl group concentration on the surface than SBA-15 made by syntheses involving high-temperature treatments. These properties are beneficial if the silica is to be further modified with other functional groups.

This method was exploited to selectively modify the surface of SBA-15; first, the mesopores were functionalized and then palladium nanoparticles were deposited in the micropores. The series of preparation steps is illustrated in Figure 2.30 *(600)*. The mesopores of as-synthesized SBA-15 (A) were first opened by treatment with sulfuric acid, that is, the accessible fraction of P-123 was cleaved and removed (B). The exposed mesopore surface and the external surface of SBA-15 were functionalized with trimethylchlorosilane (TMCS) (C). Afterwards, the material was heated to 250 °C to remove the block polymer from the micropores while leaving the trimethylsilyl (TMS) groups intact (D). The open micropores were then functionalized by using trivinylchlorosilane (TVCS) (E), and the resultant bifunctional SBA-15 was allowed to react with dichlorobis(acetonitrile)palladium ($PdCl_2(MeCN)_2$)
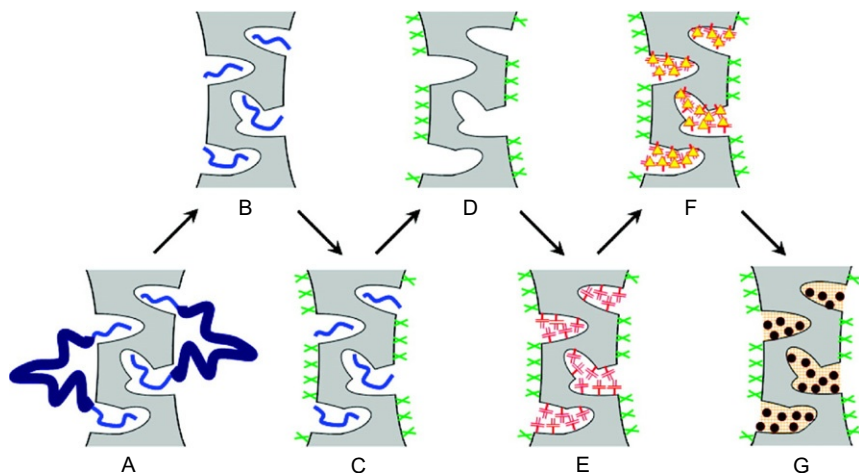
Figure 2.30 Schematic presentation of selective surface functionalization and selective deposition of palladium nanoparticles in the micropores of SBA-15 *(600)*. The sequence of steps is described in the text. *Adapted with permission from the American Chemical Society.*

to give metal complexes in the micropores (F). Subsequent reduction produced a material with fully accessible mesopores and palladium nanoparticles in the micropores (G). All the steps were monitored by various characterization methods to demonstrate the efficacy of the reaction steps.

The catalytic activity of the palladium-containing nanocomposites for the Heck reaction was investigated, and a correlation between the yield and the location (in the micropores or in the mesopores) of the palladium nanoparticles was observed. This pathway provides a blueprint for generating a heterogeneous local environment within the nanometer-sized pore structure and could be promising for the preparation of novel nanocomposite catalysts.

By use of a similar preparation method, the role of various properties of the functional sites in the vapor-phase Beckmann rearrangement of cyclohexanone oxime to ε-caprolactam on modified SBA-15 materials was investigated *(601)*. It was shown that the combination of a micropore and a mesopore system in SBA-15 allows the investigation of the influence of pore dimensions, concentration and strength of acid sites, and location of the sites on the catalytic behavior. The porous silica was calcined at various temperatures to tune the silanol group concentration, and the silanols on the mesopore surface were selectively rendered inactive by reaction with various agents, therefore allowing an independent investigation of the catalytic activity in the micropores and that in the mesopores.

Table 2.5 Catalytic activity for Beckmann rearrangement of cyclohexanone oxime to ε-caprolactam (capr.) after 1 h on stream in a flow reactor, related to the catalyst mass or normalized to the concentration of surface silanols

SBA-15 Treatments	Productivity $(mmol_{capr}g_{cat}^{-1}h^{-1})$	Productivity $(mol_{capr}mol_{SiOH}^{-1}h^{-1})$
	SBA–15 aged at 60 °C	
Calc. 550 °C (A)	2.94	1.07
H_2SO_4, calc. 300 °C (B)	3.13	0.78
H_2SO_4, TMCS, 300 °C (C)	1.44	0.51
Calc. 550 °C, TMSI (D)	0.50	
H_2SO_4, 300 °C, TMSI (E)	0.38	
	SBA–15 aged at 100 °C	
Calc. 550 °C (A)	2.80	0.76
H_2SO_4, calc. 300 °C (B)	2.96	0.55
H_2SO_4, TMCS, 300 °C (C)	0.91	0.36
Calc. 550 °C, TMSI (D)	0.39	
H_2SO_4, 300 °C, TMSI (E)	0.27	

Productivity was determined by ^{29}Si NMR spectroscopy (601).
The left column presents the following catalysts: SBA-15 calcined at 550 °C (A), SBA-15 treated with H_2SO_4 and calcined at 300 °C (B), SBA-15 treated with H_2SO_4, functionalized with trimethylchlorosilane (TMCS) and subsequently calcined at 300 °C (C), SBA-15 calcined at 550 °C and functionalized with trimethylsilylimidazole (TMSI) (D), SBA-15 treated with H_2SO_4, calcined at 300 °C and subsequently functionalized with TMSI (E).
Adapted with permission from Elsevier.

Independent of the specific treatment conditions, high catalytic activity was observed in the Beckmann rearrangement, as shown in Table 2.5. It was observed that acid-treated, low-temperature-calcined SBA-15 samples (B) exhibited the highest activities, corresponding to the very high total silanol concentration, whereas calcination at 550 °C (A) led to a lower activity, which is attributed to the reduction in the concentration of silanol groups. Materials with trimethylsilylated mesopore surfaces (C) still showed catalytic activity, albeit at a lower level, a result that emphasizes that both the micropore and the mesopore surfaces are involved in the catalytic reaction. Correlation of the catalytic activity with the surface silanol group concentration allowed the calculation of the intrinsic activity of the silanol groups. The results suggest that the contribution to the catalytic activity from acid sites in the mesopores was greater than that of the silanol groups in the micropores. Acid site strength
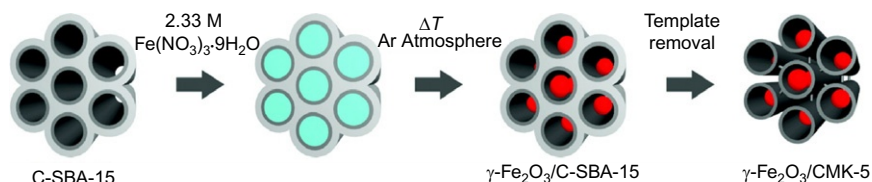
Figure 2.31 Schematic representation of the synthesis of γ-Fe$_2$O$_3$ nanoparticles confined within the tubes of CMK-5 carbon *(551)*. *Adapted with permission from the American Chemical Society.*

is an additional characteristic that influences activity in the reaction, together with the acid site density. It was concluded that the medium-strength acidity of silanol groups located in the mesopores was advantageous for the Beckmann rearrangement. The location of the silanol groups in mesostructured SBA-15 silica thus influences their acid strength and, correspondingly, the activity of the material for acid-catalyzed reactions.

CMK-5 type materials are appealing for patterned surface modification, because they provide two different types of surfaces, those on the inside of the carbon tubes and those on the outside *(602)*. Lu *et al.* *(551)* immobilized γ-Fe$_2$O$_3$ nanoparticles selectively within one of the pore systems of CMK-5 carbons and within a carbon-SBA-15 composite by following the strategy illustrated in Figure 2.31. To selectively immobilize Fe$_2$O$_3$ within the tubes of CMK-5 carbons and leave the mesopores between the tubes open, the iron precursor was impregnated into the carbon–silica composite (CS), because only the pores within the tubes are open and accessible. First, an iron precursor, Fe(NO$_3$)$_3$·9H$_2$O, was impregnated into the pore space of CS. Then the samples were dried at room temperature and calcined at a high temperature in an argon atmosphere. Then the silica was removed by an aqueous NaOH solution. The resultant γ-Fe$_2$O$_3$/CMK-5 material showed the highest ammonia decomposition activity of all the previously reported iron-containing catalysts. Furthermore, Fe$_2$O$_3$-carbon-SBA-15 catalysts were found to be highly stable for extended reaction times. The excellent performance was attributed to the spatial confinement in the pores and the strong interaction with the silica in the composite support, preventing nanoparticle migration and subsequent sintering.

5. PERSPECTIVE: CATALYST DESIGN ON THE NANOSCALE

Many important industrial catalysts are high-surface-area solids onto which an active component is dispersed in the form of particles with dimensions of several nanometers. Because size, composition, and the distribution

of these particles affect their catalytic activity, selectivity, and stability, the prospects for design of such catalysts on the nanometer scale have recently gained wide attention. To achieve a true design on the nanoscale, the function of each component in the catalysts (i.e., metal or metal oxide particles, oxide supports, and their interfaces) must be understood, requiring a high level of sophistication in catalyst preparation and characterization, and in the characterization of catalyst performance.

Parameters that—among others—control the performance of a solid catalyst include particle size, composition, and shape of the active phase, support composition, surface area, pore size, and pore size distribution. Furthermore, the organizational structure of the porous network (including the possible presence of hierarchical pore systems) is important. The complex interplay of the different characteristics of a catalyst poses a serious challenge to the prospect of synthetic control and design of solid catalysts. A suitable approach to the problem is to isolate one parameter at a time and learn how to control it in a methodical way and then to examine its effect on catalytic performance. OMMs—especially silica-containing materials—are ideally suited to such an approach. They are often used as supports in various catalytic reactions. Because the effects of their properties have been eludicated to a significant degree, as discussed above, they allow study of the influence of pore size, pore topology, size of the supported phase (via pore confinement), or surface curvature in a wide range of catalytic reactions.

The active phase is usually deposited in the form of a molecular precursor after the support material has been created. Several methods have been developed for the effective deposition of the active phase, such as impregnation or deposition–precipitation. However, notwithstanding the uniform, confining pore system of OMMs, nanoparticles generated on the support generally are not uniform in size and shape, and these properties play an important role in catalysis. The nonuniformity of the supported species results because these types of composites are created by growth of the inorganic nanocrystals inside the pores after the synthesis of the mesopore system, and such processes generally lead to nonuniform structures. Alternatively, a different sequence of steps can be used, in which the nanoparticles are formed first, and then the mesopore structure can be grown around the nanoparticles. Thus, design of novel catalysts is possible by encapsulation strategies. This approach was followed relatively early after the discovery of OMMs. Preformed palladium clusters were added to the synthesis mixture of MCM–41 and thus incorporated directly in the pore system *(490)*. However, these particles decomposed upon calcination of the material, and for CO oxidation catalysis, incipient wetness impregnation with the cluster solution was found to be more suitable.

Konya *et al.* *(603)* reported a similar approach by which platinum and gold nanocrystals were directly incorporated during SBA–15 synthesis. Cubic platinum nanoparticles were prepared by using P-123 as capping agent. The synthesis of the mesoporous material was carried out in the presence of the nanoparticles, as follows: To conform to optimal synthesis conditions for SBA–15, an excess of P-123 was added to the nanoparticle solutions. The solution was acidified with concentrated HCl, and then tetramethyl orthosilicate (TMOS) was added. The solution was stirred for 24 h at 30 °C and then held at 80 °C for 1 day. The product was filtered, washed, dried, and calcined at 550 °C for 12 h to remove the template. By this method, nanoparticles were encapsulated in the mesopores of silica in a one–pot process. It was found that at a low concentration, the nanoparticles, which are larger in diameter than the pore diameter typically obtained with the structure-directing agent used, acted to expand the entire mesopore structure uniformly.

A similar strategy was also used for growth of mesoporous SBA–15 silica in the presence of polyvinylpyrrolidone (PVP)-stabilized platinum nanoparticles *(604)*. Monodisperse platinum nanoparticles with diameters in the range of 1.7–7.1 nm were synthesized by alcohol reduction methods and incorporated into mesoporous SBA–15 silica during hydrothermal synthesis. When the SBA–15 synthesis was performed under acidic conditions, upon addition of the PVP-capped platinum nanoparticles, these particles aggregated, and the resultant silica was disordered. Therefore, SBA–15 was prepared under neutral conditions with sodium fluoride and a different organosilicon source, TMOS. PVP-capped platinum particles with diameters of 1.7, 2.9, 3.6, and 7.1 nm were introduced into the reaction mixture with a neutral pH. In a typical reaction, the platinum colloidal solution was mixed with an aqueous polymer solution at 40 °C and stirred for 1 h to ensure complete dispersion of the platinum particles. It was observed that brown precipitates were formed 5 min after the addition of NaF solution and TMOS. The supernatant solution was colorless and transparent, which shows that all the platinum colloids had been incorporated in the silica matrix. The slurry was aged for a day at 40 °C and placed in an oven and held at 100 °C for an additional day. Pt/SBA–15 catalysts were obtained by calcination of the raw materials under optimal conditions. TEM images of the Pt/SBA–15 catalysts indicated that platinum nanoparticles were located within the surfactant micelles during silica formation, leading to their dispersion throughout the silica structure (Figure 2.32).

The catalytic activities of the samples in the series were investigated for ethylene hydrogenation and for ethane hydrogenolysis. The latter reaction
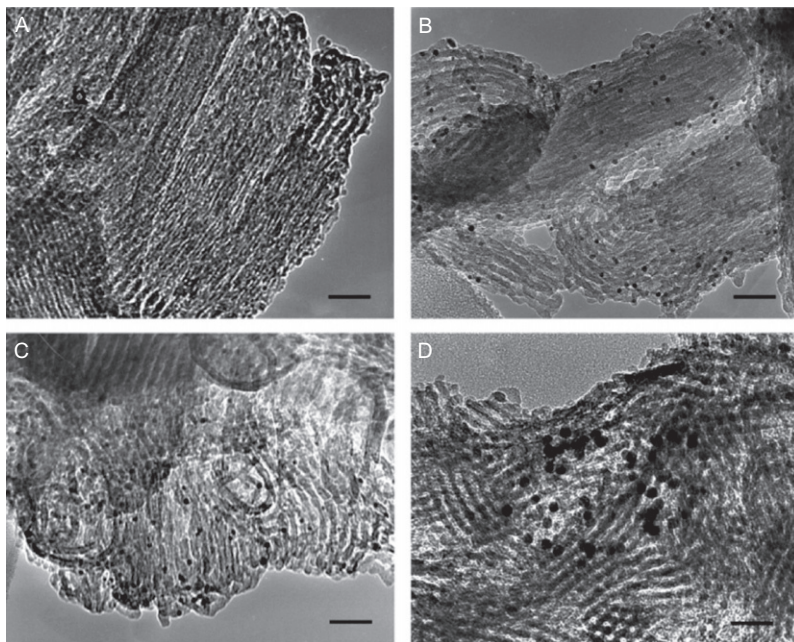
Figure 2.32 TEM images of Pt(*X*)/SBA-15 catalysts. *X* is the nanoparticle diameter in nm. (A) *X* = 1.7, (B) *X* = 2.9, (C) *X* = 3.6, and (D) *X* = 7.1. The scale bars represent 40 nm *(604)*. *Adapted with permission from the American Chemical Society.*

was characterized by a noteworthy structure sensitivity in the particle diameter range of 1–7 nm; the apparent activation energy increased linearly up to a platinum particle diameter of 4 nm and then remained constant. The observed dependence of rate on particle size was attributed to a higher reactivity of coordinatively unsaturated surface atoms in small particles relative to atoms on low-index surfaces, which are prevalent in large particles. The design strategy of this investigation illustrates that the ability to design catalytic structures with tunable properties by rational synthetic methods has advanced in a major way—even if such syntheses are not yet feasible on industrial scale, they are extremely valuable for the establishment of accurate structure–function relationships in heterogeneous reaction kinetics.

Recent developments in colloidal synthesis have facilitated the precise control of the size, shape, and composition of catalytic metal nanoparticles *(605)*, enabling their use as model catalysts for systematic investigations of the atomic-scale properties affecting catalytic activity and selectivity. The organic capping agents stabilizing colloidal nanoparticles, however, often limit the application of the catalysts in high-temperature reactions. Coating

of nanoparticles with mesoporous silica shells can provide a solution to this problem. For instance, Joo *et al.* *(606)* reported the design of a high-temperature-stable model catalyst that consists of a platinum metal core coated with a mesoporous silica shell (Pt@mSiO$_2$). Platinum nanoparticles were synthesized by the use of tetradecyltrimethylammonium bromide (TTAB) surfactant as the capping agent, and they were used as the core particles in the synthesis of core–shell catalysts. Second, Pt@SiO$_2$ particles were prepared by polymerizing TEOS around the TTAB-capped platinum cores. Then the as-synthesized Pt@SiO$_2$ particles were converted to Pt@mSiO$_2$ particles by calcination. The synthetic approach to obtain mesoporous Pt@SiO$_2$ is shown in Figure 2.33A. The calcination step is required because the as-synthesized Pt@SiO$_2$ nanoparticles contained a significant amount of the TTAB, which hinders the transport of reactant and product molecules in catalytic applications. To remove the TTAB, the as-synthesized Pt@SiO$_2$ sample was calcined at 350 °C to form mesoporous Pt@mSiO$_2$ nanoparticles. TEM images of Pt@mSiO$_2$ nanoparticles after calcination (Figure 2.33C and D) show mesopores with diameters of 2–3 nm in the silica shells. The inorganic silica shells are able to protect the platinum cores in air at temperatures up to 750 °C (Figure 2.33E), and the mesopores providing direct access to the platinum core made the Pt@mSiO$_2$ nanoparticles catalytically as active as bare platinum metal for ethylene hydrogenation and CO oxidation. The high thermal stability of Pt@mSiO$_2$ nanoparticles enabled high-temperature CO oxidation experiments, including determination of the ignition behavior, which was not possible for bare platinum nanoparticles because of the deformation or aggregation of the nanoparticles. These results suggest that such encapsulated nanoparticles are excellent materials for high-temperature reactions, and the design concept used in the Pt@mSiO$_2$ core–shell catalyst can be extended to other metal/metal oxide compositions *(606,607)*.

Selectively surface-modified OMMs provide even more options for catalysts in which functionality could be designed on the nanometer scale. Surface modification can be used to tune hydrophobicity, adsorption properties, or acid–base catalytic functionality. As mentioned before, many methods, such as pyrolysis of heteroatom-containing organic precursors, chemical vapor deposition, atomic layer deposition, impregnation, oxidation, reduction, and surface grafting can be used to modify the surfaces of OMMs. Ordered mesoporous carbon (OMC) of the CMK–5 type especially appears to be interesting for selective modification, because it has two types of pore systems that are generated in different steps of the synthesis. To obtain different functional groups on ordered mesoporous carbon, the most
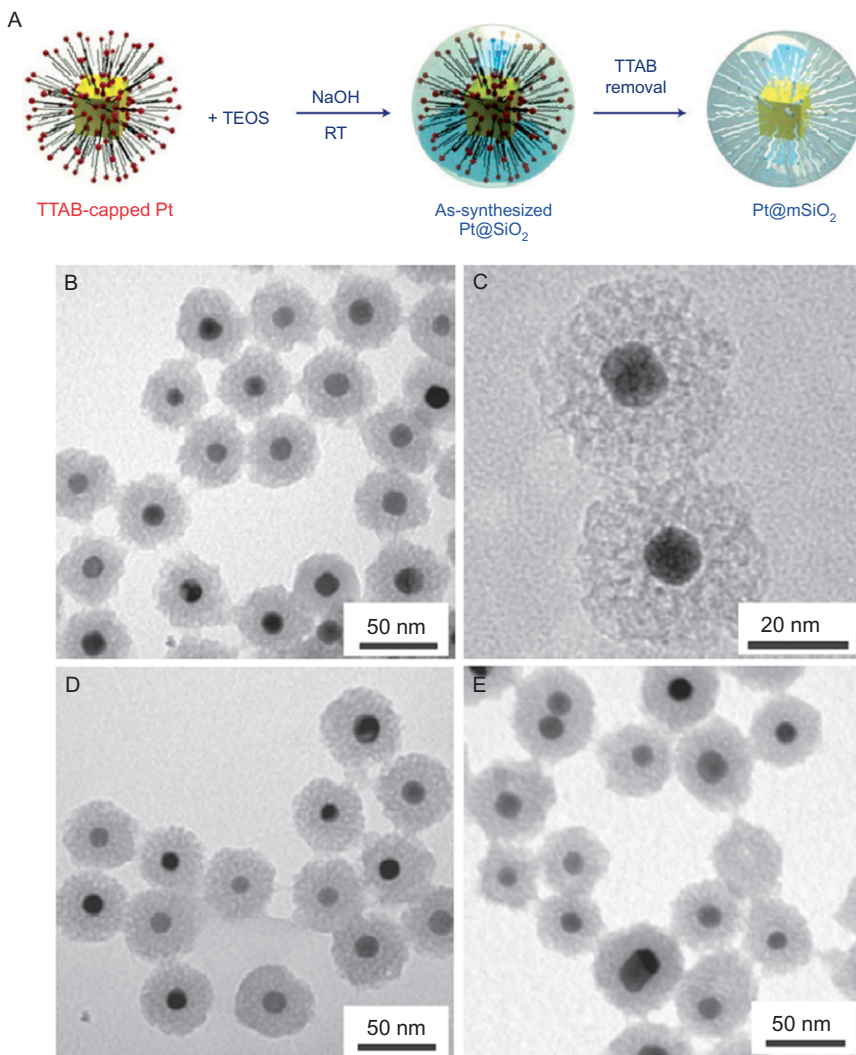
Figure 2.33 (A) Illustration of synthetic approach to Pt@mSiO₂ nanoparticles: coating of TTAB-capped platinum nanoparticle with silica, removal of the surfactant, and resulting mesoporous core–shell structure. Thermal stability of Pt@mSiO₂ nanoparticles (B–E), TEM images of Pt@mSiO₂ nanoparticles after calcination at 350 °C (B and C), 550 °C (D), and 750 °C (E) (606). Adapted with permission from Nature Publishing Group.

common methods are the direct pyrolysis of precursors, mostly organic precursors, resulting in the deposition of heteroatoms such as nitrogen (608,609), sulfur (610), and fluorine (611).

Several approaches have been applied to modify the surfaces of OMCs by post-treatment procedures, including chemical reduction of diazonium

species *(612)*, fluorination *(613)*, ammoniation *(584)*, oxidation in nitric acid *(602)* and in ammonium persulfate in dilute H_2SO_4 solution *(614)*. Although these approaches allow fine-tuning of the surface properties of OMCs, they typically lead to complete functionalization of all the accessible pore surfaces of the materials.

We recently investigated approaches to the selective functionalization of OMCs in a spatially controlled manner—to target specific pore surfaces by taking the structure and flexible synthetic procedure of the OMMs into account *(615)*. As mentioned above, CMK-5 has two independent pore systems, which are separated from each other by the walls of carbon tubes. The first type of mesopores is the unoccupied space of the mesoporous channels of SBA-15 that remains after surface coating with a thin layer of carbon. The second type of voids is created after removal of silica—creating the space where the silica walls had formerly been. Because these two pore systems are created at different stages during synthesis, in principle the opportunity is provided for the independent modification of the inner and outer surfaces of the tubes. Figure 2.34 illustrates schematically how such selective functionalization might be achieved. Starting from a carbon/SBA-15 composite, carboxylic acid moieties are formed on the surface of the coated carbon layer by nitric acid oxidation. The carboxylic acid groups can then be activated by thionyl chloride (SOCl₂), followed by reaction with an amine. Considering the fact that the carbon in the carbon/SBA-15 composite is actually tightly bonded to the silica pore wall, one can imagine that because of the steric hindrance offered by the silica walls, the exposed inner tube surfaces are preferentially accessed by the reactant molecules. This sequence of treatment
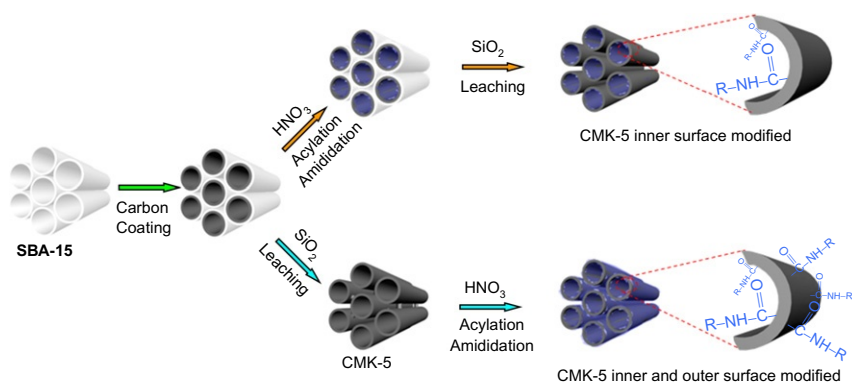

Figure 2.34 Schematic illustration of a proposed selective surface functionalization of ordered mesoporous carbons *(615)*.

steps should thus lead to selective functionalization of the inner tube surfaces. Ordered mesoporous carbons for which both the inner and the outer surface are modified should be accessible by removing the silica before any post-treatment step. One can even imagine more complex protocols of selective functionalization if one uses the reversible pore protection strategies introduced by Lu *et al.* (616) for the deposition of magnetic cobalt nanoparticles exclusively on the external surface of SBA-15.

6. CONCLUSIONS AND OUTLOOK

OMMs offer unique properties, including high surface areas, tailored porosities, narrow pore size distributions, patterned arrangement of surface functionalities, and convex surfaces. The composition, structure, crystallinity, morphology, topology, surface area, pore size, and wall thickness of an OMM can easily be tuned by virtue of the flexibility of the syntheses. Moreover, the materials can easily be modified with a variety of additional species, such as anchored complexes or nanoparticles, the size of which can be limited by the confining pore system.

These properties make this class of material highly interesting for applications in catalysis. Although some of the properties can also be realized with other, cheaper materials, some of the features are unique to OMMs, and so they are central to an assessment of the role of these materials as catalysts. Many research groups, following the discovery of the first OMMs, MCM-41, have worked in the preceding two decades to elucidate the roles of the unique properties of OMMs in catalysis and to evaluate the perspectives of these materials in practical catalysis.

In a number of cases the superiority of OMMs as catalysts or as catalyst supports has been demonstrated. However, so far, industrial applications are limited, if they have been realized at all. This lack of applications is to a large extent probably related to the high costs of production of OMMs, which may not be justified by the enhanced performance they offer.

We emphasize that the prospects of industrial applications, desirable as they may be, are not the only motivation for investigating OMMs in catalysis. Because they offer highly regular porous structures, they allow clear elucidation of key characteristics governing catalytic performance. Moreover, the regularity and periodicity of the structures also substantially facilitate the analysis of the materials, which makes establishing structure–performance relationships much easier and more reliable than for most solid catalysts. Thus, even if OMMs do not find many industrial applications, there are substantial

fundamental insights to be gained from catalytic studies of this class of solid. Moreover, the assembly of complex catalysts—designed on the nanometer scale and made possible by the availability of such a controllable class of materials—may provide the blueprint for similar materials that will be less expensive and competitive with existing catalysts. Thus, research on catalysis by OMMs may have a substantial industrial relevance in the future, even if the materials are not applied directly.

REFERENCES

1. Yanagisawa, T.; Shimizu, T.; Kuroda, K.; Kato, C. *Bull. Chem. Soc. Jpn.* **1990**, *63*, 988.
2. Kresge, C.T.; Leonowicz, M.E.; Roth, W.J.; Vartuli, J.C.; Beck, J.S. *Nature* **1992**, *359*, 710.
3. Beck, J.S.; Vartuli, J.C.; Roth, W.J.; Leonowicz, M.E.; Kresge, C.T.; Schmitt, K.D.; Chu, C.T.W.; Olson, D.H.; Sheppard, E.W.; McCullen, S.B.; Higgins, J.B.; Schlenker, J.L. *J. Am. Chem. Soc.* **1992**, *114*, 10834.
4. Corma, A. *Chem. Rev. (Washington, D.C.)* **1997**, *97*, 2373.
5. Ciesla, U.; Schüth, F. *Microporous Mesoporous Mater.* **1999**, *27*, 131.
6. Linden, M.; Schacht, S.; Schüth, F.; Steel, A.; Unger, K.K. *J. Porous Mater.* **1998**, *5*, 177.
7. Tuel, A. *Microporous Mesoporous Mater.* **1999**, *27*, 151.
8. Selvam, P.; Bhatia, S.K.; Sonwane, C.G. *Ind. Eng. Chem. Res.* **2001**, *40*, 3237.
9. Liu, Y.; Pinnavaia, T.J. *J. Mater. Chem.* **2002**, *12*, 3179.
10. Thomas, J.M. *Angew. Chem. Int. Ed.* **1999**, *38*, 3589.
11. Anwander, R. *Chem. Mater.* **2001**, *13*, 4419.
12. Ying, J.Y.; Mehnert, C.P.; Wong, M.S. *Angew. Chem. Int. Ed.* **1999**, *38*, 56.
13. He, X.; Antonelli, D. *Angew. Chem. Int. Ed.* **2001**, *41*, 214.
14. Wight, A.P.; Davis, M.E. *Chem. Rev.* **2002**, *102*, 3589.
15. De Vos, D.E.; Dams, M.; Sels, B.F.; Jacobs, P.A. *Chem. Rev.* **2002**, *102*, 3615.
16. Soler-illia, G.J.D.; Sanchez, C.; Lebeau, B.; Patarin, J. *Chem. Rev.* **2002**, *102*, 4093.
17. On, D.T.; Desplantier-Giscard, D.; Danumah, C.; Kaliaguine, S. *Appl. Catal. A-Gen.* **2003**, *253*, 543.
18. Wingen, A.; Kleitz, F.; Schüth, F. In *Basic Principles in Applied Catalysis*; Baerns, M., Ed.; Springer: Berlin, 2003; p 281.
19. Schüth, F. *Chem. Mater.* **2001**, *13*, 3184.
20. Di Renzo, F.; Galarneau, A.; Trens, P.; Fajula, F. In *Handbook of Porous Solids*; Schüth, F., Sing, K.S.W., Weitkamp, J., Eds.; Wiley-VCH: Weinheim, 2002; p 1311.
21. Taguchi, A.; Schüth, F. *Microporous Mesoporous Mater.* **2005**, *77*, 1.
22. Wan, Y.; Zhao, D.Y. *Chem. Rev.* **2007**, *107*, 2821.
23. Soler-Illia, G.J.A.A.; Azzaroni, O. *Chem. Soc. Rev.* **2011**, *40*, 1107.
24. Shi, Y.; Wan, Y.; Zhao, D. *Chem. Soc. Rev.* **2011**, *40*, 3854.
25. Mehdi, A.; Reye, C.; Corriu, R. *Chem. Soc. Rev.* **2011**, *40*, 563.
26. Garcia-Bennett, A.E. *Nanomedicine* **2011**, *6*, 867.
27. Wang, S. *Microporous Mesoporous Mater.* **2009**, *117*, 1.
28. Wan, Y.; Shi, Y.; Zhao, D. *Chem. Mater.* **2008**, *20*, 932.
29. Van der Voort, P.; Vercaemst, C.; Schaubroeck, D.; Verpoort, F. *Phys. Chem. Chem. Phys.* **2008**, *10*, 347.
30. Wan, Y.; Shi, Y.; Zhao, D. *Chem. Commun.* **2007**, 897.
31. Wan, Y.; Yang, H.; Zhao, D. *Acc. Chem. Res.* **2006**, *39*, 423.

32. Lee, J.; Kim, J.; Hyeon, T. *Adv. Mater.* **2006**, *18*, 2073.

33. Kapoor, M.P.; Inagaki, S. *Bull. Chem. Soc. Jpn.* **2006**, *79*, 1463.

34. Hatton, B.; Landskron, K.; Whitnall, W.; Perovic, D.; Ozin, G.A. *Acc. Chem. Res.* **2005**, *38*, 305.

35. Stein, A.; Schroden, R.C. *Curr. Opin. Solid State Mater. Sci.* **2001**, *5*, 553.

36. Sayari, A.; Hamoudi, S. *Chem. Mater.* **2001**, *13*, 3151.

37. Ren, Y.; Ma, Z.; Bruce, P.G. *Chem. Soc. Rev.* **2012**, *41*, 4909.

38. Hartmann, M. *Chem. Mater.* **2005**, *17*, 4577.

39. Yang, Q.; Liu, J.; Zhang, L.; Li, C. *J. Mater. Chem.* **2009**, *19*, 1945.

40. Corma, A. *Top. Catal.* **1997**, *4*, 249.

41. Karge, H.G.; Hunger, M.; Beyer, H.K. In *Catalysis and Zeolites – Fundamentals and Applications*; Weitkamp, J., Ed.; Springer: Berlin, Heidelberg, 1999; p 198.

42. Kühl, G. In *Catalysis and Zeolites – Fundamentals and Applications*; Weitkamp, J., Ed.; Springer: Berlin, Heidelberg, 1999; p 140.

43. Davis, M.E.; Saldarriaga, C.; Montes, C.; Garces, J.; Crowder, C. *Zeolites* **1988**, *8*, 362.

44. Jiang, J.X.; Yu, J.H.; Corma, A. *Angew. Chem. Int. Ed.* **2010**, *49*, 3120.

45. Tosheva, L.; Valtchev, V.P. *Chem. Mater.* **2005**, *17*, 2494.

46. Mehdipourghazi, M.; Moheb, A.; Kazemian, H. *Microporous Mesoporous Mater.* **2010**, *136*, 18.

47. Ni, Y.; Sun, A.; Wu, X.; Hai, G.; Hu, J.; Li, T.; Li, G. *Microporous Mesoporous Mater.* **2011**, *143*, 435.

48. Sun, L.; Guo, X.; Xiong, G.; Wang, X. *Catal. Commun.* **2012**, *25*, 18.

49. Tago, T.; Konno, H.; Nakasaka, Y.; Masuda, T. *Catal. Surv. Asia* **2012**, *16*, 148.

50. Tago, T.; Konno, H.; Sakamoto, M.; Nakasaka, Y.; Masuda, T. *Appl. Catal. A-Gen.* **2011**, *403*, 183.

51. Xue, T.; Wang, Y.M.; He, M.-Y. *Microporous Mesoporous Mater.* **2012**, *156*, 29.

52. Lynch, J.; Raatz, F.; Dufresne, P. *Zeolites* **1987**, 7, 333.

53. Choifeng, C.; Hall, J.B.; Huggins, B.J.; Beyerlein, R.A. *J. Catal.* **1993**, *140*, 395.

54. Cizmek, A.; Subotic, B.; Aiello, R.; Crea, F.; Nastro, A.; Tuoto, C. *Microporous Mater.* **1995**, *4*, 159.

55. Ogura, M.; Shinomiya, S.Y.; Tateno, J.; Nara, Y.; Nomura, M.; Kikuchi, E.; Matsukata, M. *Appl. Catal. A-Gen.* **2001**, *219*, 33.

56. Groen, J.C.; Bach, T.; Ziese, U.; Donk, A.M.P.V.; de Jong, K.P.; Moulijn, J.A.; Perez-Ramirez, J. *J. Am. Chem. Soc.* **2005**, *127*, 10792.

57. Ordomsky, V.V.; Murzin, V.Y.; Monakhova, Y.V.; Zubavichus, Y.V.; Knyazeva, E.E.; Nesterenko, N.S.; Ivanova, I.I. *Microporous Mesoporous Mater.* **2007**, *105*, 101.

58. Zhang, Z.T.; Han, Y.; Zhu, L.; Wang, R.W.; Yu, Y.; Qiu, S.L.; Zhao, D.Y.; Xiao, F.S. *Angew. Chem. Int. Ed.* **2001**, *40*, 1258.

59. Meng, X.; Nawaz, F.; Xiao, F.-S. *Nano Today* **2009**, *4*, 292.

60. Corma, A.; Fornes, V.; Pergher, S.B.; Maesen, T.L.M.; Buglass, J.G. *Nature* **1998**, *396*, 353.

61. Corma, A.; Fornes, V.; Guil, J.M.; Pergher, S.; Maesen, T.L.M.; Buglass, J.G. *Microporous Mesoporous Mater.* **2000**, *38*, 301.

62. Wei, X.T.; Smirniotis, P.G. *Microporous Mesoporous Mater.* **2006**, *89*, 170.

63. Moushey, D.L.; Smirniotis, P.G. *Catal. Lett.* **2009**, *129*, 20.

64. Martinez, A.; Arribas, M.A.; Derewinski, M.; Burkat-Dulak, A. *Appl. Catal. A-Gen.* **2010**, *379*, 188.

65. Jacobsen, C.J.H.; Madsen, C.; Houzvicka, J.; Schmidt, I.; Carlsson, A. *J. Am. Chem. Soc.* **2000**, *122*, 7116.

66. Schmidt, I.; Boisen, A.; Gustavsson, E.; Stahl, K.; Pehrson, S.; Dahl, S.; Carlsson, A.; Jacobsen, C.J.H. *Chem. Mater.* **2001**, *13*, 4416.

67. Tao, Y.S.; Kanoh, H.; Kaneko, K. *J. Am. Chem. Soc.* **2003**, *125*, 6044.
68. Tao, Y.S.; Kanoh, H.; Kaneko, K. *Langmuir* **2005**, *21*, 504.
69. Holland, B.T.; Abrams, L.; Stein, A. *J. Am. Chem. Soc.* **1999**, *121*, 4308.
70. Fang, Y.; Hu, H. *J. Am. Chem. Soc.* **2006**, *128*, 10636.
71. Chen, H.; Wydra, J.; Zhang, X.; Lee, P.–S.; Wang, Z.; Fan, W.; Tsapatsis, M. *J. Am. Chem. Soc.* **2011**, *133*, 12390.
72. Cho, H.S.; Ryoo, R. *Microporous Mesoporous Mater.* **2012**, *151*, 107.
73. Lu, A.-H.; Schüth, F. *Adv. Mater.* **2006**, *18*, 1793.
74. Tiemann, M. *Chem. Mater.* **2008**, *20*, 961.
75. Choi, M.; Cho, H.S.; Srivastava, R.; Venkatesan, C.; Choi, D.-H.; Ryoo, R. *Nat. Mater.* **2006**, *5*, 718.
76. Srivastava, R.; Choi, M.; Ryoo, R. *Chem. Commun. (Cambridge, U.K.)* **2006**, 4489.
77. Shetti, V.N.; Kim, J.; Srivastava, R.; Choi, M.; Ryoo, R. *J. Catal.* **2008**, *254*, 296.
78. Choi, M.; Na, K.; Kim, J.; Sakamoto, Y.; Terasaki, O.; Ryoo, R. *Nature* **2009**, *461*, 246.
79. Na, K.; Choi, M.; Park, W.; Sakamoto, Y.; Terasaki, O.; Ryoo, R. *J. Am. Chem. Soc.* **2010**, *132*, 4169.
80. Na, K.; Jo, C.; Kim, J.; Cho, K.; Jung, J.; Seo, Y.; Messinger, R.J.; Chmelka, B.F.; Ryoo, R. *Science* **2011**, *333*, 328.
81. Pierre, A.C.; Pajonk, G.M. *Chem. Rev.* **2002**, *102*, 4243.
82. Husing, N.; Schubert, U. *Angew. Chem. Int. Ed.* **1998**, *37*, 23.
83. Brinker, C. J.; Scherer, G. W. In *Sol-Gel Science*: The Physics and Chemistry of Sol-Gel Processing; A. Press (Ed.), Boston, 1990.
84. Baumann, T.F.; Gash, A.E.; Fox, G.A.; Satcher, J.H., Jr.; Hrubesh, L.W. In *Handbook of Porous Solids*; Schüth, F., Sing, K.S.W., Weitkamp, J., Eds.; Wiley-VCH: Weinheim, 2002; p 2014.
85. Fricke, J.; Petricevic, R. In *Handbook of Porous Solids*; Schüth, F., Sing, K.S.W., Weitkamp, J., Eds.; Wiley-VCH: Weinheim, 2002; p 2037.
86. Morales-Torres, S.; Maldonado-Hodar, F.J.; Perez-Cadenas, A.F.; Carrasco-Marin, F. *Microporous Mesoporous Mater.* **2012**, *153*, 24.
87. Pons, A.; Casas, L.; Estop, E.; Molins, E.; Harris, K.D.M.; Xu, M. *J. Non-Cryst. Solids* **2012**, *358*, 461.
88. Gesser, H.D.; Goswami, P.C. *Chem. Rev.* **1989**, *89*, 765.
89. Dorcheh, A.S.; Abbasi, M.H. *J. Mater. Process. Technol.* **2008**, *199*, 10.
90. James, S.L. *Chem. Soc. Rev.* **2003**, *32*, 276.
91. Lee, J.; Farha, O.K.; Roberts, J.; Scheidt, K.A.; Nguyen, S.T.; Hupp, J.T. *Chem. Soc. Rev.* **2009**, *38*, 1450.
92. Zhou, H.C.; Long, J.R.; Yaghi, O.M. *Chem. Rev.* **2012**, *112*, 673.
93. O'Keeffe, M.; Yaghi, O.M. *Chem. Rev.* **2012**, *112*, 675.
94. Yaghi, O.M.; Li, H.L.; Davis, C.; Richardson, D.; Groy, T.L. *Acc. Chem. Res.* **1998**, *31*, 474.
95. Li, H.; Eddaoudi, M.; O'Keeffe, M.; Yaghi, O.M. *Nature* **1999**, *402*, 276.
96. O'Keeffe, M.; Eddaoudi, M.; Li, H.L.; Reineke, T.; Yaghi, O.M. *J. Solid State Chem.* **2000**, *152*, 3.
97. Eddaoudi, M.; Moler, D.B.; Li, H.L.; Chen, B.L.; Reineke, T.M.; O'Keeffe, M.; Yaghi, O.M. *Acc. Chem. Res.* **2001**, *34*, 319.
98. Yaghi, O.M.; O'Keeffe, M.; Ockwig, N.W.; Chae, H.K.; Eddaoudi, M.; Kim, J. *Nature* **2003**, *423*, 705.
99. Chae, H.K.; Siberio-Perez, D.Y.; Kim, J.; Go, Y.; Eddaoudi, M.; Matzger, A.J.; O'Keeffe, M.; Yaghi, O.M. *Nature* **2004**, *427*, 523.
100. Rowsell, J.L.C.; Yaghi, O.M. *Microporous Mesoporous Mater.* **2004**, *73*, 3.
101. Rowsell, J.L.C.; Yaghi, O.M. *J. Am. Chem. Soc.* **2006**, *128*, 1304.

102. Eddaoudi, M.; Kim, J.; Rosi, N.; Vodak, D.; Wachter, J.; O'Keeffe, M.; Yaghi, O.M. *Science* **2002**, *295*, 469.

103. Tranchemontagne, D.J.; Park, K.S.; Furukawa, H.; Eckert, J.; Knobler, C.B.; Yaghi, O.M. *J. Phys. Chem. C* **2012**, *116*, 13143.

104. Fracaroli, A.M.; Tashiro, K.; Yaghi, O.M. *Inorg. Chem.* **2012**, *51*, 6437.

105. Coskun, A.; Hmadeh, M.; Barin, G.; Gandara, F.; Li, Q.W.; Choi, E.; Strutt, N.L.; Cordes, D.B.; Slawin, A.M.Z.; Stoddart, J.F.; Sauvage, J.P.; Yaghi, O.M. *Angew. Chem. Int. Ed.* **2012**, *51*, 2160.

106. Mori, W.; Takamizawa, S.; Kato, C.N.; Ohmura, T.; Sato, T. *Microporous Mesoporous Mater.* **2004**, *73*, 31.

107. Kaskel, S. In *Handbook of Porous Solids*; Schüth, F., Sing, K.S.W., Weitkamp, J., Eds.; Wiley-VCH: Weinheim, 2002; p 1190.

108. Ferey, G. *Chem. Soc. Rev.* **2008**, *37*, 191.

109. Bourrelly, S.; Llewellyn, P.L.; Serre, C.; Millange, F.; Loiseau, T.; Ferey, G. *J. Am. Chem. Soc.* **2005**, *127*, 13519.

110. Loiseau, T.; Serre, C.; Huguenard, C.; Fink, G.; Taulelle, F.; Henry, M.; Bataille, T.; Ferey, G. *Chem. Eur. J.* **2004**, *10*, 1373.

111. Dinca, M.; Yu, A.F.; Long, J.R. *J. Am. Chem. Soc.* **2006**, *128*, 8904.

112. Dinca, M.; Long, J.R. *Angew. Chem. Int. Ed.* **2008**, *47*, 6766.

113. Gedrich, K.; Senkovska, I.; Klein, N.; Stoeck, U.; Henschel, A.; Lohe, M.R.; Baburin, I.A.; Mueller, U.; Kaskel, S. *Angew. Chem. Int. Ed.* **2010**, *49*, 8489.

114. Klein, N.; Senkovska, I.; Gedrich, K.; Stoeck, U.; Henschel, A.; Mueller, U.; Kaskel, S. *Angew. Chem. Int. Ed.* **2009**, *48*, 9954.

115. Mueller, U.; Schubert, M.; Teich, F.; Puetter, H.; Schierle-Arndt, K.; Pastre, J. *J. Mater. Chem.* **2006**, *16*, 626.

116. Wang, Q.M.; Shen, D.M.; Bulow, M.; Lau, M.L.; Deng, S.G.; Fitch, F.R.; Lemcoff, N.O.; Semanscin, J. *Microporous Mesoporous Mater.* **2002**, *55*, 217.

117. Masuda, H.; Yamada, H.; Satoh, M.; Asoh, H.; Nakao, M.; Tamamura, T. *Appl. Phys. Lett.* **1997**, *71*, 2770.

118. Lee, W.; Ji, R.; Goesele, U.; Nielsch, K. *Nature Mater.* **2006**, *5*, 741.

119. Zaraska, L.; Sulka, G.D.; Szeremeta, J.; Jaskula, M. *Electrochim. Acta* **2010**, *55*, 4377.

120. Platschek, B.; Keilbach, A.; Bein, T. *Adv. Mater.* **2011**, *23*, 2395.

121. Tanev, P.T.; Chibwe, M.; Pinnavaia, T.J. *Nature* **1994**, *368*, 321.

122. Monnier, A.; Schüth, F.; Huo, Q.; Kumar, D.; Margolese, D.; Maxwell, R.S.; Stucky, G.D.; Krishnamurty, M.; Petroff, P.; Firouzi, A.; Janicke, M.; Chmelka, B.F. *Science* **1993**, *261*, 1299.

123. Corma, A.; Navarro, M.T.; Pariente, J.P. *J. Chem. Soc. Chem. Commun.* **1994**, 147.

124. Franke, O.; Rathousky, J.; Schulzekloff, G.; Starek, J.; Zukal, A. *Stud. Surf. Sci. Catal.* **1994**, *84*, 77.

125. Ciesla, U.; Demuth, D.; Leon, R.; Petroff, P.; Stucky, G.; Unger, K.; Schüth, F. *J. Chem. Soc. Chem. Comm* **1994**, 1387.

126. Huo, Q.S.; Margolese, D.I.; Ciesla, U.; Feng, P.Y.; Gier, T.E.; Sieger, P.; Leon, R.; Petroff, P.M.; Schüth, F.; Stucky, G.D. *Nature* **1994**, *368*, 317.

127. Antonelli, D.M.; Ying, J.Y. *Angew. Chem. Int. Ed.* **1995**, *34*, 2014.

128. Ciesla, U.; Schacht, S.; Stucky, G.D.; Unger, K.K.; Schüth, F. *Angew. Chem. Int. Ed.* **1996**, *35*, 541.

129. Thomas, A.; Goettmann, F.; Antonietti, M. *Chem. Mater.* **2008**, *20*, 738.

130. Vartuli, J.C.; Kresge, C.T.; Leonowicz, M.E.; Chu, A.S.; Mccullen, S.B.; Johnsen, I.D.; Sheppard, E.W. *Chem. Mater.* **1994**, *6*, 2070.

131. Ishikawa, T.; Matsuda, M.; Yasukawa, A.; Kandori, K.; Inagaki, S.; Fukushima, T.; Kondo, S. *J. Chem. Soc. Faraday Trans.* **1996**, *92*, 1985.

132. Kresge, C.T.; Vartuli, J.C.; Roth, W.J.; Leonowicz, M.E. *Stud. Surf. Sci. Catal.* **2004**, *148*, 53.
133. Huo, Q.S.; Margolese, D.I.; Ciesla, U.; Demuth, D.G.; Feng, P.Y.; Gier, T.E.; Sieger, P.; Firouzi, A.; Chmelka, B.F.; Schüth, F.; Stucky, G.D. *Chem. Mater.* **1994**, *6*, 1176.
134. Stucky, G.D.; Monnier, A.; Schüth, F.; Huo, Q.; Margolese, D.; Kumar, D.; Krishnamurty, M.; Petroff, P.; Firouzi, A.; Janicke, M.; Chmelka, B.F. *Mol. Cryst. Liq. Crys. A* **1994**, *240*, 187.
135. Kuroda, K. *Stud. Surf. Sci. Catal.* **2004**, *148*, 73.
136. Inagaki, S.; Fukushima, Y.; Kuroda, K. *J. Chem. Soc. Chem. Commun.* **1993**, 680.
137. Kimura, T.; Kamata, T.; Fuziwara, M.; Takano, Y.; Kaneda, M.; Sakamoto, Y.; Terasaki, O.; Sugahara, Y.; Kuroda, K. *Angew. Chem. Int. Ed.* **2000**, *39*, 3855.
138. Huo, Q.S.; Margolese, D.I.; Stucky, G.D. *Chem. Mater.* **1996**, *8*, 1147.
139. Huo, Q.S.; Leon, R.; Petroff, P.M.; Stucky, G.D. *Science* **1995**, *268*, 1324.
140. Israelachvili, J.N.; Mitchell, D.J.; Ninham, B.W. *J. Chem. Soc. Faraday Trans 2* **1976**, *72*, 1525.
141. Antonietti, M. *Curr. Opin. Colloid Interface Sci.* **2001**, *6*, 244.
142. Palmqvist, A.E.C. *Curr. Opin. Colloid Interface Sci.* **2003**, *8*, 145.
143. Tanev, P.T.; Pinnavaia, T.J. *Science* **1995**, *267*, 865.
144. Tanev, P.T.; Pinnavaia, T.J. *Science* **1996**, *271*, 1267.
145. Tanev, P.T.; Liang, Y.; Pinnavaia, T.J. *J. Am. Chem. Soc.* **1997**, *119*, 8616.
146. Bagshaw, S.A.; Pinnavaia, T.J. *Angew. Chem. Int. Ed.* **1996**, *35*, 1102.
147. Attard, G.S.; Glyde, J.C.; Goltner, C.G. *Nature* **1995**, *378*, 366.
148. Zhao, D.Y.; Feng, J.L.; Huo, Q.S.; Melosh, N.; Fredrickson, G.H.; Chmelka, B.F.; Stucky, G.D. *Science* **1998**, *279*, 548.
149. Yang, P.D.; Zhao, D.Y.; Margolese, D.I.; Chmelka, B.F.; Stucky, G.D. *Nature* **1998**, *396*, 152.
150. Yang, P.D.; Zhao, D.Y.; Margolese, D.I.; Chmelka, B.F.; Stucky, G.D. *Chem. Mater.* **1999**, *11*, 2813.
151. Zhao, D.Y.; Huo, Q.S.; Feng, J.L.; Chmelka, B.F.; Stucky, G.D. *J. Am. Chem. Soc.* **1998**, *120*, 6024.
152. Sakamoto, Y.; Kaneda, M.; Terasaki, O.; Zhao, D.Y.; Kim, J.M.; Stucky, G.; Shim, H.J.; Ryoo, R. *Nature* **2000**, *408*, 449.
153. Zhao, L.; Dong, Y.; Zhan, X.; Cheng, Y.; Zhu, Y.; Yuan, F.; Fu, H. *Catal. Lett.* **2012**, *142*, 619.
154. Matos, J.R.; Kruk, M.; Mercuri, L.P.; Jaroniec, M.; Zhao, L.; Kamiyama, T.; Terasaki, O.; Pinnavaia, T.J.; Liu, Y. *J. Am. Chem. Soc.* **2003**, *125*, 821.
155. Fan, J.; Yu, C.Z.; Gao, T.; Lei, J.; Tian, B.Z.; Wang, L.M.; Luo, Q.; Tu, B.; Zhou, W.Z.; Zhao, D.Y. *Angew. Chem. Int. Ed.* **2003**, *42*, 3146.
156. Huang, L.A.; Yan, X.W.; Krut, M. *Langmuir* **2010**, *26*, 14871.
157. Huang, L.; Kruk, M. *J. Colloid Interface Sci.* **2012**, *365*, 137.
158. Kruk, M.; Hui, C.M. *Microporous Mesoporous Mater.* **2008**, *114*, 64.
159. Kim, T.W.; Kleitz, F.; Paul, B.; Ryoo, R. *J. Am. Chem. Soc.* **2005**, *127*, 7601.
160. Choi, M.; Kleitz, F.; Liu, D.N.; Lee, H.Y.; Ahn, W.S.; Ryoo, R. *J. Am. Chem. Soc.* **2005**, *127*, 1924.
161. Kleitz, F.; Liu, D.N.; Anilkumar, G.M.; Park, I.S.; Solovyov, L.A.; Shmakov, A.N.; Ryoo, R. *J. Phys. Chem. B* **2003**, *107*, 14296.
162. Kleitz, F.; Choi, S.H.; Ryoo, R. *Chem. Commun.* **2003**, 2136.
163. Brunel, D. *Microporous Mesoporous Mater.* **1999**, *27*, 329.
164. Stein, A.; Melde, B.J.; Schroden, R.C. *Adv. Mater.* **2000**, *12*, 1403.
165. MacLachlan, M.J.; Asefa, T.; Ozin, G.A. *Chem. Eur. J.* **2000**, *6*, 2507.

166. Schüth, F.; Wang, Y.; Yang, C.-M.; Zibrowius, B. In *Organosilicon Chemistry VI*; Auner, N., Ed.; Wiley-VCH: Heidelberg, 2005; p 860.
167. Inagaki, S.; Guan, S.; Fukushima, Y.; Ohsuna, T.; Terasaki, O. *J. Am. Chem. Soc.* **1999**, *121*, 9611.
168. Melde, B.J.; Holland, B.T.; Blanford, C.F.; Stein, A. *Chem. Mater.* **1999**, *11*, 3302.
169. Asefa, T.; MacLachlan, M.J.; Coombs, N.; Ozin, G.A. *Nature* **1999**, *402*, 867.
170. Inagaki, S.; Guan, S.; Ohsuna, T.; Terasaki, O. *Nature* **2002**, *416*, 304.
171. Ryoo, R.; Joo, S.H.; Jun, S. *J. Phys. Chem. B* **1999**, *103*, 7743.
172. Schüth, F. *Angew. Chem. Int. Ed.* **2003**, *42*, 3604.
173. Ryoo, R.; Joo, S.H. *Stud. Surf. Sci. Catal.* **2004**, *148*, 241.
174. Polarz, S.; Antonietti, M. *Chem. Commun.* **2002**, 2593.
175. Yu, C.Z.; Tian, B.Z.; Zhao, D.Y. *Curr. Opin. Solid State Mater. Sci.* **2003**, 7, 191.
176. Yang, H.F.; Zhao, D.Y. *J. Mater. Chem.* **2005**, *15*, 1217.
177. Valdes-Solis, T.; Fuertes, A.B. *Mater. Res. Bull.* **2006**, *41*, 2187.
178. Lu, A.-H.; Wan, Y.; Zhao Nanocasting, D.Y. *A Versatile Strategy for Creating Nanostructured Porous Materials*. Royal Society of Chemistry: Cambridge, 2010.
179. Tüysüz, H. Novel Mesostructured Metal Oxides, Ph.D. Thesis, Ruhr Universität Bochum, Bochum, 2008, pp 171.
180. Joo, S.H.; Choi, S.J.; Oh, I.; Kwak, J.; Liu, Z.; Terasaki, O.; Ryoo, R. *Nature* **2001**, *412*, 169.
181. Lee, J.; Yoon, S.; Hyeon, T.; Oh, S.M.; Kim, K.B. *Chem. Commun.* **1999**, 2177.
182. Kyotani, T.; Nagai, T.; Inoue, S.; Tomita, A. *Chem. Mater.* **1997**, *9*, 609.
183. Shin, H.J.; Ryoo, R.; Liu, Z.; Terasaki, O. *J. Am. Chem. Soc.* **2001**, *123*, 1246.
184. Lu, A.H.; Schmidt, W.; Taguchi, A.; Spliethoff, B.; Tesche, B.; Schüth, F. *Angew. Chem. Int. Ed.* **2002**, *41*, 3489.
185. Kang, M.; Yi, S.H.; Lee, H.I.; Yie, J.E.; Kim, J.M. *Chem. Commun.* **2002**, 1944.
186. Roggenbuck, J.; Tiemann, M. *J. Am. Chem. Soc.* **2005**, *127*, 1096.
187. Roggenbuck, J.; Koch, G.; Tiemann, M. *Chem. Mater.* **2006**, *18*, 4151.
188. Li, J.X.; Dai, W.L.; Fan, K. *J. Phys. Chem. C* **2008**, *112*, 17657.
189. Dibandjo, P.; Bois, L.; Chassagneux, F.; Cornu, D.; Letoffe, J.M.; Toury, B.; Babonneau, F.; Miele, P. *Adv. Mater.* **2005**, *17*, 571.
190. Dibandjo, P.; Chassagneux, F.; Bois, L.; Sigala, C.; Miele, P. *J. Mater. Chem.* **2005**, *15*, 1917.
191. Liu, Q.; Wang, A.Q.; Wang, X.D.; Zhang, T. *Chem. Mater.* **2006**, *18*, 5153.
192. Wu, Z.X.; Li, Q.A.; Peng, D.; Webley, P.A.; Zhao, D.Y. *J. Am. Chem. Soc.* **2010**, *132*, 12042.
193. Sakithivel, A.; Huang, S.; Chen, W.; Kim, T.; Ryoo, R.; Chiang, A.S.T.; Chen, K.; Liu, S. *Stud. Surf. Sci. Catal.* **2004**, *154*, 394.
194. Lai, X.Y.; Li, X.T.; Geng, W.C.; Tu, J.C.; Li, J.X.; Qiu, S.L. *Angew. Chem. Int. Ed.* **2007**, *46*, 738.
195. Wagner, T.; Waitz, T.; Roggenbuck, J.; Froba, M.; Kohl, C.D.; Tiemann, M. *Thin Solid Films* **2007**, *515*, 8360.
196. Polarz, S.; Orlov, A.V.; Schüth, F.; Lu, A.H. *Chem. Eur. J.* **2007**, *13*, 592.
197. Waitz, T.; Tiemann, M.; Klar, P.J.; Sann, J.; Stehr, J.; Meyer, B.K. *Appl. Phys. Lett.* **2007**, *90*.
198. West, C.; Mokaya, R. *Chem. Mater.* **2009**, *21*, 4080.
199. Tian, B.Z.; Liu, X.Y.; Yang, H.F.; Xie, S.H.; Yu, C.Z.; Tu, B.; Zhao, D.Y. *Adv. Mater.* **2003**, *15*, 1370.
200. Tian, B.Z.; Liu, X.Y.; Solovyov, L.A.; Liu, Z.; Yang, H.F.; Zhang, Z.D.; Xie, S.H.; Zhang, F.Q.; Tu, B.; Yu, C.Z.; Terasaki, O.; Zhao, D.Y. *J. Am. Chem. Soc.* **2004**, *126*, 865.

201. Wang, Y.Q.; Yang, C.M.; Schmidt, W.; Spliethoff, B.; Bill, E.; Schüth, F. *Adv. Mater.* **2005**, *17*, 53.
202. Rumplecker, A.; Kleitz, F.; Salabas, E.L.; Schüth, F. *Chem. Mater.* **2007**, *19*, 485.
203. Tüysüz, H.; Salabas, E.L.; Weidenthaler, C.; Schüth, F. *J. Am. Chem. Soc.* **2008**, *130*, 280.
204. Tüysüz, H.; Lehmann, C.W.; Bongard, H.; Tesche, B.; Schmidt, R.; Schüth, F. *J. Am. Chem. Soc.* **2008**, *130*, 11510.
205. Shi, Y.F.; Meng, Y.; Chen, D.H.; Cheng, S.J.; Chen, P.; Yang, T.F.; Wan, Y.; Zhao, D.Y. *Adv. Funct. Mater.* **2006**, *16*, 561.
206. Wang, Y.M.; Wu, Z.Y.; Wang, H.J.; Zhu, J.H. *Adv. Funct. Mater.* **2006**, *16*, 2374.
207. Yan, J.; Wang, A.J.; Kim, D.P. *Microporous Mesoporous Mater.* **2007**, *100*, 128.
208. Li, G.S.; Zhang, D.Q.; Yu, J.C. *Chem. Mater.* **2008**, *20*, 3983.
209. Luo, Q.L.; Shen, S.D.; Lu, G.Z.; Xiao, X.Z.; Mao, D.S.; Wang, Y.Q. *J. Mater. Chem.* **2009**, *19*, 8079.
210. Mohanty, P.; Landskron, K. *J. Mater. Chem.* **2009**, *19*, 2400.
211. Shi, Y.F.; Guo, B.K.; Corr, S.A.; Shi, Q.H.; Hu, Y.S.; Heier, K.R.; Chen, L.Q.; Seshadri, R.; Stucky, G.D. *Nano Lett.* **2009**, *9*, 4215.
212. Deng, J.G.; Zhang, L.; Dai, H.X.; Xia, Y.S.; Jiang, H.Y.; Zhang, H.; He, H. *J. Phys. Chem. C* **2010**, *114*, 2694.
213. Lai, X.Y.; Wang, D.; Han, N.; Du, J.; Li, J.; Xing, C.J.; Chen, Y.F.; Li, X.T. *Chem. Mater.* **2010**, *22*, 3033.
214. Puertolas, B.; Solsona, B.; Agouram, S.; Murillo, R.; Mastral, A.M.; Aranda, A.; Taylor, S.H.; Garcia, T. *Appl. Catal. B-Environ.* **2010**, *93*, 395.
215. Wan, L.M.; Cui, X.Z.; Chen, H.R.; Shi, J.L. *Mater. Lett.* **2010**, *64*, 1379.
216. Xiao, Q.; Gao, L.; Zhang, X. *J. Inorg. Mater.* **2011**, *26*, 1256.
217. Zhao, J.; Wang, W.N.; Liu, Y.P.; Ma, J.M.; Li, X.W.; Du, Y.; Lu, G.Y. *Sensor. Actuat. B-Chem.* **2011**, *160*, 604.
218. Fang, X.P.; Yu, X.Q.; Liao, S.F.; Shi, Y.F.; Hu, Y.S.; Wang, Z.X.; Stucky, G.D.; Chen, L.Q. *Microporous Mesoporous Mater.* **2012**, *151*, 418.
219. Luo, Q.L.; Shen, S.D.; Lu, G.Z.; Xiao, X.Z.; Mao, D.S.; Wang, Y.Q. *RSC Adv.* **2012**, *2*, 616.
220. Zhang, Y.H.; Wang, A.Q.; Huang, Y.Q.; Xu, Q.Q.; Yin, J.Z.; Zhang, T. *Catal. Lett.* **2012**, *142*, 275.
221. Borchardt, L.; Kockrick, E.; Wollmann, P.; Kaskel, S.; Guron, M.M.; Sneddon, L.G.; Geiger, D. *Chem. Mater.* **2010**, *22*, 4660.
222. Zhu, K.K.; Yue, B.; Zhou, W.Z.; He, H.Y. *Chem. Commun.* **2003**, 98.
223. Jiao, F.; Jumas, J.C.; Womes, M.; Chadwick, A.V.; Harrison, A.; Bruce, P.G. *J. Am. Chem. Soc.* **2006**, *128*, 12905.
224. Jiao, F.; Harrison, A.; Hill, A.H.; Bruce, P.G. *Adv. Mater.* **2007**, *19*, 4063.
225. Ren, Y.; Bruce, P.G.; Ma, Z. *J. Mater. Chem.* **2011**, *21*, 9312.
226. Tüysüz, H.; Liu, Y.; Weidenthaler, C.; Schüth, F. *J. Am. Chem. Soc.* **2008**, *130*, 14108.
227. Tüysüz, H.; Weidenthaler, C.; Schüth, F. *Chem. Eur. J.* **2012**, *18*, 5080.
228. Sun, Y.Y.; Ji, G.B.; Zheng, M.B.; Chang, X.F.; Li, S.D.; Zhang, Y. *J. Mater. Chem.* **2010**, *20*, 945.
229. Tüysüz, H.; Salabas, E.L.; Bill, E.; Bongard, H.; Spliethoff, B.; Lehmann, C.W.; Schüth, F. *Chem. Mater.* **2012**, *24*, 2493.
230. Yen, H.; Seo, Y.; Guillet-Nicolas, R.; Kaliaguine, S.; Kleitz, F. *Chem. Commun.* **2011**, *47*, 10473.
231. Gu, X.; Zhu, W.M.; Jia, C.J.; Zhao, R.; Schmidt, W.; Wang, Y.Q. *Chem. Commun.* **2011**, *47*, 5337.
232. Shi, Y.F.; Wan, Y.; Zhang, R.Y.; Zhao, D.Y. *Adv. Funct. Mater.* **2008**, *18*, 2436.
233. Braun, P.V.; Osenar, P.; Stupp, S.I. *Nature* **1996**, *380*, 325.

234. Osenar, P.; Braun, P.V.; Stupp, S.I. *Adv. Mater.* **1996**, *8*, 1022.

235. Braun, P.V.; Stupp, S.I. *Mater. Res. Bull* **1999**, *34*, 463.

236. Braun, P.V.; Osenar, P.; Tohver, V.; Kennedy, S.B.; Stupp, S.I. *J. Am. Chem. Soc.* **1999**, *121*, 7302.

237. Lubeck, C.R.; Han, T.Y.J.; Gash, A.E.; Satcher, J.H.; Doyle, F.M. *Adv. Mater.* **2006**, *18*, 781.

238. Shi, Y.F.; Wan, Y.; Liu, R.L.; Tu, B.; Zhao, D.Y. *J. Am. Chem. Soc.* **2007**, *129*, 9522.

239. Zhang, F.; Wan, Y.; Shi, Y.F.; Tu, B.; Zhao, D.Y. *Chem. Mater.* **2008**, *20*, 3778.

240. Liang, C.D.; Hong, K.L.; Guiochon, G.A.; Mays, J.W.; Dai, S. *Angew. Chem. Int. Ed.* **2004**, *43*, 5785.

241. Meng, Y.; Gu, D.; Zhang, F.; Shi, Y.; Cheng, L.; Feng, D.; Wu, Z.; Chen, Z.; Wan, Y.; Stein, A.; Zhao, D. *Chem. Mater.* **2006**, *18*, 4447.

242. Meng, Y.; Gu, D.; Zhang, F.Q.; Shi, Y.F.; Yang, H.F.; Li, Z.; Yu, C.Z.; Tu, B.; Zhao, D.Y. *Angew. Chem. Int. Ed.* **2005**, *44*, 7053.

243. Tatsumi, T.; Koyano, K.A.; Tanaka, Y.; Nakata, S. *Chem. Lett.* **1997**, 469.

244. Boger, T.; Roesky, R.; Glaser, R.; Ernst, S.; Eigenberger, G.; Weitkamp, J. *Microporous Mater.* **1997**, *8*, 79.

245. Tatsumi, T.; Koyano, K.A.; Tanaka, Y.; Nakata, S. *J. Porous Mater.* **1999**, *6*, 13.

246. Desplantier–Giscard, D.; Galarneau, A.; Di Renzo, F.; Fajula, F. *Mater. Sci. Eng. C-Bio. S* **2003**, *23*, 727.

247. Schacht, S.; Huo, Q.; VoigtMartin, I.G.; Stucky, G.D.; Schüth, F. *Science* **1996**, *273*, 768.

248. Bruinsma, P.J.; Kim, A.Y.; Liu, J.; Baskaran, S. *Chem. Mater.* **1997**, *9*, 2507.

249. Lu, Y.F.; Fan, H.Y.; Stump, A.; Ward, T.L.; Rieker, T.; Brinker, C.J. *Nature* **1999**, *398*, 223.

250. Huo, Q.S.; Feng, J.L.; Schüth, F.; Stucky, G.D. *Chem. Mater.* **1997**, *9*, 14.

251. Grun, M.; Lauer, I.; Unger, K.K. *Adv. Mater.* **1997**, *9*, 254.

252. Xia, Y.D.; Mokaya, R. *Adv. Mater.* **2004**, *16*, 886.

253. Botterhuis, N.E.; Sun, Q.Y.; Magusin, P.; van Santen, R.A.; Sommerdijk, N. *Chem. Eur. J.* **2006**, *12*, 1448.

254. Yang, H.; Kuperman, A.; Coombs, N.; MamicheAfara, S.; Ozin, G.A. *Nature* **1996**, *379*, 703.

255. Zhao, D.; Yang, P.; Melosh, N.; Feng, J.; Chmelka, B.F.; Stucky, G.D. *Adv. Mater.* **1998**, *10*, 1380.

256. Crepaldi, E.L.; Soler-Illia, G.; Bouchara, A.; Grosso, D.; Durand, D.; Sanchez, C. *Angew. Chem. Int. Ed.* **2003**, *42*, 347.

257. Grosso, D.; Boissiere, C.; Smarsly, B.; Brezesinski, T.; Pinna, N.; Albouy, P.A.; Amenitsch, H.; Antonietti, M.; Sanchez, C. *Nat. Mater.* **2004**, *3*, 787.

258. Grosso, D.; Soler-Illia, G.; Babonneau, F.; Sanchez, C.; Albouy, P.A.; Brunet-Bruneau, A.; Balkenende, A.R. *Adv. Mater.* **2001**, *13*, 1085.

259. Huo, Q.S.; Zhao, D.Y.; Feng, J.L.; Weston, K.; Buratto, S.K.; Stucky, G.D.; Schacht, S.; Schüth, F. *Adv. Mater.* **1997**, *9*, 974.

260. Marlow, F.; Spliethoff, B.; Tesche, B.; Zhao, D.Y. *Adv. Mater.* **2000**, *12*, 961.

261. Marlow, F.; Kleitz, F. *Microporous Mesoporous Mater.* **2001**, *44*, 671.

262. Kleitz, F.; Marlow, F.; Stucky, G.D.; Schüth, F. *Chem. Mater.* **2001**, *13*, 3587.

263. Wang, J.F.; Zhang, J.P.; Asoo, B.Y.; Stucky, G.D. *J. Am. Chem. Soc.* **2003**, *125*, 13966.

264. Lin, H.P.; Mou, C.Y. *Science* **1996**, *273*, 765.

265. Kleitz, F.; Wilczok, U.; Schüth, F.; Marlow, F. *Phys. Chem. Chem. Phys.* **2001**, *3*, 3486.

266. Wu, X.W.; Ruan, J.F.; Ohsuna, T.; Terasaki, O.; Che, S.N. *Chem. Mater.* **2007**, *19*, 1577.

267. Tolbert, S.H.; Firouzi, A.; Stucky, G.D.; Chmelka, B.F. *Science* **1997**, *278*, 264.

268. Smatt, J.H.; Schunk, S.; Linden, M. *Chem. Mater.* **2003**, *15*, 2354.

269. Smatt, J.H.; Weidenthaler, C.; Rosenholm, J.B.; Linden, M. *Chem. Mater.* **2006**, *18*, 1443.
270. Sun, Z.; Deng, Y.; Wei, J.; Gu, D.; Tu, B.; Zhao, D. *Chem. Mater.* **2011**, *23*, 2176.
271. Florent, M.; Xue, C.; Zhao, D.; Goldfarb, D. *Chem. Mater.* **2012**, *24*, 383.
272. Wang, H.; Jeong, H.Y.; Imura, M.; Wang, L.; Radhakrishnan, L.; Fujita, N.; Castle, T.; Terasaki, O.; Yamauchi, Y. *J. Am. Chem. Soc.* **2011**, *133*, 14526.
273. Vartuli, J.C.; Schmitt, K.D.; Kresge, C.T.; Roth, W.J.; Leonowicz, M.E.; Mccullen, S.B.; Hellring, S.D.; Beck, J.S.; Schlenker, J.L.; Olson, D.H.; Sheppard, E.W. *Chem. Mater.* **1994**, *6*, 2317.
274. Tsoncheva, T.; Linden, A.; Areva, S.; Minchev, C. *Catal. Commun.* **2006**, 7, 357.
275. Tsoncheva, T.; Rosenholm, J.; Teixeira, C.V.; Dimitrov, M.; Linden, M.; Minchev, C. *Microporous Mesoporous Mater.* **2006**, *89*, 209.
276. Yang, H.; Coombs, N.; Sokolov, I.; Ozin, G.A. *Nature* **1996**, *381*, 589.
277. Aksay, I.A.; Trau, M.; Manne, S.; Honma, I.; Yao, N.; Zhou, L.; Fenter, P.; Eisenberger, P.M.; Gruner, S.M. *Science* **1996**, *273*, 892.
278. Ogawa, M. *Chem. Commun.* **1996**, 1149.
279. Ogawa, M. *J. Am. Chem. Soc.* **1994**, *116*, 7941.
280. Lu, Y.F.; Ganguli, R.; Drewien, C.A.; Anderson, M.T.; Brinker, C.J.; Gong, W.L.; Guo, Y.X.; Soyez, H.; Dunn, B.; Huang, M.H.; Zink, J.I. *Nature* **1997**, *389*, 364.
281. Choi, S.Y.; Mamak, M.; Coombs, N.; Chopra, N.; Ozin, G.A. *Adv. Funct. Mater.* **2004**, *14*, 335.
282. Jiang, X.; Oveisi, H.; Nemoto, Y.; Suzuki, N.; Wu, K.C.W.; Yamauchi, Y. *Dalton Trans.* **2011**, *40*, 10851.
283. Kuemmel, M.; Grosso, D.; Boissiere, U.; Smarsly, B.; Brezesinski, T.; Albouy, P.A.; Amenitsch, H.; Sanchez, C. *Angew. Chem. Int. Ed.* **2005**, *44*, 4589.
284. Wan, L.J.; Fu, H.G.; Shi, K.Y.; Tian, X.Q. *Microporous Mesoporous Mater.* **2008**, *115*, 301.
285. Wang, Y.; Brezesinski, T.; Antonietti, M.; Smarsly, B. *ACS Nano* **2009**, *3*, 1373.
286. Brezesinski, T.; Fischer, A.; Iimura, K.-i.; Sanchez, C.; Grosso, D.; Antonietti, M.; Smarsly, B.M. *Adv. Funct. Mater.* **2006**, *16*, 1433.
287. Brezesinski, T.; Antonietti, M.; Groenewolt, M.; Pinna, N.; Smarsly, B. *New J. Chem.* **2005**, *29*, 237.
288. Katou, T.; Lee, B.; Lu, D.L.; Kondo, J.N.; Hara, M.; Domen, K. *Angew. Chem. Int. Ed.* **2003**, *42*, 2382.
289. Katou, T.; Lee, B.; Lu, D.; Kondo, J.N.; Hara, M.; Domen, K. *Stud. Surf. Sci. Catal.* **2003**, *146*, 251.
290. Ravikovitch, P.I.; Neimark, A.V. *Langmuir* **2002**, *18*, 1550.
291. Ravikovitch, P.I.; Neimark, A.V. *J. Phys. Chem. B* **2001**, *105*, 6817.
292. Thommes, M.; Kohn, R.; Froba, M. *Appl. Surf. Sci.* **2002**, *196*, 239.
293. Jaroniec, M.; Kruk, M. *Stud. Surf. Sci. Catal.* **2003**, *146*, 263.
294. Kruk, M.; Jaroniec, M. *Microporous Mesoporous Mater.* **2001**, *44*, 725.
295. Kruk, M.; Jaroniec, M.; Ryoo, R.; Kim, J.M. *Microporous Mater.* **1997**, *12*, 93.
296. Setzer, C.; von Essche, G.; Pryor, N. In *Handbook of Porous Solids*; Schüth, F., Sing, K.S.W., Weitkamp, J., Eds.; Wiley-VCH: Weinheim, 2002; p 1543.
297. Wingen, A.; Anastasievic, N.; Hollnagel, A.; Werner, D.; Schüth, F. *J. Catal.* **2000**, *193*, 248.
298. Froba, M.; Kohn, R.; Bouffaud, G.; Richard, O.; van Tendeloo, G. *Chem. Mater.* **1999**, *11*, 2858.
299. Kohn, R.; Paneva, D.; Dimitrov, M.; Tsoncheva, T.; Mitov, I.; Minchev, C.; Froba, M. *Microporous Mesoporous Mater.* **2003**, *63*, 125.
300. Huwe, H.; Froba, M. *Anal. Bioanal. Chem.* **2006**, *384*, 817.
301. Huwe, H.; Froba, M. *Microporous Mesoporous Mater.* **2003**, *60*, 151.

302. Cao, J.M.; He, N.Y.; Li, C.; Dong, J.L.; Xu, Q.H. *Stud. Surf. Sci. Catal.* **1998**, *117*, 461.
303. He, N.Y.; Bao, S.L.; Xu, Q.H. *Stud. Surf. Sci. Catal.* **1997**, *105*, 85.
304. Bachari, K.; Millet, J.M.M.; Benaichouba, B.; Cherifi, O.; Figueras, F. *J. Catal.* **2004**, *221*, 55.
305. Sun, Y.Y.; Walspurger, S.; Tessonnier, J.P.; Louis, B.; Sommer, J. *Appl. Catal. A* **2006**, *300*, 1.
306. Okumura, K.; Nishigaki, K.; Niwa, M. *Microporous Mesoporous Mater.* **2001**, *44*, 509.
307. Li, X.K.; Ji, W.J.; Zhao, J.; Wang, S.J.; Au, C.T. *J. Catal.* **2005**, *236*, 181.
308. Xiong, H.F.; Zhang, Y.H.; Wang, S.G.; Liew, K.Y.; Li, J.L. *J. Phys. Chem. C* **2008**, *112*, 9706.
309. Chary, K.; Srikanth, C. *Catal. Lett.* **2009**, *128*, 164.
310. Landau, M.V.; Dafa, E.; Kaliya, M.L.; Sen, T.; Herskowitz, M. *Microporous Mesoporous Mater.* **2001**, *49*, 65.
311. de P, A.L.V.; Alarcon, E.; de Correa, C.M. *Chem. Commun.* **2002**, 2654.
312. Gruene, P.; Wolfram, T.; Pelzer, K.; Schlogl, R.; Trunschke, A. *Catalysis Today* **2010**, *157*, 137.
313. Liu, Y.M.; Cao, Y.; Zhu, K.K.; Yan, S.R.; Dai, W.L.; He, H.Y.; Fan, K.N. *Chem. Commun.* **2002**, 2832.
314. Liu, Y.M.; Cao, Y.; Yi, N.; Feng, W.L.; Dai, W.L.; Yan, S.R.; He, H.Y.; Fan, K.N. *J. Catal.* **2004**, *224*, 417.
315. Zhang, Q.H.; Wang, Y.; Ohishi, Y.; Shishido, T.; Takehira, K. *J. Catal.* **2001**, *202*, 308.
316. Solsona, B.; Blasco, T.; Nieto, J.M.L.; Pena, M.L.; Rey, F.; Vidal-Moya, A. *J. Catal.* **2001**, *203*, 443.
317. Sulikowski, B.; Olejniczak, Z.; Wloch, E.; Rakoczy, J.; Valenzuela, R.X.; Corberan, V.C. *Appl. Catal. A-Gen* **2002**, *232*, 189.
318. Bruckner, A.; Rybarczyk, P.; Kosslick, H.; Wolf, G.U.; Baerns, M. *Stud. Surf. Sci. Catal.* **2002**, *142*, 1141.
319. Hess, C.; Drake, I.J.; Hoefelmeyer, J.D.; Tilley, T.D.; Bell, A.T. *Catal. Lett.* **2005**, *105*, 1.
320. Xu, J.; Chen, M.; Liu, Y.M.; Cao, Y.; He, H.Y.; Fan, K.N. *Microporous Mesoporous Mater.* **2009**, *118*, 354.
321. Berndt, H.; Martin, A.; Bruckner, A.; Schreier, E.; Muller, D.; Kosslick, H.; Wolf, G.U.; Lucke, B. *J. Catal.* **2000**, *191*, 384.
322. Lin, B.M.; Wang, X.X.; Guo, Q.; Yang, W.; Zhang, Q.H.; Wang, Y. *Chem. Lett.* **2003**, *32*, 860.
323. Fornes, V.; Lopez, C.; Lopez, H.H.; Martinez, A. *Appl. Catal. A* **2003**, *249*, 345.
324. Dai, L.X.; Teng, Y.H.; Tabata, K.; Suzuki, E.; Tatsumi, T. *Microporous Mesoporous Mater.* **2001**, *44*, 573.
325. Gao, X.T.; Wachs, I.E.; Wong, M.S.; Ying, J.Y. *J. Catal.* **2001**, *203*, 18.
326. Trejda, M.; Tuel, A.; Kujawa, J.; Kilos, B.; Ziolek, M. *Microporous Mesoporous Mater.* **2008**, *110*, 271.
327. Euzen, P.; Raybaud, P.; Krokidis, X.; Toulhoat, H.; Le Loarer, J.-L.; Jolivet, J.-P.; Froidefond, C. In *Handbook of Porous Solids*; Schüth, F., Sing, K.S.W., Weitkamp, J., Eds.; Wiley-VCH: Weinheim, 2002; p 1591.
328. Gonzalez-Pena, V.; Marquez-Alvarez, C.; Sastre, E.; Perez-Pariente, J. *Stud. Surf. Sci. Catal.* **2002**, *142*, 1283.
329. Cabrera, S.; El Haskouri, J.; Alamo, J.; Beltran, A.; Beltran, D.; Mendioroz, S.; Marcos, M.D.; Amoros, P. *Adv. Mater.* **1999**, *11*, 379.
330. Yada, M.; Machida, M.; Kijima, T. *Chem. Commun.* **1996**, 769.
331. Valange, S.; Guth, J.L.; Kolenda, F.; Lacombe, S.; Gabelica, Z. *Microporous Mesoporous Mater.* **2000**, *35–6*, 597.

332. Sicard, L.; Lebeau, B.; Patarin, J.; Kolenda, F. *Stud. Surf. Sci. Catal.* **2002**, *143*, 209.
333. Schüth, F.; Czuryskiewicz, T.; Kleitz, F.; Linden, M.; Lu, A.H.; Rosenholm, J.; Schmidt, W.; Taguchi, A. *Stud. Surf. Sci. Catal.* **2003**, *146*, 399.
334. Yuan, Q.; Yin, A.-X.; Luo, C.; Sun, L.-D.; Zhang, Y.-W.; Duan, W.-T.; Liu, H.-C.; Yan, C.-H. *J. Am. Chem. Soc.* **2008**, *130*, 3465.
335. Li, L.-L.; Duan, W.-T.; Yuan, Q.; Li, Z.-X.; Duan, H.-H.; Yan, C.-H. *Chem. Commun.* **2009**, 6174.
336. Onaka, M.; Oikawa, T. *Chem. Lett.* **2002**, 850.
337. Zhen-Xing, L.; Fu-Bo, S.; Le-Le, L.; Tao, Z.; Chun-Hua, Y. *Phys. Chem. Chem. Phys.* **2011**, *13*, 2488.
338. Armatas, G.S.; Katsoulidis, A.P.; Petrakis, D.E.; Pomonis, P.J. *J. Mater. Chem.* **2010**, *20*, 8631.
339. Vaudry, F.; Khodabandeh, S.; Davis, M.E. *Chem. Mater.* **1996**, *8*, 1451.
340. Velu, S.; Kapoor, M.P.; Inagaki, S.; Suzuki, K. *Appl. Catal. A-Gen.* **2003**, *245*, 317.
341. Chang, P.Y.; Huang, C.H.; Doong, R.A. *Carbon* **2012**, *50*, 4259.
342. Liu, S.; Guo, E.Y.; Yin, L.W. *J. Mater. Chem.* **2012**, *22*, 5031.
343. Zhao, J.Q.; Wan, P.; Xiang, J.; Tong, T.; Dong, L.; Gao, Z.N.; Shen, X.Y.; Tong, H. *Microporous Mesoporous Mater.* **2011**, *138*, 200.
344. Kao, L.H.; Hsu, T.C.; Cheng, K.K. *J. Colloid Interface Sci.* **2010**, *341*, 359.
345. Zhang, F.L.; Zheng, Y.H.; Cao, Y.N.; Chen, C.Q.; Zhan, Y.Y.; Lin, X.Y.; Zheng, Q.; Wei, K.M.; Zhu, J.F. *J. Mater. Chem.* **2009**, *19*, 2771.
346. Li, G.S.; Zhang, D.Q.; Yu, J.C. *Phys. Chem. Chem. Phys.* **2009**, *11*, 3775.
347. Ergun, O.; Karslioglu, O.; Yilmaz, A.; Uner, D. *Turk. J. Chem.* **2007**, *31*, 501.
348. Pan, J.H.; Lee, W.I. *Chem. Mater.* **2006**, *18*, 847.
349. Tang, J.; Wu, Y.Y.; McFarland, E.W.; Stucky, G.D. *Chem. Commun.* **2004**, 1670.
350. Perkas, N.; Koltypin, Y.; Palchik, O.; Gedanken, A.; Chandrasekaran, S. *App. Catal. A-Gen.* **2001**, *209*, 125.
351. Gedanken, A.; Tang, X.H.; Wang, Y.Q.; Perkas, N.; Koltypin, Y.; Landau, M.V.; Vradman, L.; Herskowitz, M. *Chem. Eur. J.* **2001**, 7, 4546.
352. Yoshitake, H.; Tatsumi, T. *Chem. Mater.* **2003**, *15*, 1695.
353. Stone, V.F.; Davis, R.J. *Chem. Mater.* **1998**, *10*, 1468.
354. Yusuf, M.M.; Imai, H.; Hirashima, H. *J. Sol-Gel Sci. Technol.* **2002**, *25*, 65.
355. Takahara, Y.; Kondo, J.N.; Takata, T.; Lu, D.L.; Domen, K. *Chem. Mater.* **2001**, *13*, 1194.
356. Uchida, M.; Kondo, J.N.; Lu, D.L.; Domen, K. *Chem. Lett.* **2002**, 498.
357. Hisatomi, T.; Otani, M.; Nakajima, K.; Teramura, K.; Kako, Y.; Lu, D.; Takata, T.; Kondo, J.N.; Domen, K. *Chem. Mater.* **2010**, *22*, 3854.
358. Wang, X.C.; Maeda, K.; Thomas, A.; Takanabe, K.; Xin, G.; Carlsson, J.M.; Domen, K.; Antonietti, M. *Nat. Mater.* **2009**, *8*, 76.
359. Antonelli, D.M.; Ying, J.Y. *Angew. Chem. Int. Ed.* **1996**, *35*, 426.
360. Vettraino, M.; He, X.; Trudeau, M.; Drake, J.E.; Antonelli, D.M. *Adv. Funct. Mater.* **2002**, *12*, 174.
361. Brodsky, C.J.; Ko, E.I. *J. Non-Cryst. Solids* **1995**, *186*, 88.
362. Landau, M.V. In *Handbook of Porous Solids*; Schüth, F., Sing, K.S.W., Weitkamp, J., Eds.; Wiley-VCH: Weinheim, 2002; p 1677.
363. Serre, C.; Auroux, A.; Gervasini, A.; Hervieu, M.; Ferey, G. *Angew. Chem. Int. Ed.* **2002**, *41*, 1594.
364. Carreon, M.A.; Guliants, V.V.; Pierelli, F.; Cavani, F. *Catal. Lett.* **2004**, *92*, 11.
365. Bluhm, H.; Havecker, M.; Kleimenov, E.; Knop-Gericke, A.; Liskowski, A.; Schlögl, R.; Su, D.S. *Top. Catal.* **2003**, *23*, 99.
366. Tüysüz, H.; Comotti, M.; Schüth, F. *Chem. Commun.* **2008**, 4022.

367. Wu, J.-M.; Antonietti, M.; Gross, S.; Bauer, M.; Smarsly, B.M. *Chemphyschem* **2008**, *9*, 748.
368. Brezesinski, K.; Ostermann, R.; Hartmann, P.; Perlich, J.; Brezesinski, T. *Chem. Mater.* **2010**, *22*, 3079.
369. Reitz, C.; Brezesinski, K.; Haetge, J.; Perlich, J.; Brezesinski, T. *RSC Adv.* **2012**, *2*, 5130.
370. Chen, C.Y.; Li, H.X.; Davis, M.E. *Microporous Mater.* **1993**, *2*, 17.
371. Corma, A.; Fornes, V.; Navarro, M.T.; Perezpariente, J. *J. Catal.* **1994**, *148*, 569.
372. Auroux, A. *Top. Catal.* **2002**, *19*, 205.
373. Galarneau, A.; Barodawalla, A.; Pinnavaia, T.J. *Nature* **1995**, *374*, 529.
374. Galarneau, A.; Desplantier-Giscard, D.; Di Renzo, F.; Fajula, F. *Catal. Today* **2001**, *68*, 191.
375. Cassiers, K.; Linssen, T.; Mathieu, M.; Benjelloun, M.; Schrijnemakers, K.; Van Der Voort, P.; Cool, P.; Vansant, E.F. *Chem. Mater.* **2002**, *14*, 2317.
376. Igarashi, N.; Koyano, K.A.; Tanaka, Y.; Nakata, S.; Hashimoto, K.; Tatsumi, T. *Microporous Mesoporous Mater.* **2003**, *59*, 43.
377. Mokaya, R. *Angew. Chem. Int. Ed.* **1999**, *38*, 2930.
378. O'Neil, A.S.; Mokaya, R.; Poliakoff, M. *J. Am. Chem. Soc.* **2002**, *124*, 10636.
379. Kisler, J.M.; Gee, M.L.; Stevens, G.W.; O'Connor, A.J. *Chem. Mater.* **2003**, *15*, 619.
380. Ryoo, R.; Jun, S. *J. Phys. Chem. B* **1997**, *101*, 317.
381. Karlsson, A.; Stocker, M.; Schmidt, R. *Microporous Mesoporous Mater.* **1999**, *27*, 181.
382. Kloetstra, K.R.; van Bekkum, H.; Jansen, J.C. *Chem. Commun.* **1997**, 2281.
383. Liu, Y.; Zhang, W.Z.; Pinnavaia, T.J. *Angew. Chem. Int. Ed.* **2001**, *40*, 1255.
384. Guo, W.P.; Huang, L.M.; Deng, P.; Xue, Z.Y.; Li, Q.Z. *Microporous Mesoporous Mater.* **2001**, *44*, 427.
385. Meng, X.J.; Li, D.F.; Yang, X.Y.; Yu, Y.; Wu, S.; Han, Y.; Yang, Q.; Jiang, D.Z.; Xiao, F.S. *J. Phys. Chem. B* **2003**, *107*, 8972.
386. Kremer, S.P.B.; Kirschhock, C.E.A.; Aerts, A.; Villani, K.; Martens, J.A.; Lebedev, O.I.; Van Tendeloo, G. *Adv. Mater.* **2003**, *15*, 1705.
387. On, D.T.; Kaliaguine, S. *Angew. Chem. Int. Ed.* **2002**, *41*, 1036.
388. Trong-On, D.; Ungureanu, A.; Kaliaguine, S. *Phys. Chem. Chem. Phys.* **2003**, *5*, 3534.
389. On, D.T.; Kaliaguine, S. *Stud. Surf. Sci. Catal.* **2003**, *146*, 561.
390. Kozhevnikov, I.V.; Sinnema, A.; Jansen, R.J.J.; Pamin, K.; van Bekkum, H. *Catal. Lett.* **1995**, *30*, 241.
391. Kozhevnikov, I.V.; Kloetstra, K.R.; Sinnema, A.; Zandbergen, H.W.; van Bekkum, H. *J. Mol. Catal. A: Chem.* **1996**, *114*, 287.
392. Marme, F.; Coudurier, G.; Vedrine, J.C. *Microporous Mesoporous Mater.* **1998**, *22*, 151.
393. Blasco, T.; Corma, A.; Martinez, A.; Martinez-Escolano, P. *J. Catal.* **1998**, *177*, 306.
394. Ghanbari-Siahkali, A.; Philippou, A.; Dwyer, J.; Anderson, M.W. *Appl. Catal. A-Gen.* **2000**, *192*, 57.
395. Jalil, P.A.; Al-Daous, M.A.; Al-Arfaj, A.R.A.; Al-Amer, A.M.; Beltramini, J.; Barri, S.A.I. *Appl. Catal. A-Gen.* **2001**, *207*, 159.
396. Choi, S.M.; Wang, Y.; Nie, Z.M.; Liu, J.; Peden, C.H.F. *Catal. Today* **2000**, *55*, 117.
397. Lim, M.H.; Blanford, C.F.; Stein, A. *Chem. Mater.* **1998**, *10*, 467.
398. Van Rhijn, W.M.; De Vos, D.E.; Sels, B.F.; Bossaert, W.D.; Jacobs, P.A. *Chem. Commun.* **1998**, 317.
399. Bossaert, W.D.; De Vos, D.E.; Van Rhijn, W.M.; Bullen, J.; Grobet, P.J.; Jacobs, P.A. *J. Catal.* **1999**, *182*, 156.
400. Diaz, I.; Marquez-Alvarez, C.; Mohino, F.; Perez-Pariente, J.; Sastre, E. *J. Catal.* **2000**, *193*, 283.
401. Diaz, I.; Marquez-Alvarez, C.; Mohino, F.; Perez-Pariente, J.; Sastre, E. *J. Catal.* **2000**, *193*, 295.

402. Diaz, I.; Marquez-Alvarez, C.; Mohino, F.; Perez–Pariente, J.; Sastre, E. *Microporous Mesoporous Mater.* **2001**, *44*, 295.
403. Diaz, I.; Mohino, F.; Perez–Pariente, J.; Sastre, E. *Appl. Catal. A-Gen*. **2001**, *205*, 19.
404. Margolese, D.; Melero, J.A.; Christiansen, S.C.; Chmelka, B.F.; Stucky, G.D. *Chem. Mater.* **2000**, *12*, 2448.
405. Melero, J.A.; Stucky, G.D.; van Grieken, R.; Morales, G. *J. Mater. Chem.* **2002**, *12*, 1664.
406. Zeidan, R.K.; Hwang, S.-J.; Davis, M.E. *Angew. Chem. Int. Ed.* **2006**, *45*, 6332.
407. Melero, J.A.; van Grieken, R.; Morales, G.; Nuno, V. *Catal. Commun.* **2004**, *5*, 131.
408. Yang, C.M.; Zibrowius, B.; Schmidt, W.; Schüth, F. *Chem. Mater.* **2003**, *15*, 3739.
409. Yang, C.M.; Zibrowius, B.; Schüth, F. *Chem. Commun.* **2003**, 1772.
410. Yang, C.M.; Wang, Y.Q.; Zibrowius, B.; Schüth, F. *Phys. Chem. Chem. Phys.* **2004**, *6*, 2461.
411. Alvaro, M.; Corma, A.; Das, D.; Fornes, V.; Garcia, H. *Chem. Commun.* **2004**, 956.
412. Alvaro, M.; Corma, A.; Das, D.; Fornes, V.; Garcia, H. *J. Catal.* **2005**, *231*, 48.
413. Martinez, F.; Morales, G.; Martin, A.; van Grieken, R. *Appl. Catal. A-Gen.* **2008**, *347*, 169.
414. Shen, W.; Gu, Y.; Xu, H.L.; Dube, D.; Kaliaguine, S. *Appl. Catal. A-Gen.* **2010**, *377*, 1.
415. Fujiwara, M.; Kuraoka, K.; Yazawa, T.; Xu, Q.; Tanaka, M.; Souma, Y. *Chem. Commun.* **2000**, 1523.
416. Kloetstra, K.R.; van Bekkum, H. *J. Chem. Soc. Chem. Comm* **1995**, 1005.
417. Kloetstra, K.R.; van Laren, M.; van Bekkum, H. *J. Chem. Soc. Faraday Trans.* **1997**, *93*, 1211.
418. Brunel, D.; Cauvel, A.; Fajula, F.; DiRenzo, F. *Stud. Surf. Sci. Catal.* **1995**, *97*, 173.
419. Sutra, P.; Brunel, D. *Chem. Commun.* **1996**, 2485.
420. Cauvel, A.; Renard, G.; Brunel, D. *J. Org. Chem.* **1997**, *62*, 749.
421. Lasperas, M.; Llorett, T.; Chaves, L.; Rodriguez, I.; Cauvel, A.; Brunel, D. *Stud. Surf. Sci. Catal.* **1997**, *108*, 75.
422. Derrien, A.; Renard, G.; Brunel, D. *Stud. Surf. Sci. Catal.* **1998**, *117*, 445.
423. Macquarrie, D.J. *Chem. Commun.* **1996**, 1961.
424. Mdoe, J.E.G.; Clark, J.H.; Macquarrie, D.J. *Synlett* **1998**, 625.
425. Alauzun, J.; Mehdi, A.; Reye, C.; Corriu, R.J.P. *J. Am. Chem. Soc.* **2006**, *128*, 8718.
426. Vartuli, J. Presentation at the Meeting on Mesoporous Crystals and Related Nanostructured Materials, Stockholm, June 1–5, 2004.
427. Da, J.W.; Song, C.M.; Qian, L.; Su, J.M.; Xu, X.Z. *J. Porous Mater.* **2008**, *15*, 189.
428. Corma, A.; Grande, M.S.; Gonzalez–Alfaro, V.; Orchilles, A.V. *J. Catal.* **1996**, *159*, 375.
429. Pater, J.P.G.; Jacobs, P.A.; Martens, J.A. *J. Catal.* **1999**, *184*, 262.
430. Seo, G.; Kim, N.H.; Lee, Y.H.; Kim, J.H. *Catal. Lett.* **1999**, *57*, 209.
431. Corma, A.; Gonzalez–Alfaro, V.; Orchilles, A.V. *J. Catal.* **2001**, *200*, 34.
432. Kubicka, D.; Kumar, N.; Maki-Arvela, P.; Tiitta, M.; Niemi, V.; Salmi, T.; Murzin, D.Y. *J. Catal.* **2004**, *222*, 65.
433. Byambajav, E.; Ohtsuka, Y. *Fuel* **2003**, *82*, 1571.
434. Twaiq, F.A.; Mohamed, A.R.; Bhatia, S. *Microporous Mesoporous Mater.* **2003**, *64*, 95.
435. Siskin, M.; Kelemen, S.R.; Eppig, C.P.; Brown, L.D.; Afeworki, M. *Energy Fuel* **2006**, *20*, 1227.
436. Xia, Q.H.; Hidajat, K.; Kawi, S. *J. Catal.* **2002**, *209*, 433.
437. Chiche, B.; Sauvage, E.; Di Renzo, F.; Ivanova, I.I.; Fajula, F. *J. Mol. Catal. A: Chem.* **1998**, *134*, 145.
438. Climent, M.J.; Corma, A.; Guil-Lopez, R.; Iborra, S.; Primo, J. *J. Catal.* **1998**, *175*, 70.
439. Climent, M.J.; Corma, A.; Iborra, S.; Navarro, M.C.; Primo, J. *J. Catal.* **1996**, *161*, 783.
440. Liu, Y.; Kim, S.S.; Pinnavaia, T.J. *J. Catal.* **2004**, *225*, 381.

441. Armengol, E.; Cano, M.L.; Corma, A.; Garcia, H.; Navarro, M.T. *J. Chem. Soc. Chem. Commun.* **1995**, 519.
442. Hu, X.C.; Foo, M.L.; Chuah, G.K.; Jaenicke, S. *J. Catal.* **2000**, *195*, 412.
443. Wang, Y.; Kim, A.Y.; Li, X.S.; Wang, L.-Q.; Peden, C.H.F.; Bunker, B.C. *ACS Symp. Ser.* **2000**, *738*, 353.
444. Stoylkova, T.Y.; Chanev, C.D.; Lechert, H.T.; Bezouhanova, C.P. *Catal. Lett.* **2000**, *69*, 109.
445. Singh, A.P. *Catal. Lett.* **1992**, *16*, 431.
446. Nowinska, K.; Kaleta, W. *Appl. Catal. A-Gen.* **2000**, *203*, 91.
447. Das, D.; Lee, J.F.; Cheng, S.F. *J. Catal.* **2004**, *223*, 152.
448. Wang, X.Q.; Liu, R.; Waje, M.M.; Chen, Z.W.; Yan, Y.S.; Bozhilov, K.N.; Feng, P.Y. *Chem. Mater.* **2007**, *19*, 2395.
449. Wang, W.; Zhuang, X.; Zhao, Q.F.; Wan, Y. *J. Mater. Chem.* **2012**, *22*, 15874.
450. Jana, S.K.; Kugita, T.; Namba, S. *Appl. Catal. A-Gen.* **2004**, *266*, 245.
451. Maki-Arvela, P.; Kumar, N.; Nieminen, V.; Sjoholm, R.; Salmi, T.; Murzin, D.Y. *J. Catal.* **2004**, *225*, 155.
452. Hu, S.; Liu, D.; Li, L.; Guo, Z.; Chen, Y.; Borgna, A.; Yang, Y. *Chem. Eng. J.* **2010**, *165*, 916.
453. Corma, A.; Iborra, S.; Rodriguez, I.; Iglesias, M.; Sanchez, F. *Catal. Lett.* **2002**, *82*, 237.
454. Doyaguez, E.G.; Calderon, F.; Sanchez, F.; Fernandez-Mayoralas, A. *J. Org. Chem.* **2007**, *72*, 9353.
455. Srivastava, R. *J. Mol. Catal. A: Chem* **2007**, *264*, 146.
456. Wang, X.G.; Lin, K.S.K.; Chan, J.C.C.; Cheng, S. *Chem. Commun.* **2004**, 2762.
457. Kaskel, S.; Schlichte, K.; Zibrowius, B. *Phys. Chem. Chem. Phys.* **2002**, *4*, 1675.
458. Farrusseng, D.; Schlichte, K.; Spliethoff, B.; Wingen, A.; Kaskel, S.; Bradley, J.S.; Schüth, F. *Angew. Chem. Int. Ed.* **2001**, *40*, 4204.
459. Taramasso, M.; Perego, G.; Notari, B. U.S. Patent 4 410 501, USA 1982.
460. Clerici, M.G.; Bellussi, G.; Romano, U. *J. Catal.* **1991**, *129*, 159.
461. Clerici, M.G.; Ingallina, P. *J. Catal.* **1993**, *140*, 71.
462. Corma, A.; Camblor, M.A.; Esteve, P.; Martinez, A.; Perezpariente, J. *J. Catal.* **1994**, *145*, 151.
463. Corma, A.; Esteve, P.; Martinez, A.; Valencia, S. *J. Catal.* **1995**, *152*, 18.
464. Corma, A.; Iglesias, M.; Sanchez, F. *Catal. Lett.* **1996**, *39*, 153.
465. Haruta, M.; Uphade, B.S.; Tsubota, S.; Miyamoto, A. *Res. Chem. Intermed.* **1998**, *24*, 329.
466. van der Waal, J.C.; Rigutto, M.S.; van Bekkum, H. *Appl. Catal. A-Gen.* **1998**, *167*, 331.
467. Blasco, T.; Corma, A.; Navarro, M.T.; Pariente, J.P. *J. Catal.* **1995**, *156*, 65.
468. Mandache, I.; Parvulescu, V.I.; Popescu, A.; Parvulescu, L.; Banciu, M.D.; Amoros, P.; Beltran, D.; On, D.T.; Kaliaguine, S. *Microporous Mesoporous Mater.* **2005**, *81*, 115.
469. Lin, W.Y.; Frei, H. *J. Phys. Chem. B* **2005**, *109*, 4929.
470. Nakamura, R.; Frei, H. *J. Am. Chem. Soc.* **2006**, *128*, 10668.
471. Han, H.; Frei, H. *J. Phys. Chem. C* **2008**, *112*, 8391.
472. Kureshy, R.I.; Ahmad, I.; Khan, N.H.; Abdi, S.H.R.; Pathak, K.; Jasra, R.V. *J. Catal.* **2006**, *238*, 134.
473. Kondo, J.N.; Domen, K. *Chem. Mater.* **2008**, *20*, 835.
474. Karimi, B.; Abedi, S.; Clark, J.H.; Budarin, V. *Angew. Chem. Int. Ed.* **2006**, *45*, 4776.
475. Katou, T.; Lu, D.L.; Kondo, J.N.; Domen, K. *J. Mater. Chem.* **2002**, *12*, 1480.
476. Noda, Y.; Lee, B.; Domen, K.; Kondo, J.N. *Chem. Mater.* **2008**, *20*, 5361.
477. Tanaka, M.; Shima, H.; Yokoi, T.; Tatsumi, T.; Kondo, J.N. *Catal. Lett.* **2011**, *141*, 283.

478. Ismail, A.A.; Bahnemann, D.W.; Robben, L.; Yarovyi, V.; Wark, M. *Chem. Mater.* **2010**, *22*, 108.
479. Bernardoni, F.; Kouba, M.; Fadeev, A.Y. *Chem. Mater.* **2008**, *20*, 382.
480. Kidder, M.K.; Buchanan, A.C. *J. Phys. Chem. C* **2008**, *112*, 3027.
481. Kidder, M.K.; Chaffee, A.L.; Nguyen, M.-H.T.; Buchanan, A.C., III *J. Org. Chem.* **2011**, *76*, 6014.
482. Kidder, M.K.; Britt, P.F.; Chaffee, A.L.; Buchanan, A.C. *Chem. Commun.* **2007**, 52.
483. Shylesh, S.; Singh, A.R. *J. Catal.* **2006**, *244*, 52.
484. Dal Santo, V.; Liguori, F.; Pirovano, C.; Guidotti, M. *Molecules* **2010**, *15*, 3829.
485. Thomas, J.M.; Raja, R. *Top. Catal.* **2006**, *40*, 3.
486. Jones, M.D.; Raja, R.; Thomas, J.M.; Johnson, B.F.G.; Lewis, D.W.; Rouzaud, J.; Harris, K.D.M. *Angew. Chem. Int. Ed.* **2003**, *42*, 4326.
487. Corma, A.; Martinez, A.; Martinezsoria, V.; Monton, J.B. *J. Catal.* **1995**, *153*, 25.
488. Corma, A.; Martinez, A.; MartinezSoria, V. *J. Catal.* **1997**, *169*, 480.
489. Junges, U.; Jacobs, W.; Voigtmartin, I.; Krutzsch, B.; Schüth, F. *J. Chem. Soc. Chem. Commun.* **1995**, 2283.
490. Junges, U.; Schüth, F.; Schmid, G.; Uchida, Y.; Schlögl, R. *Ber. Bunsen. Phys. Chem.* **1997**, *101*, 1631.
491. Mehnert, C.P.; Ying, J.Y. *Chem. Commun.* **1997**, 2215.
492. Schiesser, W.; Vinek, H.; Jentys, A. *Catal. Lett.* **1998**, *56*, 189.
493. Haruta, M.; Tsubota, S.; Kobayashi, T.; Kageyama, H.; Genet, M.J.; Delmon, B. *J. Catal.* **1993**, *144*, 175.
494. Iizuka, Y.; Tode, T.; Takao, T.; Yatsu, K.; Takeuchi, T.; Tsubota, S.; Haruta, M. *J. Catal.* **1999**, *187*, 50.
495. Haruta, M. *J. New Mater. Electrochem. Syst.* **2004**, 7, 163.
496. Comotti, M.; Li, W.C.; Spliethoff, B.; Schüth, F. *J. Am. Chem. Soc.* **2006**, *128*, 917.
497. Yang, C.M.; Kalwei, M.; Schüth, F.; Chao, K.J. *Appl. Catal. A-Gen.* **2003**, *254*, 289.
498. Liotta, L.F.; Pantaleo, G.; Puleo, F.; Venezia, A.M. *Catal. Today* **2012**, *187*, 10.
499. Escamilla-Perea, L.; Peza-Ledesma, C.L.; Nava, R.; Rivera-Munoz, E.M.; Pawelec, B.; Fierro, J.L.G. *Catal. Commun.* **2011**, *15*, 108.
500. Peza-Ledesma, C.L.; Escamilla-Perea, L.; Nava, R.; Pawelec, B.; Fierro, J.L.G. *Appl. Catal. A-Gen.* **2010**, *375*, 37.
501. Rombi, E.; Cutrufello, M.G.; Cannas, C.; Casu, M.; Gazzoli, D.; Occhiuzzi, M.; Monacia, R.; Ferinoa, I. *Phys. Chem. Chem. Phys.* **2009**, *11*, 593.
502. Lee, B.; Ma, Z.; Zhang, Z.; Park, C.; Dai, S. *Microporous Mesoporous Mater.* **2009**, *122*, 160.
503. Gonzalez-Arellano, C.; Corma, A.; Iglesias, M.; Sanchez, F. *Eur. J. Inorg. Chem.* **2008**, 1107.
504. Bandyopadhyay, M.; Korsak, O.; van den Berg, M.W.E.; Grunert, W.; Birkner, A.; Li, W.; Schüth, F.; Gies, H. *Microporous Mesoporous Mater.* **2006**, *89*, 158.
505. Chi, Y.S.; Lin, H.P.; Mou, C.Y. *Appl. Catal. A-Gen.* **2005**, *284*, 199.
506. Liu, J.H.; Chi, Y.S.; Lin, H.P.; Mou, C.Y.; Wan, B.Z. *Catal. Today* **2004**, *93–5*, 141.
507. Reddy, K.M.; Wei, B.L.; Song, C.S. *Catal. Today* **1998**, *43*, 261.
508. Naik, B.; Hazra, S.; Prasad, V.S.; Ghosh, N.N. *Catal. Commun.* **2011**, *12*, 1104.
509. Huang, W.; Kuhn, J.N.; Tsung, C.-K.; Zhang, Y.; Habas, S.E.; Yang, P.; Somorjai, G.A. *Nano Lett.* **2008**, *8*, 2027.
510. Barau, A.; Budarin, V.; Caragheorgheopol, A.; Luque, R.; Macquarrie, D.J.; Prelle, A.; Teodorescu, V.S.; Zaharescu, M. *Catal. Lett.* **2008**, *124*, 204.
511. Albuquerque, M.C.G.; Jimenez-Urbistondo, I.; Santamaria-Gonzalez, J.; Merida-Robles, J.M.; Moreno-Tost, R.; Rodriguez-Castellon, E.; Jimenez-Lopez, A.; Azevedo, D.C.S.; Cavalcante, C.L., Jr.; Maireles-Torres, P. *Appl. Catal. A-Gen.* **2008**, *334*, 35.
512. Sacaliuc, E.; Beale, A.M.; Weckhuysen, B.M.; Nijhuis, T.A. *J. Catal.* **2007**, *248*, 235.

513. Magureanu, M.; Mandache, N.B.; Hu, J.; Richards, R.; Florea, M.; Parvulescu, V.I. *Appl. Catal. B* **2007**, *76*, 275.
514. Chytil, S.; Glomm, W.R.; Kvande, I.; Zhao, T.; Walmsley, J.C.; Blekkan, E.A. *Top. Catal.* **2007**, *45*, 93.
515. Zhu, H.G.; Liang, C.D.; Yan, W.F.; Overbury, S.H.; Dai, S. *J. Phys. Chem. B* **2006**, *110*, 10842.
516. Tu, C.H.; Wang, A.Q.; Zheng, M.Y.; Wang, X.D.; Zhang, T. *Appl. Catal. A-Gen.* **2006**, *297*, 40.
517. Karimi, B.; Abedi, S.; Clark, J.H.; Budarin, V. *Ang. Chem. Inter. Ed.* **2006**, *45*, 4776.
518. Jiang, Y.J.; Gao, Q.M. *J. Am. Chem. Soc.* **2006**, *128*, 716.
519. Chiang, C.-W.; Wang, A.; Mou, C.-Y. *Catal. Today* **2006**, *117*, 220.
520. Ding, J.; Chan, K.Y.; Ren, J.W.; Xiao, F.-S. *Electrochim. Acta* **2005**, *50*, 3131.
521. Yang, C.M.; Kalwei, M.; Schüth, F.; Chao, K.J. *Appl. Catal. A-Gen.* **2003**, *254*, 289.
522. Vradman, L.; Landau, M.V.; Herskowitz, M.; Ezersky, V.; Talianker, M.; Nikitenko, S.; Koltypin, Y.; Gedanken, A. *J. Catal.* **2003**, *213*, 163.
523. Martinez, A.; Lopez, C.; Marquez, F.; Diaz, I. *J. Catal.* **2003**, *220*, 486.
524. Khodakov, A.Y.; Griboval-Constant, A.; Bechara, R.; Zholobenko, V.L. *J. Catal.* **2002**, *206*, 230.
525. Rioux, R.M.; Song, H.; Hoefelmeyer, J.D.; Yang, P.; Somorjai, G.A. *J. Phys. Chem. B* **2005**, *109*, 2192.
526. Bezemer, G.L.; Bitter, J.H.; Kuipers, H.P.C.E.; Oosterbeek, H.; Holewijn, J.E.; Xu, X.D.; Kapteijn, F.; van Dillen, A.J.; de Jong, K.P. *J. Am. Chem. Soc.* **2006**, *128*, 3956.
527. Khodakov, A.Y.; Bechara, R.; Griboval-Constant, A. *Appl. Catal. A-Gen.* **2003**, *254*, 273.
528. Xiong, H.; Zhang, Y.; Liew, K.; Li, J. *J. Mol. Catal. A: Chem.* **2008**, *295*, 68.
529. Abe, T.; Tachibana, Y.; Uematsu, T.; Iwamoto, M. *J. Chem. Soc. Chem. Commun.* **1995**, 1617.
530. Kloetstra, K.R.; van Bekkum, H. *Stud. Surf. Sci. Catal.* **1997**, *105*, 431.
531. Choudhary, V.R.; Jana, S.K.; Kiran, B.P. *J. Catal.* **2000**, *192*, 257.
532. Zecchina, A.; Scarano, D.; Spoto, G.; Bordiga, S.; Lamberti, C.; Bellussi, G. *Stud. Surf. Sci. Catal.* **1998**, *117*, 343.
533. Hu, J.C.; Wang, Y.D.; Chen, L.F.; Richards, R.; Yang, W.M.; Liu, Z.C.; Xu, W. *Microporous Mesoporous Mater.* **2006**, *93*, 158.
534. Li, E.; Rudolph, V. *Energy Fuel* **2008**, *22*, 145.
535. Nguyen, S.V.; Szabo, V.; On, D.T.; Kaliaguine, S. *Microporous Mesoporous Mater.* **2002**, *54*, 51.
536. Capek, L.; Adam, J.; Grygar, T.; Bulanek, R.; Vradman, L.; Kosova-Kucerova, G.; Cicmanec, P.; Knotek, P. *Appl. Catal. A-Gen.* **2008**, *342*, 99.
537. Liu, Y.M.; Cao, Y.; Yan, S.R.; Dai, W.L.; Fan, K.N. *Catal. Lett.* **2003**, *88*, 61.
538. Liu, W.; Lai, S.Y.; Dai, H.; Wang, S.; Sun, H.; Au, C.T. *Catal. Lett.* **2007**, *113*, 147.
539. Kustrowski, P.; Segura, Y.; Chmielarz, L.; Surman, J.; Dziembaj, R.; Cool, P.; Vansant, E.F. *Catal. Today* **2006**, *114*, 307.
540. Lopez, H.H.; Martinez, A. *Catal. Lett.* **2002**, *83*, 37.
541. Fornes, V.; Lopez, C.; Lopez, H.H.; Martinez, A. *Appl. Catal. A-Gen.* **2003**, *249*, 345.
542. Li, X.K.; Ji, W.H.; Zhao, J.; Zhang, Z.; Au, C.T. *Appl. Catal. A-Gen.* **2006**, *306*, 8.
543. Sauer, J.; Marlow, F.; Spliethoff, B.; Schüth, F. *Chem. Mater.* **2002**, *14*, 217.
544. Schüth, F.; Wingen, A.; Sauer, J. *Microporous Mesoporous Mater.* **2001**, *44*, 465.
545. Chmielarz, L.; Kustrowski, P.; Dziembaj, R.; Cool, P.; Vansant, E.F. *Appl. Catal. B.* **2006**, *62*, 369.
546. Sun, Y.Y.; Walspurger, S.; Tessonnier, J.P.; Louis, B.; Sommer, J. *Appl. Catal. A-Gen.* **2006**, *300*, 1.

547. Wang, Y.; Yang, W.; Yang, L.; Wang, X.; Zhang, Q. *Catal. Today* **2006**, *117*, 156.
548. Zhang, Q.; Li, Y.; An, D.; Wang, Y. *Appl. Catal. A-Gen.* **2009**, *356*, 103.
549. Rajabi, F.; Naserian, S.; Primo, A.; Luque, R. *Adv. Synth. Catal.* **2011**, *353*, 2060.
550. Li, Y.; Xia, H.; Fan, F.; Feng, Z.; van Santen, R.A.; Hensen, E.J.M.; Li, C. *Chem. Commun.* **2008**, 774.
551. Lu, A.-H.; Nitz, J.-J.; Comotti, M.; Weidenthaler, C.; Schlichte, K.; Lehmann, C.W.; Terasaki, O.; Schüth, F. *J. Am. Chem. Soc.* **2010**, *132*, 14152.
552. Jiao, F.; Frei, H. *Angew. Chem. Int. Ed.* **2009**, *48*, 1841.
553. Jiao, F.; Frei, H. *Chem. Commun.* **2010**, *46*, 2920.
554. Jiao, F.; Frei, H. *Energy Environ. Sci.* **2010**, *3*, 1018.
555. Nava, R.; Ortega, R.A.; Alonso, G.; Ornelas, C.; Pawelec, B.; Fierro, J.L.G. *Catal. Today* **2007**, *127*, 70.
556. Gutierrez, O.Y.; Fuentes, G.A.; Salcedo, C.; Klimova, T. *Catal. Today* **2006**, *116*, 485.
557. Ramirez, J.; Contreras, R.; Castillo, P.; Klimova, T.; Zarate, R.; Luna, R. *Appl. Catal. A-Gen.* **2000**, *197*, 69.
558. Huirache-Acuna, R.; Pawelec, B.; Rivera-Munoz, E.; Nava, R.; Espino, J.; Fierro, J.L.G. *Appl. Catal. B* **2009**, *92*, 168.
559. Valencia, D.; Klimova, T. *Catal. Commun.* **2012**, *21*, 77.
560. Alonso-Nunez, G.; Bocarando, J.; Huirache-Acuna, R.; Alvarez-Contreras, L.; Huang, Z.D.; Bensch, W.; Berhault, G.; Cruz, J.; Zepeda, T.A.; Fuentes, S. *Appl. Catal. A-Gen.* **2012**, *419*, 95.
561. Zhang, D.Q.; Duan, A.J.; Zhao, Z.; Wang, X.Q.; Jiang, G.Y.; Liu, J.; Wang, C.Y.; Jin, M.C. *Catal. Today* **2011**, *175*, 477.
562. Valencia, D.; Klimova, T. *Catal. Today* **2011**, *166*, 91.
563. Infantes-Molina, A.; Romero-Perez, A.; Sanchez-Gonzalez, V.; Pawelec, B.; Fierro, J.L.G.; Jimenez-Lopez, A.; Rodriguez-Castellon, E. *ACS Catal.* **2011**, *1*, 175.
564. Fan, Y.; Shi, G.; Liu, H.Y.; Bao, X.J. *Fuel* **2011**, *90*, 1717.
565. Klimova, T.; Gutierrez, O.; Lizama, L.; Amezcua, J. *Microporous Mesoporous Mater.* **2010**, *133*, 91.
566. Cho, K.S.; Seo, H.R.; Kim, S.H.; Lee, Y.K. *J. Jpn. Pet. Inst.* **2010**, *53*, 173.
567. Soriano, A.; Roquero, P.; Klimova, T. *Stud. Surf. Sci. Catal.* **2010**, *175*, 525.
568. Valencia, D.; Garcia-Cruz, I.; Klimova, T. *Stud. Surf. Sci. Catal.* **2010**, *175*, 529.
569. Huang, X.F.; Ji, S.F.; Wu, P.Y.; Liu, Q.Q.; Liu, H.; Zhu, J.Q.; Li, C.Y. *Acta Phys. Chim. Sinica* **2008**, *24*, 1773.
570. Gutierrez, O.Y.; Romero, K.A.; Fuentes, G.A.; Klimova, T. *Stud. Surf. Sci. Catal.* **2006**, *162*, 355.
571. Sampieri, A.; Pronier, S.; Blanchard, J.; Breysse, M.; Brunet, S.; Fajerwerg, K.; Louis, C.; Perot, G. *Catal. Today* **2005**, *107–08*, 537.
572. Chai, G.S.; Yoon, S.B.; Yu, J.S.; Choi, J.H.; Sung, Y.E. *J. Phys. Chem. B* **2004**, *108*, 7074.
573. Su, F.B.; Zeng, J.H.; Bao, X.Y.; Yu, Y.S.; Lee, J.Y.; Zhao, X.S. *Chem. Mater.* **2005**, *17*, 3960.
574. Choi, Y.S.; Joo, S.H.; Lee, S.A.; You, D.J.; Kim, H.; Pak, C.; Chang, H.; Seung, D. *Macromolecules* **2006**, *39*, 3275.
575. Joo, S.H.; Pak, C.; You, D.J.; Lee, S.-A.; Lee, H.I.; Kim, J.M.; Chang, H.; Seung, D. *Electrochim. Acta* **2006**, *52*, 1618.
576. Calvillo, L.; Lazaro, M.J.; Garcia-Bordeje, E.; Moliner, R.; Cabot, P.L.; Esparbe, I.; Pastor, E.; Quintana, J.J. *J. Power Sources* **2007**, *169*, 59.
577. Chang, H.; Joo, S.H.; Pak, C. *J. Mater. Chem.* **2007**, *17*, 3078.
578. Kim, M.; Hwang, S.; Yu, J.-S. *J. Mater. Chem.* **2007**, *17*, 1656.
579. Lin, M.-L.; Huang, C.-C.; Lo, M.-Y.; Mou, C.-Y. *J. Phys. Chem. C* **2008**, *112*, 867.
580. Antolini, E. *Appl. Catal. B* **2009**, *88*, 1.

581. Fang, B.; Kim, J.H.; Kim, M.; Yu, J.–S. *Chem. Mater.* **2009**, *21*, 789.
582. Liu, G.; Li, X.; Ganesan, P.; Popov, B.N. *Appl. Catal. B* **2009**, *93*, 156.
583. Liu, R.; Wu, D.; Feng, X.; Muellen, K. *Angew. Chem. Int. Ed.* **2010**, *49*, 2565.
584. Wang, X.; Lee, J.S.; Zhu, Q.; Liu, J.; Wang, Y.; Dai, S. *Chem. Mater.* **2010**, *22*, 2178.
585. Lu, A.H.; Li, W.C.; Hou, Z.S.; Schüth, F. *Chem. Commun.* **2007**, 1038.
586. Lu, A.H.; Tüysüz, H.; Schüth, F. *Microporous Mesoporous Mater.* **2008**, *111*, 117.
587. Lee, K.T.; Ji, X.L.; Rault, M.; Nazar, L.F. *Angew. Chem. Int. Ed.* **2009**, *48*, 5661.
588. Ismail, A.A.; Bahnemann, D.W.; Rathousky, J.; Yarovyi, V.; Wark, M. *J. Mater. Chem.* **2011**, *21*, 7802.
589. Ismail, A.A. *Microporous Mesoporous Mater.* **2012**, *149*, 69.
590. Cauvel, A.; Brunel, D.; DiRenzo, F.; Garrone, E.; Fubini, B. *Langmuir* **1997**, *13*, 2773.
591. Brunel, D.; Cauvel, A.; Di Renzo, F.; Fajula, F.; Fubini, B.; Onida, B.; Garrone, E. *New J. Chem.* **2000**, *24*, 807.
592. Moller, K.; Bein, T. *Chem. Mater.* **1998**, *10*, 2950.
593. Nakazawa, J.; Smith, B.J.; Stack, T.D.P. *J. Am. Chem. Soc.* **2012**, *134*, 2750.
594. Athens, G.L.; Shayib, R.M.; Chmelka, B.F. *Curr. Opin. Colloid Interface Sci.* **2009**, *14*, 281.
595. Dhepe, P.L.; Ohashi, M.; Inagaki, S.; Ichikawa, M.; Fukuoka, A. *Catal. Lett.* **2005**, *102*, 163.
596. Corma, A.; Das, D.; Garcia, H.; Leyva, A. *J. Catal.* **2005**, *229*, 322.
597. Mbaraka, I.K.; Shanks, B.H. *J. Catal.* **2005**, *229*, 365.
598. Jarupatrakorn, J.; Tilley, J.D. *J. Am. Chem. Soc.* **2002**, *124*, 8380.
599. Yang, C.M.; Zibrowius, B.; Schmidt, W.; Schüth, F. *Chem. Mater.* **2004**, *16*, 2918.
600. Yang, C.-M.; Lin, H.-A.; Zibrowius, B.; Spliethoff, B.; Schüth, F.; Liou, S.-C.; Chu, M.-W.; Chen, C.-H. *Chem. Mater.* **2007**, *19*, 3205.
601. Palkovits, R.; Yang, C.-M.; Olejnik, S.; Schüth, F. *J. Catal.* **2006**, *243*, 93.
602. Bazula, P.A.; Lu, A.H.; Nitz, J.J.; Schüth, F. *Microporous Mesoporous Mater.* **2008**, *108*, 266.
603. Konya, Z.; Puntes, V.F.; Kiricsi, I.; Zhu, J.; Alivisatos, A.P.; Somorjai, G.A. *Nano Lett.* **2002**, *2*, 907.
604. Song, H.; Rioux, R.M.; Hoefelmeyer, J.D.; Komor, R.; Niesz, K.; Grass, M.; Yang, P.D.; Somorjai, G.A. *J. Am. Chem. Soc.* **2006**, *128*, 3027.
605. Jia, C.J.; Schüth, F. *Phys. Chem. Chem. Phys.* **2011**, *13*, 2457.
606. Joo, S.H.; Park, J.Y.; Tsung, C.K.; Yamada, Y.; Yang, P.D.; Somorjai, G.A. *Nat. Mater.* **2009**, *8*, 126.
607. Arnal, P.M.; Comotti, M.; Schüth, F. *Angew. Chem. Int. Ed.* **2006**, *45*, 8224.
608. Lu, A.H.; Kiefer, A.; Schmidt, W.; Schüth, F. *Chem. Mater.* **2004**, *16*, 100.
609. Xia, Y.D.; Mokaya, R. *Adv. Mater.* **2004**, *16*, 1553.
610. Shin, Y.S.; Fryxell, G.; Um, W.Y.; Parker, K.; Mattigod, S.V.; Skaggs, R. *Adv. Funct. Mater.* **2007**, *17*, 2897.
611. Wan, Y.; Qian, X.; Jia, N.Q.; Wang, Z.Y.; Li, H.X.; Zhao, D.Y. *Chem. Mater.* **2008**, *20*, 1012.
612. Li, Z.J.; Yan, W.F.; Dai, S. *Langmuir* **2005**, *21*, 11999.
613. Li, Z.J.; Del Cul, G.D.; Yan, W.F.; Liang, C.D.; Dai, S. *J. Am. Chem. Soc.* **2004**, *126*, 12782.
614. Vinu, A.; Hossian, K.Z.; Srinivasu, P.; Miyahara, M.; Anandan, S.; Gokulakrishnan, N.; Mori, T.; Ariga, K.; Balasubramanian, V.V. *J. Mater. Chem.* **2007**, *17*, 1819.
615. Lu, A.-H.; Nitz, J.-J.; Tüysüz, H.; Weidenthaler, C.; Bongard, H.-J.; Schüth, F. in preparation.
616. Lu, A.H.; Li, W.C.; Kiefer, A.; Schmidt, W.; Bill, E.; Fink, G.; Schüth, F. *J. Am. Chem. Soc.* **2004**, *126*, 8616.
617. Lin, W.Y.; Frei, H. *J. Am. Chem. Soc.* **2005**, *127*, 1610.